AN ABSTRACT OF A DISSERTATION

ON THE BRANCH FORMATION AND MOBILITY OF LINKAGES

Changyu Xue

Doctor of Philosophy in Engineering

In this dissertation, the N-bar rotatability laws are extended to N-bar chains containing prismatic joints. The extension is based on the principle that a prismatic joint may be regarded as a revolute joint located at infinity in the direction normal to the sliding path. The extension provides a consistent method to understand all aspects of linkage rotatability disregarding the existence of prismatic joints.

Mobility of linkages refers to the problems concerning branch, full rotatability, singularities, and order of motion. By using the stretch rotation to one of the four-bar loop, a Watt six-bar linkage is equivalent to a Stephenson six-bar linkage. The equivalency offers a simple and clear visual explanation on the formation of branches and sub-branches and how Watt and Stephenson linkages differ in mobility.

The concept of virtual loops is presented to describe the essential geometry behind spatial linkages. Spatial group 1, 2, 3, or 4 linkages can be regarded as a virtual spherical linkage formed by one or more virtual loops. From the viewpoint of linkage mobility and displacement analysis, simple RCRCR and group 2 linkages with parallel joint axes are virtually equivalent to Stephenson six-bar linkages. The concept of virtual loops is subtle but significant. It establishes a unified view on planar, spherical, and spatial linkages and a useful model to view or even understand complex spatial linkages.

The current use of branch points for branch identification is limited to linkages with simple topology and singularity conditions, such as Stephenson-type linkages, which are simplified versions of group 2 mechanisms. In this dissertation, branch points in Stephenson-type linkages are generalized to explain and define the interaction between two virtual five-bar loops. The discovery of tangent points and the concept of generalized branch points offer an explicit explanation and prediction about the branch formation of spatial group 2 linkage.

The mobility of spatial group 2 linkages is governed by two fundamental equations and how they influence each other. Under the concepts of virtual loops and generalized branch points, it becomes possible to explore the mobility theory of general group 2 linkages and other complex linkages.

ON THE BRANCH FORMATION AND MOBILITY OF LINKAGES

A Dissertation

Presented to

The Faculty of the Graduate School

Tennessee Technological University

by

Changyu Xue

In Partial Fulfillment of

the Requirements for the Degree of

DOCTOR OF PHILOSOPHY

Engineering

August 2009

ProQuest LLC
789 East Eisenhower Parkway
P.O. Box 1346
Ann Arbor, MI 48106-1346

CERTIFICATE OF APPROVAL OF DISSERTATION

ON THE BRANCH FORMATION AND MOBILITY OF LINKAGES

by

Changyu Xue

Graduate Advisory Committee:

Kwun-Lon Ting, Chairperson — 5-26-09 Date

Kenneth R. Currie, Co-chair — 5-27-09 Date

Motoya Machida — 5-26-09 Date

Chris Wilson — 5-26-09 Date

Ying Zhang — 5-26-09 Date

Approved for the Faculty:

Francis Otuonye
Associate Vice President for Research
and Graduate Studies

5/29/09

Date

ACKNOWLEDGEMENTS

The author would like to take this opportunity to extend his sincere appreciation and gratitude to those who make this dissertation possible. He would like to thank his advisors Dr. Kwun-Lon Ting and Dr. Kenneth R. Currie, whose guidance, support, encouragement, and patience made the process of this dissertation and his years of the doctoral program an enjoyable and beneficial learning experience. He is deeply thankful to Dr. Motoya Machida, Dr. Chris Wilson, and Dr. Ying Zhang, members of the advisory committee, for their invaluable suggestions. Special grateful appreciation is expressed to Dr. Heidemarie Weidner, his host mother and writing coach, for her careful editing on his dissertation. The author is also thankful to Mr. Jun Wang and Mr. Bowen Yu for all their help in the last year of his doctoral program.

The author acknowledges the financial support to his graduate study provided by the Center for Manufacturing Research at Tennessee Technological University. Thanks are also given to Ms. Sue Richardson, Ms. Phyllis Stallion, Ms. Darlene Wiegand, Mr. Joel Seber, and Mr. Mike Renfro of Center for Manufacturing Research for their kind assistance.

The author would like to express his gratitude to his parents, Yongtai Xue and Naifang Wang, for their unconditional love and support. He would also like to extend his gratitude to his parents-in-laws, Guozhong Zhang and Meihua Bi, for their consistent support all the years. He is grateful to his wife, Jie, for her patience and unconditional love and support. With a thankful heart, he acknowledges his family and friends for their love and prayers. This dissertation is especially for his son, Jeffrey.

TABLE OF CONTENTS

Page

Chapter Page

LIST OF FIGURES

Page

Page

LIST OF TABLES

Page

CHAPTER 1

INTRODUCTION

1.1 Background

Linkages and manipulators are usually synthesized or programmed to navigate through discrete positions over a region. When a linkage is synthesized, it is necessary to make sure that the linkage has adequate mobility for a continuous and smooth operation. The ability for a linkage to reach the desired discrete positions typically refers to the ability to overcome or avoid discontinuity and singularity and to navigate in a desired and coordinated manner.

Fig. 1.1 shows a gear five-bar linkage, which is used to generate a tool path [1]. For a closed-loop linkage or manipulator, the mobility is an intrinsic property of the linkage geometry and cannot be altered by changing the environment or shaping the links and joints. The problems with discontinuity and singularity exist in single degree-of-freedom (DOF) linkages. In a linkage synthesis process, the mobility of numerous design candidates must be rectified. Since linkage synthesis generally involves massive design candidates, the synthesis task may become prohibitive without an intelligent mobility rectification method.

The typical application of linkages and manipulators is displayed on robots. Robots are widely used, especially in hazardous environments or in operations requiring accuracy and consistence that people easily find tedious, such as welding, painting, processing, assembly, and inspection. A robot manipulator consists of joints and should reach an object or any required point in workspace. The workspace of a manipulator refers to the accessible area of the end

effector (Figure 1.2). The joint movements (translation / rotation) are represented by joint variables, describing the robot configuration.

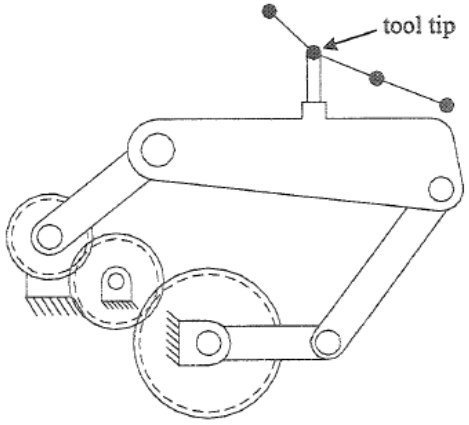

Figure 1.1 A five-bar tooling mechanism

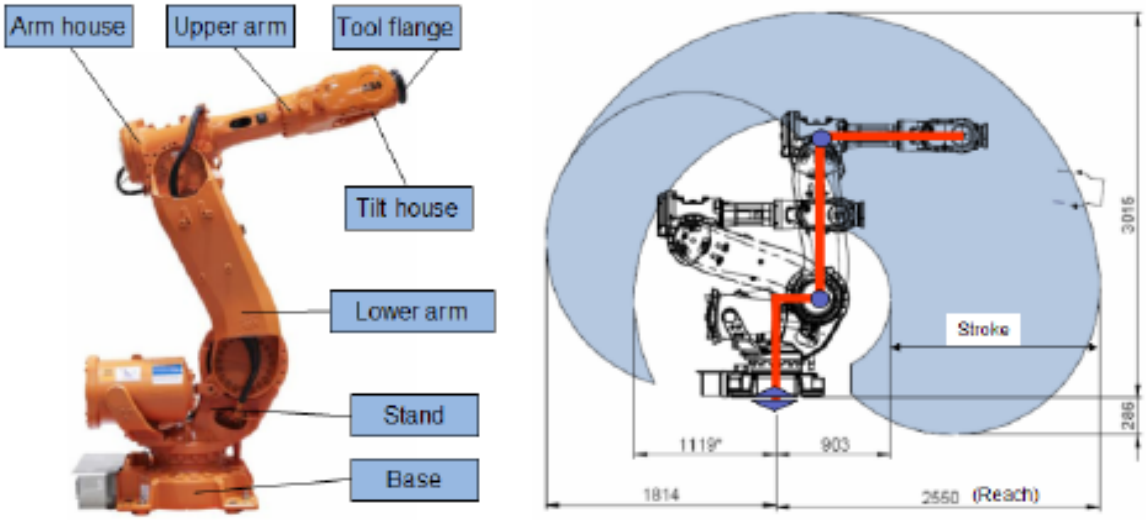

(a) (b)

Figure 1.2 (a) An ABB IRB6640-185/2.8 robot and (b) its workspace

Although mobility issues occur only in closed loop linkages, a serial or parallel manipulator will form a closed loop when the end-effector reaches a target position, travels along a designated path or surface, or cooperates with others. For example, when a computerized numerical control (CNC) machine is working on a workpiece (a CNC machine is regarded as a robot manipulator), a closed loop chain will be formed and the mobility issue may occur. A similar situation may be found during the coordination robot arms when two manipulators are capable of a synchronized operation, such as material handling and assembly, servicing, and maintenance in remote hazardous places.

The problems with linkage mobility were recognized decades ago, but they remain one of the most difficult problems in linkage analysis, synthesis, and programming. For any linkage or manipulator, it is highly desirable that a single decisive step answers the questions of if and how the desired positions can be reached in a favorable manner rather than a decision made through trial and error and a possibly endless search process. The tremendous interest in the mobility of four-bar linkages and the workspace/singularity of manipulators in recent decades were efforts motivated by such desires.

For many decades, the understanding of the mobility of conventional closed-loop linkages had been mostly restricted to planar and spherical four-bar linkages. The mobility study of four-bar linkages may be traced back to the discovery of the Grashof criterion [2], which was widely used, proved, and elaborated several decades later through approaches such as triangular inequality condition, transmission angle, and polynomial discriminant [3-8]. There were also attempts to re-derive the Grashof criterion through the intersection of the workspaces of two open-loop chains taken apart from a closed-loop four-bar linkage [9]. Other works on the mobility of four-bar

linkages include the singularity analysis and the synthesis of four-bar linkages based on their overall mobility [7, 10-14].

Traditionally, mobility issues were treated by considering the point positions on a coupler curve (i.e., the path traced by a point fixed in the coupler link of a mechanism) [15-21] or by using the discriminant function [22-25] based on the input and output relationship. There appear in the kinematics literature numerous theorems concerning the properties of coupler curves, whose geometric and algebraic properties have important implications on mechanisms synthesis, such as path generation or rigid body guidance problems [26]. A numerical method was presented to evaluate the performance of a path-generating mechanism with the use of coupler curves theorem [27]. However, the complexity of coupler curves unavoidably adds an unnecessary complexity to the problem. On the other hand, the research on the format of the input and output relationship is limited by the use of the discriminant function only.

A significant advancement in linkage mobility are the N-bar rotatability laws [28-30]. In the N-bar rotatability laws, the rotatability of a linkage is viewed as the variation of a polygon rather than a linkage. Therefore, the variety of mobility considerations due to different linkage inversions is eliminated. In fact, the N-bar rotatability laws were simplified as the full extension of the existence condition of triangles, i.e. the length sum of two sides is greater than the length of the third side in a triangle. The joint rotatability in a chaotic N-bar chain suddenly becomes easy to understand. The N-bar rotatability laws offer the first simple, complete, and systematical explanation for the rotatability of any N-bar chain ($N \geq 3$) connected with revolute joints, in which the Grashof criterion becomes a very special case.

Later on, the Grashof criterion was extended to spherical four-bar linkages [9, 14, 31-36]. Generally, for geometric properties found in planar linkages, similar properties can also be

expected in spherical linkages. The success in planar and spherical four-bar linkages was later extended to all bimodal linkages [12, 22, 24, 37-39].

The equation relating the output and input of a bimodal linkage can always be expressed in quadratic form. Based on the discriminant function of the quadratic equation, an algorithm can be derived for the mobility identification of any bimodal linkages, including RSSR, RRSS, RSCR, RSCP, and RCCC linkages (R, S, C, and P refer to the revolute, spherical, cylindrical, and prismatic joints used in the linkages) [22, 24, 37, 40, 41]. Like planar four-bar linkages, RSSR can always be classified into three classes according to the possible number of branches [40]. The RRSS linkage is an inversion of the RSSR linkage, and the classification strategy for the two is essentially identical. The geometric and algebraic properties of the coupler curves of the RSSR and RCCC mechanisms were studied and presented [42, 43]. The coupler curve equations were derived for the spherical four-bar and the RCCC mechanism [44].

The mobility problem, particularly in spatial mechanisms, becomes increasingly difficult with the addition links and an increased linkage complexity. Because of the complexity of spatial mechanisms, an undesirably lengthy mathematical treatment in considering the effects of all links and joints parameters is required while simultaneously avoiding extraneous roots. Each spatial linkage connected with revolute or cylindrical joints has a spherical indicatrix [45], which is equivalent to the case when each joint offset and the skew distance between each pair of joint axes diminishes. Realizing the large variety of spatial linkages and the similarity shared by single loop spatial mechanisms, Duffy classified them into four groups, namely as group 1, 2, 3, and 4 linkages [45, 46]. Duffy's classification is very essential for a systematic mobility study on spatial mechanisms.

Table 1.1 Classification of spatial kinematic chains

Group	Number of links	Mechanism
1	4-7	R-3C, 2R-P-2C, 3R-2P-C, 4R-3P
2	5-7	3R- 2C, 4R-P-C, 5R-2P
3	6-7	5R- C, 6R-P
4	7	7R

The aforementioned RSSR, RRSS, RSCR, RSCP, and RCCC all belong to the category of group 1. The mobility analysis of group 1 mechanisms is relatively simple, because the input-output displacement equation leads to second degree polynomials in terms of the input joint variable, i.e., an input given to a joint will lead to two possible linkage configurations.

The number of possible configurations corresponding to one input increases as the linkage topology gets complicated. On a general group 2 mechanism, the number of configurations per one input may be as high as eight, as its input / output displacement equation is an eighth degree polynomial. In other words, there appear many limit points on the travel of the mechanism, which in turn makes a mobility analysis difficult [39]. On the other hand, a linkage may have several configurations to reach a designated position. Each linkage configuration leads to different mobility properties. A linkage must reach each position with a proper configuration. So far, little progress has been achieved on group 2 mechanisms.

Although linkage synthesis or analysis provides information at discrete positions, it offers little or no clue about how to relate the configurations at different positions or even if these configuration may be related to realize a desired continuous and smooth motion. Because discontinuities and singularities are common among linkage configurations, a black box type blind search or an optimization process is not only difficult and tedious but also unreliable. The problem is further complicated if the motion must be accomplished in a specific manner.

A few researchers tried to solve the branch problem on group 2 or even more complex single-DOF spatial mechanisms. A search technique was applied to find the assembly configurations (or branch) of RRRCC, RRCRC, RRRRCR, and RRRRRRR spatial mechanisms [47, 48]. The process is similar to the plot of an input/output displacement equation, which can be directly obtained under Duffy's closure equation [45, 46]. Based on the mathematical property of quartic expression, an automatic generation algorithm was used to identify branches of general RCRCR where one input corresponds up to four outputs [49].

When the offset is zero at the revolute joint between the cylindrical joints, general RCRCR degenerates into a special case, simple RCRCR. The conditions were presented for determining the rotatability of input and output links of simple RCRCR [25], although the conditions are extremely complicated. The successful approach is displayed in [50], in which the simple RCRCR mechanism is regarded as a spherical 5R linkage with one cylindroid surface constraint formed by a virtual bimodal linkage. Another special case occurs when two adjacent axes are parallel in group 2 mechanisms. In such a situation, the inherent 5R indicatrix degenerats into a 4R indicatrix. From the rotatability point of view, simple RCRCR and group 2 mechanisms with parallel axes are similar to Stephenson six-bar linkages and their mobility issues can be solved with the same approach. Details will be explained in Chapter 2.

The algebraic input-output displacement equations of degree four was obtained on spatial five links RRSRR [51]. The eighth degree polynomial for RRSRR mechanism is derived from the input-output displacement equation, and a total of 12 limit positions of the input link are obtained by calculating the roots of the discriminant of the quadratic solution of the mechanism in [39]. However, the mobility analysis is only available for a special case when the eighth degree polynomial input-output displacement equation is reduced to a quadratic equation. The

RRRSR spatial five-bar mechanism was investigated [52]. The input-output displacement equation was derived in quartic form and the polynomial describing the coupler curve was at most of the 32nd order. This is another example that the complexity of mobility analysis will be increased with the use of coupler curve theorem.

1.2 Organization

Most mobility researches focused on a specific linkage type. In view of the large variety of linkages, one may lament how little has been resolved. Focusing on group 2 mechanisms, this dissertation seeks to describe the essential geometry hidden behind spatial linkages. A unified view on planar, spherical, and spatial linkages and a useful model to view or even understand complex spatial linkages will be established.

This dissertation is composed of eight chapters. The introduction is presented in Chapter 1. In Chapter 2, the N-bar rotatability laws are extended to N-bar chains containing prismatic joints. In Chapter 3, the stretch rotation is applied on Watt six-bar linkages. By using the stretch rotation to one of the four-bar loop, a Watt six-bar linkage is equivalent to a Stephenson six-bar linkage. Chapter 4 addresses the simplified versions of spatial group 2 linkages: simple RCRCR and group 2 linkages with parallel joint axes. Under the concept of virtual loops, they can be modeled as Stephenson-type linkages where findings for planar Stephenson linkages can be used directly. The current use of branch points for branch identification is limited to Stephenson-type linkages. In Chapter 5, the concept of branch points is generalized to explain the branch formation of spatial group 2 linkages. In Chapter 6, the mobility analysis is carried out based on the similarity of the mobility features rather than the specific or individual linkage structure. A branch

rectification scheme is presented and demonstrated with examples. Chapter 7 addresses the JRS of multiloop linkages. The extension of JRS to multiloop linkages is helpful for the explanation and prediction of the branch formation of complex linkages, particularly spatial linkages. Chapter 8 contains the conclusions of the study.

To make it easier to read, each of Chapters 2 through 6 is arranged as an independent research paper.

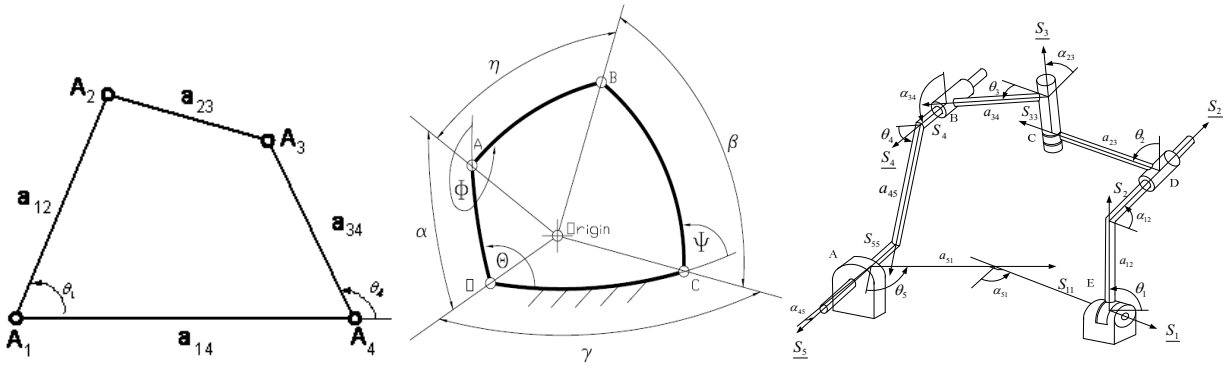

(a) Planar (b) spherical (c) spatial

Figure 1.3 Planar, spherical, and spatial linkages

REFERENCES

1. Lee, W.T., 2004, *The Design of Adjustable Spherical Mechanisms Using Plane-to-sphere and Sphere-to-plane Projections*, Ph.D dissertation, New Jersey Institute of Technology.
2. Grashof, F., 1983, *Theoretische Maschinenlehre*, Leipzig.
3. Harding, B.L., 1962, "Deviation of Grashof's Law," *ASEE Machine Design Bulletin*, pp. 1-10.
4. Paul, B., 1979, "A Reassessment of Grashof's Criterion," *ASME Journal of Mechanical Design*, pp. 515-518.
5. Midha, A., Zhao, Z., and Her, I. 1985, "Mobility Region of Plane Linkages," *ASME Journal of Mechanisms, Transmissions, and Automation in Design*, Dec., Vol.107, pp. 394-400.
6. Williams, R.L.,II and Reinholtz, C.F., 1986, "Proof of Grashof's Law Using Polynomial Discriminants," *ASME Journal of Mechanisms, Transmissions, and Automation in Design*, pp. 562-564.
7. Barker, C.R., 1985, "A Complete Classification of Planar Four-Bar Linkages," *Mechanism & Machine Theory*, v 20, n 6, pp. 535-554.
8. Angeles, J. and Callejas, M., 1984, "An Algebraic Formulation of Grashof's Mobility Criteria with Application to Linkage Optimization Using Gradient Dependent Methods," *ASME Journal of Mechanisms, Transmissions, and Automation in Design*, v 106, pp. 327-332.
9. Dobrovolskii, V.V., 1947, *Theory of the spherical mechanisms*, Machgiz 231 (in Russian).
10. Freudenstein, F., and Primrose, E.J.F., 1976, "On the Criteria for the Rotatability of the Cranks of a Skew Four-Bar Linkage," *ASME Journal of Engineering for Industry*, pp. 1285-1288.
11. Gupta, K.C., 1978, "A General Theory for Synthesizing Crank-Type Four-Bar Function Generator With Transmission Angle Control," *ASME Journal of Applied Mechanics*, Vol. 45, pp. 415-421.
12. Kazerounian, K.; Solecki, R., 1993, "Mobility Analysis of General Bi-modal Four Bar Linkages Based on Their Transmission Angle," *Mechanism & Machine Theory*, v 28, n 3, pp. 437-445.
13. Mallik, A.K., 1994, "Mobility Analysis and Type Identification of Four-Link Mechanisms," *Journal of Mechanical Design*, v 116, n 2, pp.629-633.
14. Savage, M. and Hall, A.S.Jr., 1980, "Unique Descriptions of all Spherical Four-Bar Linkages," *ASME Journal of Engineering for Industry*, v 6, n 3, series B, pp. 559-566.
15. Chase, T.R., and Mirth, J.A., 1993, "Circuit and Branches of Single Degree-of-Freedom Planar Linkages," *Journal of Mechanical Design*, Vol.115, No. 2, pp. 223-230.
16. Davis, H.P., Chase, T.R., and Mirth, J.A., 1994, "Circuit Analysis of Stephenson Chain Six-Bar Mechanisms," *ASME Mechanism Synthesis and Analysis*, DE-vol.70, pp.349–358.

17. Davis, H.P., Chase, T.R., 1994, "Stephenson Chain Branch Analysis: Four Generic Stationary Configurations and One New Linkage Polynomial," *ASME Mechanism Design and Synthesis*, DE-Vol.70, pp.359–367.

18. Guo, X.N. and Chu, J.K., 2004, "Mobility of Stephenson Six-Bar Chains-Part I: Circuit and Circuit Defect," *Proceedings of ASME DETC'04*, September 2004, Salt Lake City, Utah.

19. Guo, X.N. and Chu, J.K., 2004, "Mobility of Stephenson Six-Bar Chains-Part II: the Motion Order," *Proceedings of ASME DETC'04*, September 2004, Salt Lake City, Utah.

20. Mirth, J.A. and Chase, T.R., 1993, "Circuit Analysis of Watt Chain Six-Bar Mechanisms," *ASME Mechanical Design*, pp.214–222.

21. Guo, W.Z. and Du, R., 2006, "Mobility of Single-Loop N-Bar Linkage with Active/Passive Prismatic Joints," *Journal of Mechanical Design*, Vol. 128, no. 6, p 1261-1271.

22. Ting, K.L. and Dou, X.H., 1994, "Branch, Mobility Criteria, and Classification of RSSR and Other Bimodal Linkages," *ASME Mechanism Synthesis and Analysis*, DE-Vol.70, pp.303-310.

23. Kohli, D., Cheng, J.C. and Tsai, K.Y., 1994, "Assimilability, Circuits, Branches, Locking Positions, and Rotatability of Input Links of Mechanisms with Four Closures," *Journal of Mechanical Design, Transaction of ASME*, Vo1.116, pp.92-98.

24. Su, H.J. Collins, C.L., and McCarthy, M., 2002, "Classification of RRSS Linkages," *Mechanism and Machine Theory*, Vol. 37, pp.1413-1433.

25. Pamidi, P.R. and Freudenstein, F., 1975, "On the Motion of a Class of Five-Link, R–C–R–C–R, Spatial Mechanisms," *ASME J. Eng. Ind.*, 97 (1), pp.334–339.

26. Soni, A.H., 1974, *Mechanism Synthesis and Analysis*, McGraw-Hill Book Co, New York.

27. Ma, O. and Angeles, J., 1988, "Performance Evaluation of Path-Generating Planar, Spherical and Spatial Four-Bar Linkages," *Mechanism and Machine Theory*, 23 (4), pp.257-268.

28. Ting, K.L., 1989, "Mobility Criteria of Single-Loop N-Bar Linkages," *Journal of Mechanisms, Transmissions, and Automation in Design*, pp. 504-507.

29. Ting, K.L. and Liu, Y.W., 1991, "Rotatability Llaws for N-Bar Kinematic Chains and Their Proof," *ASME Journal of Mechanical Design*, Vol. 113, No. 1, pp. 32-39.

30. Shyu, J.H., and Ting, K.L., 1994, "Invariant Link Rotatability of N-Bar Kinematic Chains," *Journal of Mechanical Design*, Vol. 116, No.1, pp. 343-347.

31. Chiang, C.H., 1984, "On the Classification of Spherical Four-Bar Linkages," *Mechanism and Machine Theory*, Vol. 19, pp.283-287.

32. Gupta, K.C., 1986, "Rotatability Considerations for Spherical Four-Bar Linkages with Applications to Robot Wrist Design," ASME Paper No. 86-DET-18.

33. Barker, C.R., 1986, "Classification of Spherical Four-Bar Mechanisms," ASME Paper No. 86-DET-144.

34. Freudenstein, F., 1965 "On the Determination of the Type of Spherical Four-Link Mechanisms," *Contemporary Problems in the Theory of Machines and Mechanisms*, USSR Academy of Sciences, pp. 193-196.

35. Soni, A.H., 1970, "Unique Descriptions of all Spherical Four-Bar Linkages," *Discussion, ASME Journal of Engineering for Industry*, v 92, pp. 563-566.

36. Gilmartin, M.J., and Duffy, J., 1972, "Type and Mobility Analysis of the Spherical Four-Link Mechanism," *Proceedings Institution of Mechanical Engineers Conference on Mechanisms*, pp. 90-97.

37. Nolle, H., 1969, "Range of Motion Transfer by R-G-G-R Mechanisms," *Journal of Mechanisms*, 4:145-157.

38. Gupta, K. C., and Tinubu, S. O., 1983, "Synthesis of Bimodal Generating Mechanisms without Branch Defect," *J. of Mechanisms, Transmissions, and Automation in Design*, Vol. 105, pp. 641-647.

39. Lee, D., Youm, Y., and Chung, W., 1996, "Mobility Analysis of Spatial 4- and 5- Link Mechanisms of the RS Class," *Mechanism and Machine Theory*, Vol. 31, pp.673-690.

40. Williams, R.L. II and Reinholtz, C.F., 1987, "Mechanism Link Rotatability and Limit Position Analysis Using Polynomial Discriminants," *ASME Journal of Mechanisms, Transmissions, and Automation in Design*, 109 (2), pp.178–182.

41. Murray, A.P. and Larochelle, P.M., 1998, "A Classification Scheme for Planar 4R, Spherical 4R, and Spatial RCCC Linkages to Facilitate Computer Animation," *Proceedings of the 1998 ASME Design Engineering Technical Conferences: Mechanisms Conference*, Atlanta, GA.

42. Primrose, E.J.F. and Freudenstein, F., 1969, "Spatial Motions I: Point Paths of Mechanisms with Four or Fewer Links," *ASME Journal of Engineering for Industry*, Series B 91 (1), pp.103-113.

43. Marble, S.D. and Pennock, G.R., 2000, "Algebraic-Geometric Properties of the Coupler Curves of the RCCC Spatial Four-Bar Mechanism," *Mechanism and Machine Theory*, 35, pp.675-693

44. Worle, H., 1962, "Untersuchungen über Kippelkurven Viergliedriger Räumlicher Kurbelgetriebe," *Konstruktion*, 14 (10), pp.390-392.

45. Duffy, J., 1980, *Analysis of Mechanisms and Robot Manipulators*, New York, John Willey and Sons.

46. Crane III, C.D. and Duffy, J., 2008, *Kinematic Analysis of Robot Manipulators*, New York, Cambridge University Press.

47. Foster, D.E., and Cipra, R.J., 1998, "Assembly Configurations of Spatial Single-Loop Mechanisms with Revolute, Cylindrical, and Prismatic Joints," *CD-ROM Proceedings of the 1998 ASME Design Engineering Technical Conferences*, Atlanta, GA, September 13-16, Paper No. MECH-5897.

48. Foster, D.E., and Cipra, R.J., 2000, "Assembly Configurations of Spatial RRRCC, RRCRC, RRRRCR, and RRRRRRR Mechanisms," *CD-ROM Proceedings of the 2000 ASME Design Engineering Technical Conferences and Computers and Information in Engineering Conference,* Baltimore, Maryland, September 10-13, 2000, Paper No. MECH-14051.

49. Guo, X.N., 2003, *Research on Structural and Kinematic Characteristics and Parameterized Solid Kinematic Simulation of Linkages*, Ph.D dissertation, Xi'an University of Technology.

50. Dou, X. and Ting, K.L., 1996, "Classification, Rotatability, and Branch Identification of Simple RCRCR Mechanisms," *ASME Design Engineering Technical Conference and the Computer in Engineering*, Paper No. 96-DETC/FAS-1363

51. Wallace, D., 1968, *Displacement Analysis of Spatial Mechanisms with More Than Four Links*, Ph.D dissertation, Columbia University.

52. Chen, M.Z., 1983, "Some Properties of the Coupler Curve of the Spatial RRRSR Mechanism," *Mechanism and Machine Theory*, 18 (1), pp.63-71.

CHAPTER 2

MOBILITY CRITERIA OF PLANAR SINGLE-LOOP N-BAR CHAINS WITH PRISMATIC JOINTS[1]

ABSTRACT

The paper presents the extension of the N-bar rotatability laws to N-bar chains containing prismatic joints. The extension is based on the principle that a prismatic joint may be regarded as a revolute joint located at infinity in the direction normal to the sliding path. The effects of long and short links, full rotatability, linkage classification, and the formation of branches and sub-branches are discussed. The extension provides a consistent method to understand all aspects of linkage rotatability disregarding the existence of prismatic joints. The results are demonstrated by several examples.

[1] Published by the ASME 2008 International Design Engineering Technical Conferences & Computers and Information in Engineering Conference (IDETC/CIE), August 3 – 6, 2008, Brooklyn, New York, USA.

2.1 Introduction

The Grashof Criterion [1] is well known for the ability to predict the full rotatability of four-bar linkages. The N-bar rotatability laws proposed by Ting [2-5] offer a systematic treatment for almost all aspects of the mobility issues, such as branch, sub-branch, full rotatability, singularities, and order of motions, regarding single-loop N-bar chains connected with revolute (R) joints exclusively. Recently, Gao et al., introduced the concept of virtual link to investigate the mobility of five-bar 4R1P-type linkages [6] and that of N-bar linkages containing one prismatic (P) joint [7-8]. When the P-joint variable is given, the length of a virtual link can be determined and the N-bar rotatability laws govern the rotatability of the linkage. Basically, a prismatic joint may be regarded as a special revolute joint located at infinity in the direction normal to the path of the slider. Hence the applicability of the N-bar rotatability laws to N-bar chains containing any number of P-joints is expected. The question, which is the focus of the paper, is how to express it in the most general and simplest manner. Essential elements of the N-bar rotatability laws are briefed below.

In the following discussion, λ_i ($i = 1, 2, 3, ---, N$) will be the link lengths of an N-bar chain and $\lambda_1 \leq \lambda_2 \leq \lambda_3 \leq \lambda_4 \leq -----\lambda_N$, where $N \geq 3$. The link numbers represent the magnitude order of the links rather than the order of connection.

Long and short links: A link in a single-loop chain may be conveniently distinguished as a long or short link. The concept of long and short links offers simple and better understanding to the N-bar rotatability laws. A link, say link i, is called

(a) a short link if $(\lambda_N + \lambda_i) \leq$ (the total length of all other links), or

(b) a long link if $(\lambda_N + \lambda_i) >$ (the total length of all other links).

Revolvability: The ability of full revolution at a joint is a main concern in a closed loop chain. Two links may have full revolution with respect to each other if and only if the angle between them can reach 0° and 180°.

A short link may have a full revolution with respect to any link in the loop while a long link cannot have a complete revolution with respect to any other long link. Therefore, a joint on a short link is a revolvable joint while a joint between long links is a non-revolvable joint.

Full Rotatability: An N-bar linkage has full rotatability if and only if

(1) $(\lambda_N + \lambda_1 + \lambda_2 + - - - + \lambda_{N-3}) < (\lambda_{N-1} + \lambda_{N-2})$, and

(2) there is one and only one non-input joint between any two long links.

Classification: Single-loop N-bar chains are classified into three classes.

1. Class I chains if $(\lambda_N + \lambda_1 + \lambda_2 + - - - + \lambda_{N-3}) < (\lambda_{N-1} + \lambda_{N-2})$,
2. Class II chains if $(\lambda_N + \lambda_1 + \lambda_2 + - - - + \lambda_{N-3}) > (\lambda_{N-1} + \lambda_{N-2})$,
3. Class III chains if $(\lambda_N + \lambda_1 + \lambda_2 + - - - + \lambda_{N-3}) = (\lambda_{N-1} + \lambda_{N-2})$.

Branch: A branch (or circuits [9-11]) refers to a way of chain construction of a linkage or a configuration space, in which configurations may be transformed from one to another continuously.

Because two long links may become collinear or parallel only in Class II chains, class I N-bar chain has two branches while a class II chain has only one branch. A class I chain contains three long links exactly. In a class II chain, no short link exists in the case with N = 4 and the number of short links may range from 0 to N if $N \geq 5$.

Invariant link rotatability: The rotatability between any pair of links in single loop chains formed by the same set of links is independent of the order of link connection [12].

2.2 Single-Loop N-Bar Chains with One Prismatic Joint

The principle of invariant link rotatability is also true with an N-bar chain containing a prismatic joint.

Link lengths: A general single-loop N-bar chain with a prismatic joint is shown in Fig. 2.1(a). Let λ_i ($i = 1, 2, 3, ---, N-2$) be the (finite) link lengths between revolute joints and $\lambda_1 \leq \lambda_2 \leq \lambda_3 \leq \lambda_4 \leq -----\lambda_{N-2}$, where $N \geq 3$. It is noted that the effect of a prismatic joint in a linkage is essentially determined by the direction of the sliding path. The location of the sliding path does not affect the kinematic property of the linkage. Examples are shown in Fig. 2.1, in which the sliding paths in (a) and (b) are oriented in the same direction and hence both of them represent the same kinematic chain. For two links connected by a prismatic joint, the link and joint parameters can be uniquely represented, respectively, by h and s as shown in Fig. 2.2, in which AB is the hypotenuse of the right triangle ABC with AC in the direction of the sliding path and AC = s, BC = h. In Fig. 2.2, s is a joint variable and h is a link parameter. If the value of s is given, the link and joint rotatability of the remaining loop can be determined by the N-bar rotatability laws [2-5]. This paper presents the supplement to the N-bar rotatability laws when one or more revolute joints are replaced by prismatic joints. The rotatability of a joint in an N-bar chain is the intrinsic property of the chain.

In the following discussion an N-bar chain refers to a chain containing revolute joints exclusively while a chain containing a P-joint will be referred as an N-bar (1P) chain.

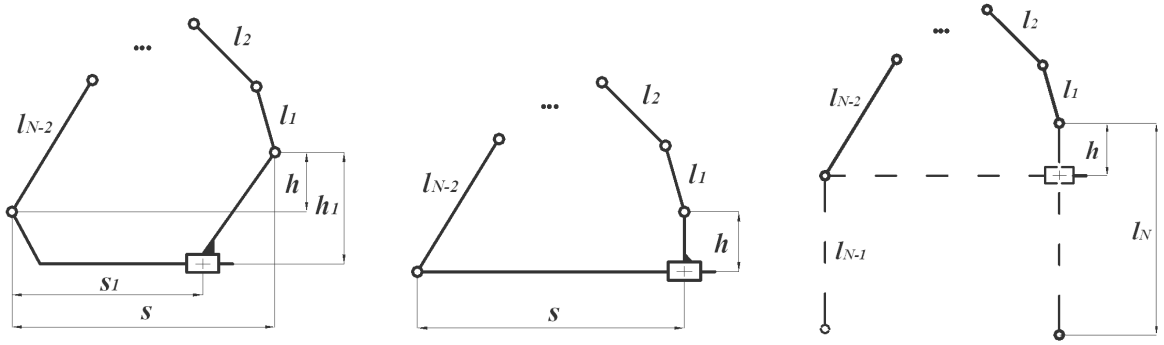

(a) (b) (c)

Figure 2.1 Representation of an N-bar chain with a P-joint

Assemblability condition: A single-loop N-bar (1P) chain may be regarded as a chain containing two links with very long (fictitious) link lengths (Fig. 2.1(c)) oriented in the direction perpendicular to the sliding path and connected by a revolute joint. The length difference between the two fictitious long links is h. Based on the N-bar rotatability laws, the following criterion can be derived.

A set of links with link lengths $\lambda_1, \lambda_2, \lambda_3, ---, \lambda_{N-2}$, *and* h *can form a planar single-loop N-bar (1P) chain, if and only if* $h \leq \lambda_1 + \lambda_2 + ---+ \lambda_{N-2}$.

For $N = 3$, the N-bar chain is reduced to a right triangle. One may note that the above assemblability condition reflects the right triangular inequality condition. To form a right triangle, for any s value, the hypotenuse λ_1 cannot be less than h. For $N > 3$, the above inequality equation represents the condition of forming a right triangle ABC in the N-bar chain.

Long and short links: A link between revolute joints in an N-bar (1P) chain can be distinguished as a long or short link. A link, say link i, is called

(a) a short link if $(h + \lambda_i) \leq (\lambda_1 + \lambda_2 + ---+ \lambda_{i-1} + \lambda_{i+1} + ---+ \lambda_{N-2})$,

i.e., $(h + \lambda_i) \leq$ (the total length of all other link parameters), or

(b) a long link if ($h + \lambda_i$) > ($\lambda_1 + \lambda_2 + \text{---} + \lambda_{i-1} + \lambda_{i+1} + \text{---} + \lambda_{N-2}$),

i.e., ($h + \lambda_i$) > (the total length of all other link parameters).

The two links connected by the P-joint may be regarded as infinite (long) links connected by an R-joint at infinity. In the following discussion, a long link will refer to a finite long link and an infinite long link will refer to a link connected by the P-joint.

Link and joint revolvability: The property of long and short links is also valid to N-bar (1P) chains. *In an N-bar (1P) chain, a short link may have a full revolution with respect to any link in the loop while a long link cannot have a complete revolution with respect to any other long link.* There is no rotatability between the two infinite long links. A revolute joint may allow a complete revolution only if it connects a short link.

Classification: Single-loop N-bar chains with a prismatic joint can be classified into three classes.

1. Class I chains if ($h + \lambda_1 + \lambda_2 + \text{---} + \lambda_{N-3}$) < λ_{N-2},
2. Class II chains if ($h + \lambda_1 + \lambda_2 + \text{---} + \lambda_{N-3}$) > λ_{N-2},
3. Class III chains if ($h + \lambda_1 + \lambda_2 + \text{---} + \lambda_{N-3}$) = λ_{N-2}.

A Class III chain may form an indeterminate configuration with all links lie on a straight line normal to the sliding path. For N = 4, this is the "change-point" configuration.

Rotatability between long links: In a Class I chain, any pair of long links can never become collinear or parallel and therefore, the oscillation angle between any pair of long links is less than 180°. On the other hand, in a Class II chain, two long links may become collinear or parallel. Therefore the oscillation angle between a pair of (finite or infinite) long links of a Class II chain is less than 360°.

Uncertainty singularity: Like a single-loop N-bar chain without any prismatic joint, any single-loop N-bar (1P) chain has (*N*-3) degree-of-freedom and requires (*N*-3) inputs.

There are always three passive (non-input) joints. If the P-joint is an input joint, when the three passive joints lie on a common straight line, the linkage is at an uncertainty singularity or a dead center position, where the linkage may lose control. If the P-joint is a passive joint, the linkage is at an uncertainty singularity when the other two passive joints are on a line normal to the sliding path.

Full rotatability: An N-bar (1P) chain is said fully rotatable if for any set of values assigned to the (*N*-3) independent inputs, there is no danger of encountering an uncertainty singularity.

If the P-joint is not an input joint, the linkage has full rotatability if and only if

(1) it has a Class I chain, i.e. $(h + \lambda_1 + \lambda_2 + \text{---} + \lambda_{N-3}) < \lambda_{N-2}$, *and*

(2) there is one and only one passive joint between the (finite) long link and any of the link connected by the prismatic joint. In other words, there is one and only one passive joint between any two (finite or infinite) long links.

Obviously, if the P-joint is used as an input joint, the linkage has no full rotatability.

Branch: A Class I chain always has one finite long link and (*N-3*) short links and the long link can never become normal to the sliding path. Therefore, *a Class I chain has two branches.* On the other hand, any link of a Class II chain may become normal to the sliding path and hence, *a Class II chain has only one branch.* Branch problem exists only in Class I chains and the branch identification criterion can be stated as below.

In a Class I N-bar (1P) chain, where $N \geq 3$, let **u** and **v** be unit vectors along the long link and the normal to the sliding path and φ the angle measured from **v** to **u**, where φ is defined in the range of [0˚, 360˚). Then linkage configurations with $\varphi \in (0^\circ, 180^\circ)$ are in one branch and those

with φ ∈ (180˚, 360˚) are in the other branch. One may note that a configuration with φ = 0˚ or 180˚ may occur only in non-Class I chains.

Sub-Branch: A sub-branch refers to a configuration space, in which each configuration may be transformed to another configuration continuously without encountering an uncertainty singularity or dead center position, where the linkage may lose control. In an N-bar chain connected exclusively by R-joints, an uncertainty singularity occurs when the three passive joints become collinear [2-5]. By treating the P-joint as an R-joint connecting two infinite links at infinity, a sub-branch can be identified with the following criterion.

Let **r** and **s** be unit vectors from a passive R-joint to the other two passive joints and ψ the angle measured from **r** to **s**, where ψ ∈ (0˚, 360˚). For linkage configurations in one branch, configurations with ψ ∈ (0˚, 180˚) are in one sub-branch and those with ψ ∈ (180˚, 360˚) are in the other sub-branch. If the P-joint is a passive joint, one of the unit vectors **r** or **s** is in the direction normal to the sliding path. One may note that the above sub-branch identification criterion is to keep ψ from reaching 0° or 180°.

2.3 Examples

The above criteria are illustrated in the following examples.

N=3: 2R1P chains

Although with N= 3 the linkage has no mobility, it does offer interesting insight on how the mobility laws are rooted in the property of right triangles. One may have the following observations from the right triangles in Fig. 2.2.

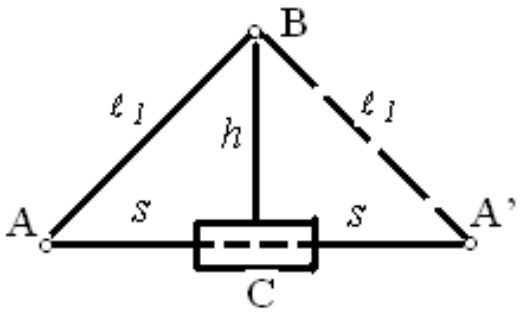

Figure 2.2 Two branches of a right triangular linkage

a. Since $h < \lambda_1$, a three-bar chain is always Class I; λ_1 is a long link.

b. φ is the angle between the long link λ_1 and the line normal to the sliding path. $\cos \varphi = (h / \lambda_1)$ yields two roots, i.e. $\varphi = \cos^{-1}(h / \lambda_1)$ and $2\pi - \cos^{-1}(h / \lambda_1)$, corresponding to two possible right triangle configurations in the ranges (0˚, 180˚) and (180˚, 360˚), respectively. These two configurations can never be brought to overlap in a planar motion and they represent two branches of the three-bar chain. Hence, the linkage has two branches.

c. If additional short links are connected to it to form an N-bar (1P) chain, such that the total length of all short links, i.e. $(\lambda_1 + \lambda_2 + \text{---} + \lambda_{N-3})$ is not longer than the long link λ_{N-2}, the resulting chain will remain a Class I chain and the two-branch feature as well as the branch identification criterion is preserved.

d. In a three-bar chain, no input can be given and all three joints are passive. As shown in Fig. 2.2, singularity occurs when AB becomes normal to the sliding path where the right triangle diminishes. Such singularity feature is also preserved in N-bar (1P) chains. If the P-joint is a passive joint, an uncertainty singularity occurs when the two passive R-joints are on a line normal to the sliding path.

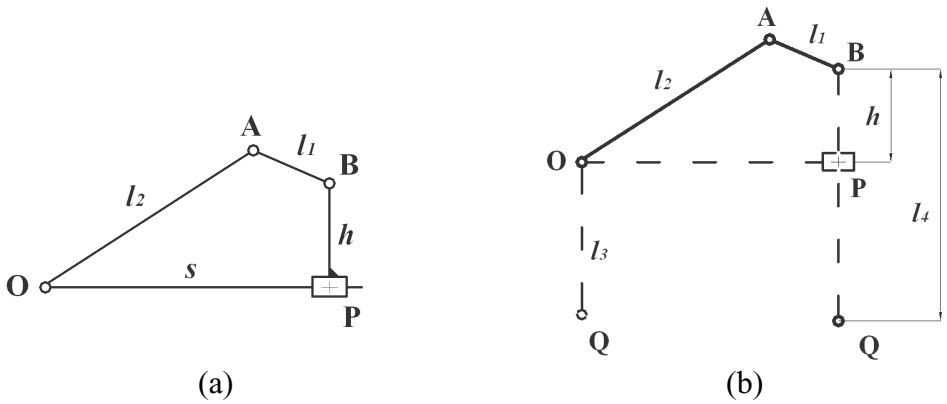

Figure 2.3 A 3R1P-type chain

N=4: 3R1P chains

This is the case with slider-crank mechanisms or inverted slider crank mechanisms (Fig. 2.3). With $\lambda_1 < \lambda_2$, the mechanism has a Class I chain if $(h + \lambda_1) < \lambda_2$ or a Class II chain if $(h + \lambda_1) > \lambda_2$. A Class I chain always has only one short link which may revolve against any link. A Class II chain does not have any short link and no link may have a full revolution with respect to any link. One may note that if $h = 0$, the linkage is always a Class I chain, as the condition $(h + \lambda_1) < \lambda_2$ is always met. One may have the following observations from the following two cases.

Case 1: $(h, \lambda_1, \lambda_2) = (9, 4, 12)$

a. Since $(h+\lambda_1) > \lambda_2$, it is a Class II chain, which has only one branch.
b. All links are long links. Joints A, B and O, without connecting any short link, do not allow full revolution. The linkage has no full rotatability.
c. If the input is given to the P-joint, then an uncertainty singularity configuration may occur, where all passive joints A, B, and O lie on a common straight line. Linkage configurations with $\theta_A \in (0^\circ, 180^\circ)$ are in one sub-branch and those with $\theta_A \in (180^\circ, 360^\circ)$ are in the other sub-branch.

d. If the input is given to any R-joint (say O), then an uncertainty singularity configuration may occur, where the other two R- joints (say A and B) are on a line normal to the sliding path. For linkage configurations with $\theta_B \in (0^\circ, 180^\circ)$ are in one sub-branch and those with $\theta_B \in (180^\circ, 360^\circ)$ are in the other sub-branch.

Case 2: $(h, \lambda_1, \lambda_2) = (5, 4, 12)$

a. Since $(h+\lambda_1) < \lambda_2$, it is a Class I chain. The short link is AB; the long link is OA. It has two branches.

b. The angle between the long link OA and the normal to the sliding path is used to identify the branch. If the angle is in the range $(0^\circ, 180^\circ)$, the corresponding linkage configuration is in one branch; if the angle is in the range $(180^\circ, 360^\circ)$, the corresponding linkage configuration is in the other branch.

c. The joints on short link AB, i.e. joints A and B may allow complete revolution. If the input is given through R-joint A or B, the linkage will have full rotatability.

d. If the input is given to the P-joint, then an uncertainty singularity configuration may occur, where all passive joints A, B, and O lie on a common straight line. For linkage configurations in one branch, configurations with $\theta_A \in (0^\circ, 180^\circ)$ are in one sub-branch and those with $\theta_A \in (180^\circ, 360^\circ)$ are in the other sub-branch.

e. If the input is given to the R-joint O, then an uncertainty singularity configuration may occur, where the other two R-joints A and B are on a line normal to the sliding path. For linkage configurations in one branch, configurations with $\theta_B \in (0^\circ, 180^\circ)$ are in one sub-branch and those with $\theta_B \in (180^\circ, 360^\circ)$ are in the other sub-branch.

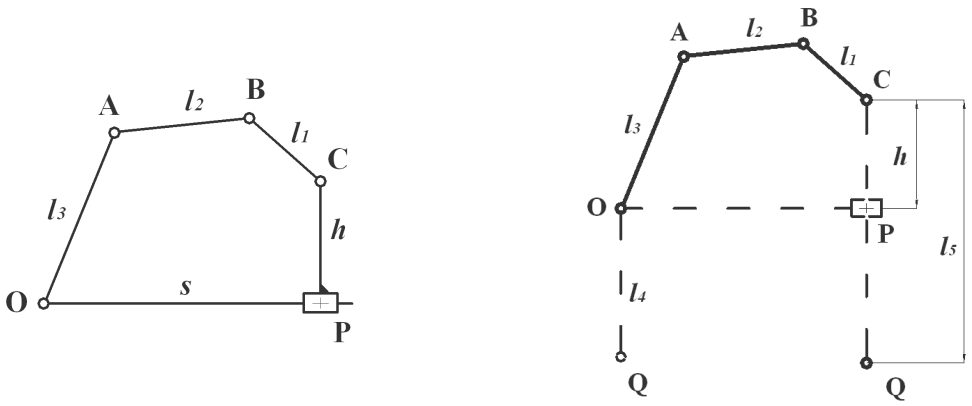

(a) (b)

Figure 2.4 A 4R1P-type chain

N=5: 4R1P chains

Fig. 2.4 shows a five-bar chain 4R1P in which $\lambda_1 < \lambda_2 < \lambda_3$, the mechanism has a Class I chain if $(h + \lambda_1 + \lambda_2) < \lambda_3$ or a Class II chain if $(h + \lambda_1 + \lambda_2) > \lambda_3$. One may have the following observations from the following two cases.

Case 1: $(h, \lambda_1, \lambda_2, \lambda_3) = (10, 4, 8, 20)$.

a. Since $(h+\lambda_1+\lambda_2) > \lambda_3$, it is a Class II chain, which has only one branch.

b. Since $(h + \lambda_2) < (\lambda_1 + \lambda_3)$ and $(h + \lambda_3) > (\lambda_1 + \lambda_2)$, links AB and BC are short links and link OA is a long link. The joints on links AB and BC, i.e. joints A, B, and C may allow complete revolution. Joint O, which does not connect a short link, does not allow full revolution.

c. If the two inputs are given through R-joints A and B (or C), although both input joints may allow complete revolution between the connected links, the linkage still has no full rotatability.

d. If the two inputs are given to the P-joint and one R-joint (say O), then an uncertainty singularity configuration may occur, where all passive joints A, B, and C lie on a

common straight line. For linkage configurations with $\theta_B \in (0^\circ, 180^\circ)$ are in one sub-branch and those with $\theta_B \in (180^\circ, 360^\circ)$ are in the other sub-branch.

e. If the two inputs are given to two R-joints (say O and A), then an uncertainty singularity configuration may occur, where the other two R-joints (say B and C) are on a line normal to the sliding path. For linkage configurations with $\theta_C \in (0^\circ, 180^\circ)$ are in one sub-branch and those with $\theta_C \in (180^\circ, 360^\circ)$ are in the other sub-branch.

Case 2: $(h, \lambda_1, \lambda_2, \lambda_3) = (6, 4, 8, 20)$.

a. Since $(h+\lambda_1+\lambda_2) < \lambda_3$, it is a Class I chain and the only long link is OA. It has two branches.

b. The angle between the long link OA and the normal to the sliding path is used to identify branch. If the angle is between $(0^\circ, 180^\circ)$, the corresponding linkage configuration is in one branch; if the angle is between $(180^\circ, 360^\circ)$, the corresponding linkage configuration is in the other branch.

c. The joints on links AB and BC, i.e. joints A, B, and C may allow complete revolution. If the two inputs are given through R-joints A, B, or C, then the linkage will have full rotatability.

d. If the two inputs are given to the P-joint and R-joint O, then an uncertainty singularity configuration may occur, where all passive joints A, B, and C lie on a common straight line. For linkage configurations in one branch, configurations with $\theta_B \in (0^\circ, 180^\circ)$ are in one sub-branch and those with $\theta_B \in (180^\circ, 360^\circ)$ are in the other sub-branch.

e. If only one input is given to R-joint O or P-joint, the other input is given to R-joint A or B or C (say two inputs are given to O and A), then an uncertainty singularity configuration may occur, where the other two R-joints B and C are on a line normal to

the sliding path. For linkage configurations in one branch, configurations with $\theta_C \in (0^\circ, 180^\circ)$ are in one sub-branch and those with $\theta_C \in (180^\circ, 360^\circ)$ are in the other sub-branch.

2.4 Single-Loop N-Bar Chains with Two Prismatic Joints

A single-loop N-bar chain with two prismatic joints may have two different cases: (1) two prismatic joints are neighboring; (2) two prismatic joints are non-neighboring. The first case may be regarded as a chain with three infinite links, while the second one may be regarded as a chain with four infinite links. Let λ_i ($i = 1, 2, 3, ---, N-4$) be the finite link lengths between revolute joints and $\lambda_1 \leq \lambda_2 \leq \lambda_3 \leq \lambda_4 \leq --- \lambda_{N-4}$, where $N \geq 4$. The distances between each prismatic joint and its adjacently connecting revolute joint are h_1 and h_2, and the corresponding slide distances are s_1 and s_2, respectively (Fig. 2.5).

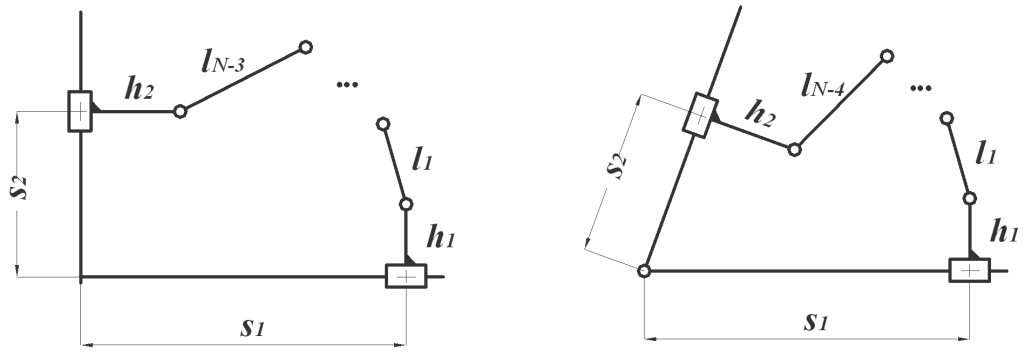

(a) neighboring 2P (b) non-neighboring 2P

Figure 2.5 N-bar (2P) chains

An N-bar (2P) chain may be regarded as a chain containing three or four links with very long (fictitious) link lengths connected by two revolute joints. The length differences among these fictitious long links are h_1 and h_2, respectively. There is no assemblability condition when two prismatic joints are involved, since a chain can always be formed. An N-bar (2P) chain has (N-3) DOF and requires (N-3) inputs. Giving (N-3) inputs, two linkage postures symmetric about a reference link can always be found. There is no way to move from one position to its symmetric position about the reference link without breaking the connection. This property leads to the existence of two branches in an N-bar (2P) chain, i.e., all N-bar (2P) chains are Class I. A finite link is always a short link, which may have a full revolution with respect to any link in the loop. A revolute joint connecting a short link may allow a complete revolution. A revolute joint connecting two prismatic joint may also allow a complete revolution if the following condition is met: $(h_1 + h_2) < (\lambda_1 + \lambda_2 + \text{---} + \lambda_{N-4})$. A linkage has full rotatability if and only if there is one and only one passive joint between any two infinite links. The use of the above criteria is demonstrated in the following four-bar 2R2P-type and five-bar 3R2P-type chains.

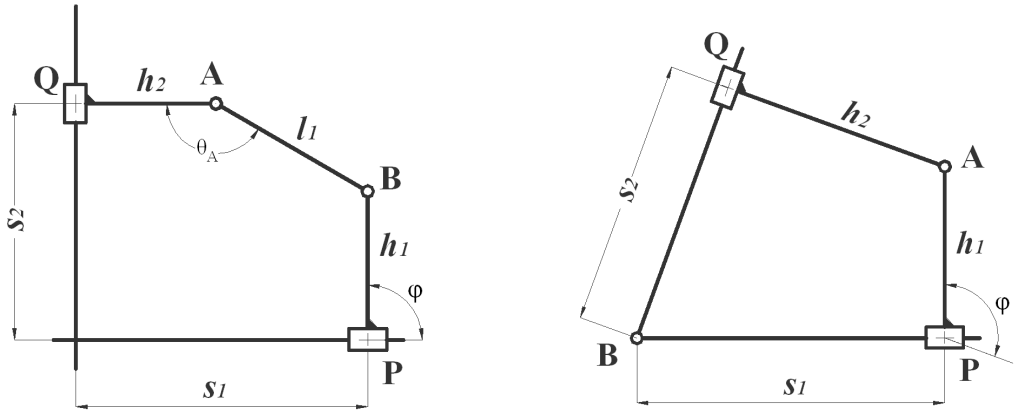

(a) neighboring 2P (b) non-neighboring 2P

Figure 2.6 2R2P chains

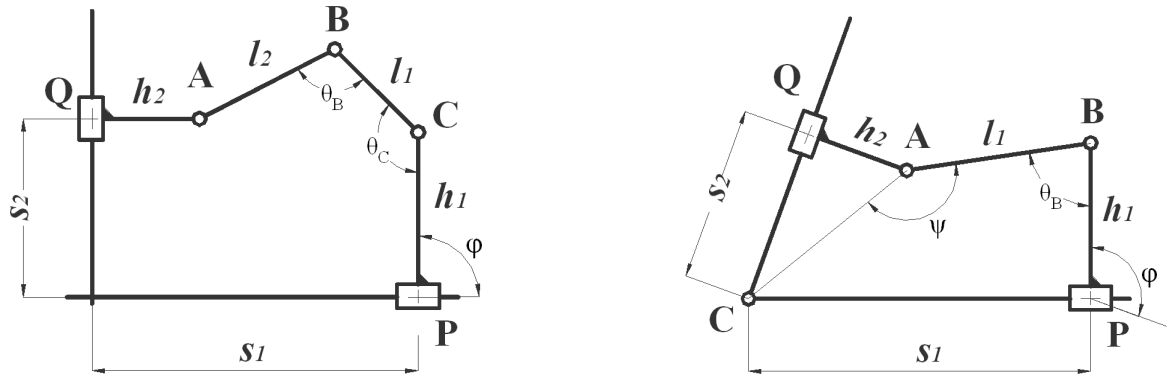

(a) neighboring 2P (b) non-neighboring 2P

Figure 2.7 3R2P chains

N=4: 2R2P chains

Fig. 2.6 shows four-bar 2R2P chains. One may have the following observations from the following two cases.

Case 1 (neighboring prismatic joints):

a. It is a Class I chain, which has two branches.

b. let **u** and **v** be unit vectors along the normal to the sliding path of both prismatic joints P and Q, and φ the angle measured from **v** to **u**, where φ is defined in the range [0˚, 360˚). Then linkage configurations with φ Є (0˚, 180˚) are in one branch and those with φ Є (180˚, 360˚) are in the other branch.

c. The only finite link AB is a short link. The joints A and B on it may allow complete revolution.

d. If the input is given through joints A or B, the linkage will have full rotatability.

e. If the input is given through one prismatic joint (say P), then the linkage has no full rotatability. An uncertainty singularity configuration may occur, where the two revolute joints A and B are on a line normal to the sliding path of the other prismatic joint (say Q).

For linkage configurations in one branch, configurations with $\theta_A \in (0^\circ, 180^\circ)$ are in one sub-branch and those with $\theta_A \in (180^\circ, 360^\circ)$ are in the other sub-branch.

Case 2 (non-neighboring prismatic joints):

a. It is a Class I chain, which has two branches.
b. let **u** and **v** be unit vectors along the normal to the sliding path of both prismatic joints P and Q, and φ the angle measured from **v** to **u**, where φ is defined in the range [0˚, 360˚). Then linkage configurations with $\varphi \in (0^\circ, 180^\circ)$ are in one branch and those with $\varphi \in (180^\circ, 360^\circ)$ are in the other branch.
c. There is no finite link. The revolute joints A and B may not allow complete revolution.
d. The linkage has no full rotatability.
e. An uncertainty singularity configuration may not occur.

N=5: 3R2P chains

Fig. 2.7 shows five-bar 3R2P chains. One may have the following observations from the following two cases.

Case 1 (neighboring prismatic joints):

a. It is a Class I chain, which has two branches.
b. let **u** and **v** be unit vectors along the normal to the sliding path of both prismatic joints P and Q, and φ the angle measured from **v** to **u**, where φ is defined in the range [0˚, 360˚). Then linkage configurations with $\varphi \in (0^\circ, 180^\circ)$ are in one branch and those with $\varphi \in (180^\circ, 360^\circ)$ are in the other branch.
c. Both finite links AB and BC are short links. The joints A, B, and C on them may allow complete revolution.

d. If the two inputs are given through joints A, B, or C, the linkage will have full rotatability.

e. If the two inputs are given to prismatic joints P and Q, then an uncertainty singularity configuration may occur, where all passive joints A, B, and C lie on a common straight line. For linkage configurations in one branch, configurations with $\theta_B \in (0^\circ, 180^\circ)$ are in one sub-branch and those with $\theta_B \in (180^\circ, 360^\circ)$ are in the other sub-branch.

f. If only one input is given to prismatic joint P or Q, the other input is given to revolute joint A or B or C (say two inputs are given to Q and A), then an uncertainty singularity configuration may occur, where the other two revolute joints B and C are on a line normal to the sliding path of the other prismatic joint P. For linkage configurations in one branch, configurations with $\theta_C \in (0^\circ, 180^\circ)$ are in one sub-branch and those with $\theta_C \in (180^\circ, 360^\circ)$ are in the other sub-branch.

Case 2 (non-neighboring prismatic joints):

a. It is a Class I chain, which has two branches.

b. let **u** and **v** be unit vectors along the normal to the sliding path of both prismatic joints P and Q, and φ the angle measured from **v** to **u**, where φ is defined in the range $[0^\circ, 360^\circ)$. Then linkage configurations with $\varphi \in (0^\circ, 180^\circ)$ are in one branch and those with $\varphi \in (180^\circ, 360^\circ)$ are in the other branch.

c. The only finite link AB is a short link. The joints A and B on it may allow complete revolution. The revolute joint C connects two prismatic joints and may also allow complete revolution if $(h_1 + h_2) < \lambda_1$.

d. If the two inputs are given through joints which allow complete revolution, the linkage will have full rotatability.

e. If the two inputs are given to prismatic joints P and Q, then an uncertainty singularity configuration may occur, where all passive joints A, B, and C lie on a common straight line. Let **r** and **s** be unit vectors from A to B and C, respectively; ψ the angle measured from **r** to **s**, where $\psi \in (0^\circ, 360^\circ)$, will be used to identify the sub-branches. For linkage configurations in one branch, configurations with $\psi \in (0^\circ, 180^\circ)$ are in one sub-branch and those with $\psi \in (180^\circ, 360^\circ)$ are in the other sub-branch.

f. If only one input is given to prismatic joint P or Q, the other input is given to revolute joint A or B or C (say two inputs are given to Q and C), then an uncertainty singularity configuration may occur, where the other two revolute joints A and B are on a line normal to the sliding path of the other prismatic joint P. For linkage configurations in one branch, configurations with $\theta_B \in (0^\circ, 180^\circ)$ are in one sub-branch and those with $\theta_B \in (180^\circ, 360^\circ)$ are in the other sub-branch.

2.5 Conclusions

The paper presents the extension of the N-bar mobility laws to linkages containing prismatic joints. The extension is based on the principle that the links connected by a prismatic joint are two very long links connected by a revolute joint. The paper shows how the concept and mobility property of short and long links, the linkage classification, the full rotatability, as well as branch and sub-branch identification in N-bar chains are preserved in N-bar chains containing prismatic joints.

REFERENCES

1. Duffy, J., Grashof, F., 1983, *Theoretische Maschinenlehre*, Leipzig.
2. Ting, K.L., 1986, "Five-bar Grashof criteria," *Journal of Mechanisms, Transmissions, and automation in Design*, Vol. 108, no. 4, pp. 533-537.
3. Ting, K.L., 1989 "Mobility criteria of single loop N-bar linkages," *Journal of Mechanisms, Transmissions and Automation in Design*, Vol.111, No. 4, pp. 504-507.
4. Ting, K.L. and Liu, Y.W., 1991, "Rotatability Laws for N-bar kinematic chains and their proof," *Journal of Mechanical Design*, Vol.113, No.1, pp.32-39.
5. Ting, K.L., 2008, "On the Input Joint Rotation Space and Mobility of Linkages," *Journal of Mechanical Design*, Vol.130, 092303.
6. Guo, W.Z., Zou, H.J., Han, B., and Zhang, Q., 2004, "Mobility of 4R1P-type five-bars using characteristics charts," *Proceedings of ASME DETC'04*, September 2004, Salt Lake City, Utah.
7. Guo, W.Z., Du, R., and Wang, J.X., 2005, "On the Mobility of Single Loop N-Bar Linkage with one Prismatic Joint," *Proceedings of ASME DETC'05*, September 2005, Long Beach, CA.
8. Guo, W.Z. and Du, R., 2006, "Mobility of single-loop N-bar linkage with active/passive prismatic joints," *Journal of Mechanical Design*, Vol. 128, no. 6, p 1261-1271.
9. Chase, T.R. and Mirth, J.A., 1993, "Circuit and branches of single Degree-of-Freedom planar linkages," *Journal of Mechanical Design*, Vol.115, No. 2, pp. 223-230.
10. Davis, H.P., Chase, T.R., and Mirth, J.A., 1994, "Circuit analysis of Stephenson chain six-bar mechanisms," *ASME Mechanism Synthesis and Analysis*, DE-vol.70, pp.349–358.
11. Davis, H.P. and Chase, T.R., 1994, "Stephenson chain branch analysis: four generic stationary configurations and one new linkage polynomial," *ASME Mechanism Design and Synthesis*, DE-Vol.70, pp.359–367.
12. Shyu, J.H. and Ting, K.L., 1994, "Invariant link rotatability of N-bar kinematic chains," *Journal of Mechanical Design*, Vol. 116, No.1, pp. 343-347.
13. Midha, A., Zhao, Z., and Her, I. 1985, "Mobility conditions for planar linkages using triangle inequality and graphical interpretation," *Journal of Mechanisms, Transmissions, and Automation in Design*, Vol.107, No. 3, pp. 394-400.

CHAPTER 3

STRETCH ROTATION AND COMPLETE MOBILITY IDENTIFICATION OF WATT SIX-BAR CHAINS[2]

ABSTRACT

Mobility of linkages refers to the problems concerning branch, full rotatability, singularities, and order of motion. This paper uses the stretch and rotation of a four-bar loop to convert a Watt six-bar linkage to an equivalent simple Stephenson linkage. It shows the mobility of a Watt six-bar linkage is affected by a hidden five-bar chain. The equivalency offers a simple and clear visual explanation on the formation of branches and sub-branches and how Watt and Stephenson linkages differ in mobility. The resulting mobility algorithm requires no stretch rotation. The dead center positions in the second four-bar loop are the branch points. It reveals that although a Watt six-bar linkage may have only up to four-branches, a branch may have up to six sub-branches. The results offer a simple algorithm suitable for automated identification of branch, sub-branch, and full rotatability. The algorithm is valid for Watt linkages with or without prismatic joints and is independent of linkage inversions. Examples are presented for illustration.

[2] Accepted on March 30, 2009 and to be published on Mechanism and Machine Theory.

3.1 Introduction

Linkage mobility refers to the problems concerning branch (or circuit) defect, full rotatability, singularities, and order of motion [1]. When a linkage is synthesized, it is necessary to make sure that the linkage has the necessary mobility for a continuous and smooth operation. The Grashof criterion [2] has been used to predict the full rotation of four-bar mechanisms for over a century. The recent N-bar rotatability laws by Ting [3, 4] offer the first simple, complete, and systematical explanation to predict the formation of branch, sub-branch, and full rotatability of any N-bar chain ($N \geq 3$). Although the methodology for the mobility analysis of single loop linkages has been well established, the mobility study of multiloop chains is far from adequate [1, 5-12] even for Watt six-bar linkages.

A Watt six-bar chain contains two four-bar loops. The mobility of both loops affects each other. Primrose, Freudenstein, and Roth developed the branch analysis criteria of a Watt six-bar linkage by visually examining the motion limits imposed on the ternary link [13]. Mirth and Chase [14, 15] examined the motion limits imposed on the ternary link and summarized the circuit (i.e. branch) composition in a chart. They concluded that the limits of motion imposed on one four-bar loop by the other might change the branches in a Watt six-bar linkage. A complete mobility analysis that takes sub-branch and full rotatability formation under any input condition into consideration and an algorithm suitable for automated mobility identification are yet to be resolved.

The mobility of a multiloop chain is affected by not only the mobility of each individual loop, which is governed by Ting's mobility laws [3, 4], but also the interaction between loops. This paper offers a simple geometric model to explain and predict the formation of branches,

sub-branches, and full rotatability of any Watt linkage regardless the choices of the fixed, input, and output links or the existence of prismatic pairs.

3.2 Basic Concepts and Terminologies

Some developed concepts and terminologies are briefed below. They are simple yet vital to understand the proposed method.

3.2.1 N-bar Rotatability Laws

In the N-bar rotatability laws proposed by Ting, links in a single loop chain are classified as short links and long links [3, 4, 16]. A short link may revolve against any other link while a long link can never revolve against any long link. A joint on a short link is revolvable while a joint between long links is non-revolvable. Ting also classified single loop chains into three classes and discussed the rotatability between long links. A Class I chain has two branches while a Class II chain has only one branch. Therefore branch problem does not exist in Class II chains. Class III is a transitional type between Class I and II chains.

3.2.2 Joint Rotation Space

The joint rotation space (JRS) of a linkage represents the maximum possible input domain or the entire configuration space of the linkage [16]. For a five-bar chain, the JRS can be regarded

as the domain of the two input joints and each point in the JRS generally corresponds to two linkage configurations. Some terminologies and concepts are explained below.

Branch: Also called circuit [14, 15]. A branch refers to a linkage assembly or configuration space, in which a configuration can be physically transformed to another configuration continuously.

Dead center position: In a single degree-of-freedom (DOF) linkage, a dead center position occurs when the input link reaches its rotation limit. For a single loop linkage, a dead center position occurs when the three non-input joints become collinear [16].

Sub-branch: A sub-branch refers to a configuration space, in which a configuration can be transformed to any other configuration continuously without reaching a dead center position. A sub-branch represents a singularity-free configuration space. Each element in a sub-branch corresponds to one and only one linkage configuration.

JRS Sheet: The JRS of a linkage branch is called a JRS sheet. It represents the configuration space of a linkage branch in the input domain. Thus, the JRS of a Class I linkage contains two sheets and that of a Class II linkage contains only one sheet. There is no motion continuity between sheets, i.e. a linkage cannot be transformed between configurations in different JRS sheets.

Edge of a JRS sheet: The edge of a JRS sheet is the boundary curve of the JRS. Each point on the boundary curve of the JRS corresponds to a unique uncertainty singularity configuration of a linkage, in which the three non-input joints are collinear.

Side of a JRS sheet: The edge of a JRS sheet separates the sheet into sides (Fig. 3.1). Each side of a JRS sheet represents the configuration space of a linkage sub-branch in the input domain. A point on one side of a JRS sheet corresponds to one and only one linkage

configuration. Since a linkage can be programmed within one side of a JRS sheet without reaching the boundary, each side of a JRS sheet represents a sub-branch or a singularity-free configuration space.

Types of JRS sheet: According to the classification of five-bar JRS [16], JRS sheets can be grouped into three types (Fig. 3.2).

1. Two (one-side) sheets: This is found only in fully rotatable [3, 4] Class I chains and the JRS contains no edge (Fig. 3.2(a)). Each sheet has only one side.
2. Two (two-side) sheets: This is found only in Class I chains (Fig. 3.2(b)). Each sheet has two sides.
3. One (two-side) sheet: Any Class II chain has such a JRS sheet. A sample is shown in Fig. 3.2(c). Each sheet has two sides.

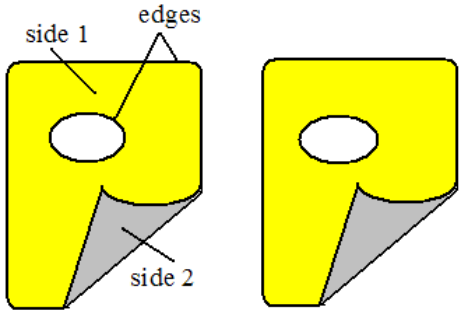

Figure 3.1 Two two-side sheets

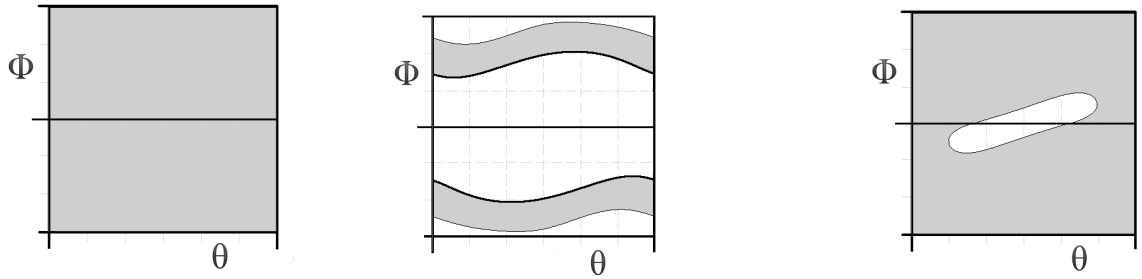

(a) two overlapping (one-side) sheets (b) two (two-side) sheets (c) one (two-side) sheet

Figure 3.2 Types of JRS sheet

3.3 Mobility Analysis of Watt Six-Bar Chains

One may note that in this paper, any Watt six-bar linkage is treated as a chain and the choice of the fixed or input link does not affect the applicability of the method. The branch identification is irrelevant to the choice of the input or fixed link and the proposed sub-branch identification method is applicable regardless the choice of the input joint. The method is suitable for fully automated mobility analysis. It is applicable to the situation when a prismatic joint is involved. In the following discussion, the branch and sub-branch formation will be explained via the stretch and rotation of a four-bar loop that converts a Watt linkage into a Stephenson linkage. The results lead to the algorithm for automated mobility identification, in which no stretch rotation is necessary.

3.3.1 Stretch and Rotation of Watt Six-Bar Chains

The concept of the stretch and rotation [17] has been used commonly in geometry and linkage design. Any linkage can be stretched, i.e. re-oriented or re-positioned, without altering the joint rotatability or angular relationships among links. Any linkage can be rotated, i.e. re-oriented or re-positioned, without affecting the geometric relationships, including joint rotatability, among links.

A Watt six-bar linkage contains two four-bar loops. When a four-bar loop is connected serially to another four-bar loop to form a Watt six-bar linkage, one may realize that the rotatability of the second four-bar loop will be affected by the output range of the first four-bar loop. However, the rotation of the second four-bar loop is not affected by its stretch and rotation. This subtle yet important principle, which has been used in Watt linkage design, can be applied

to convert a Watt six-bar linkage into an equivalent Stephenson linkage and thus form a unified mobility identification theory for all six-bar linkages.

Fig. 3.3(a) shows a Watt six-bar chain and Fig. 3.3(c) the six-bar chain after the stretch and rotation of the four-bar loop DEFGD. In Fig. 3.3(b), the four-bar loop DEFGD is stretched proportionally in the scale of (a_3/b_1) to $DE_1F_1G_1D$ so that the length of link DE_1 is equal to DC. Obviously, the rotatability of each joint, including the output angles DG_1F_1 and DGF, of the linkages before and after the stretch remains the same. In Fig. 3.3(c), the four-bar loop $DE_1F_1G_1D$ is further rotated as a solid structure through angle CDE, i.e. the angle between DC and DE of the ternary link, to $DE_2F_2G_2D$ so that DE_2 becomes coincident with DC. Since the entire four-bar is rotated as a solid structure, the rotatability of each joint remains unchanged after the rotation. The output angle DG_1F_1 of the resulting linkage is equal to the output angle DGF of the original linkage. If AG is the reference axis, one may find $\theta_{a7} = \theta_7 + \gamma$ (Fig. 3.3(a) and (c)), i.e. the measured output angles of the linkages before and after the stretch-rotation always differ by a constant γ. The characteristics of the input angle vs. the output or any other angle between neighboring links remain unchanged. In other words, the joint rotatability of the linkages before and after the stretch and rotation remains the same.

The six-bar chain after the stretch-rotation is a degenerated Stephenson six-bar chain with the coupler point at C. The degenerated Stephenson six-bar chain has a five-bar loop $ABCF_2G_2A$ and a four-bar loop ABCDA with two common joint variable at A and B as any Stephenson six-bar chain. Therefore the mobility rectification of Watt and Stephenson six-bar linkages can be treated in a unified manner as discussed below.

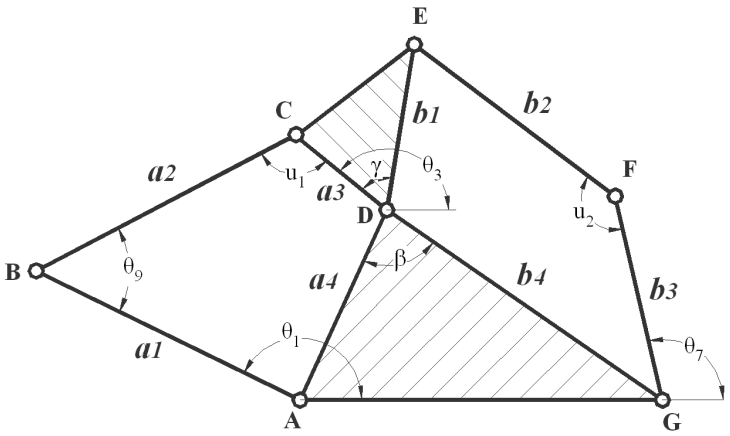

(a) before stretch-rotation

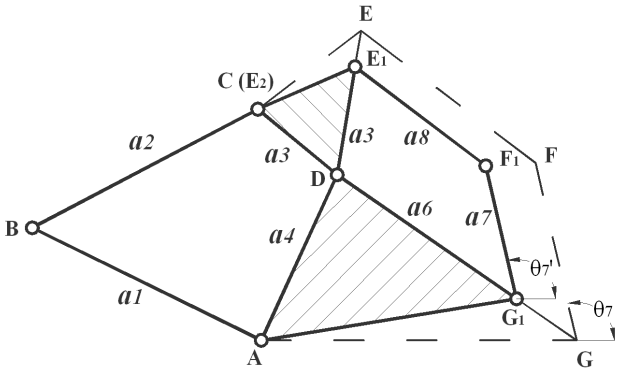

(b) stretch of the second four-bar loop

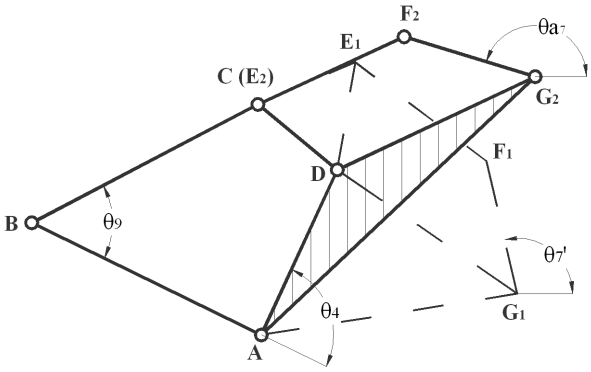

(c) rotation of the second four-bar loop

Figure 3.3 A Watt six-bar chain

3.3.2 Branch

In a Watt six-bar linkage, the input is always given to a joint of a four-bar loop and the choice of the output joint or fixed link will not affect the branch, sub-branch, or input full rotatability of the linkage. According to the choice of input, Watt six-bar linkages can be grouped into two types: (1) Input is given to joint A or B. The Watt six-bar chain after stretch-rotation has a four-bar loop ABCDA and the five-bar loop $ABCF_2G_2A$ as shown in Fig. 3.3(c). The JRS formed by the five-bar loop $ABCF_2G_2A$ may block some rotation range of the four-bar

loop ABCDA. (2) Input is given to joint C or D. It is the four-bar loop DCF_2G_2D that may block some rotation range of the four-bar loop ABCDA. The second type, its background JRS is not offered by a five-bar but a four-bar loop, may be regarded as a simplified case of the first one. The mobility analysis of these two types is same and the general one (the first type) is used to demonstrate the methodology. For convenience of discussion without losing generality, let A and B in Fig. 3.3(c) be regarded as the input and output joints, respectively.

Branch points: In the four-bar loop, the relationship between the displacements of joints A and B is a curve, which will be called as I/O curve (Fig. 3.4). If link CD is removed, the six-bar chain is reduced to a five-bar loop $ABCF_2G_2A$, from which a singular curve can be deduced. The singular curve depicts the relationship between the displacements of joints A and B when the angle between CF_2 and G_2F_2 is kept at 0 or π. The singular curve(s) is the edge of the JRS of the five-bar loop (Fig. 3.4(b) and (c)). The intersection points of the I/O curve and the singular curve are called branch points, which can be identified in the way similar to that for Stephenson six-bar linkages [1].

The maximum possible number of branch points that a Stephenson chain may have is twelve [1], which are derived from the roots of two sixth degree polynomial equations as follows.

$$W_{i1}x^6 + W_{i2}x^5 + W_{i3}x^4 + W_{i4}x^3 + W_{i5}x^2 + W_{i6}x + W_{i7} = 0 \quad (i = 1, 2)$$

In a Watt chain, the coefficients $W_{i1} = W_{i7} = 0$. Since $x \neq 0$, the above equation can be re-written as two fourth degree polynomial functions, which implies that the maximum possible number of branch points that a Watt six-bar chain may have is eight [18].

$$W_{i2}x^4 + W_{i3}x^3 + W_{i4}x^2 + W_{i5}x + W_{i6} = 0 \qquad (i = 1, 2)$$

In a branch-point induced branch, there are two branch points [16]. Because a Stephenson linkage has at most twelve branch points while a Watt linkage has no more than eight, a Stephenson linkage may have up to six branches [1] while a Watt linkage may have no more than four branches [13, 15, 18].

Dead center positions: At a dead center position, the linkage may be out of control momentarily and have zero mechanical advantage [19]. The dead center positions of a Watt six-bar linkage may correspond to the dead center positions of the first or second four-bar loops. In a Watt six-bar linkage, branch points are the dead center positions of the second four-bar loop. In order to avoid confusing, the dead center positions caused by the second four-bar loop shall be called as branch point hereafter and a dead center position will refer to a dead center position caused by the first four-bar loop exclusively. For example, in Fig. 3.4(c), M_i (i = 1,…, 6) are branch points and $A_{1,2}$, $B_{1,2}$ are dead center positions.

Branch formation: Branch is a property of the kinematic chain of a linkage. The branch formation of a linkage is irrelevant to the choices of the input, fixed, or output link. A branch may have zero or two branch points. If no branch point exists, the number of branches is two (Fig. 3.4(b)) or four (Fig. 3.4(a)). If branch points exist, there are at most eight branch points, which will lead to four branches at most. With stretch-rotation a Watt linkage become equivalent to a Stephenson linkage and the mobility identification algorithm for Stephenson linkages becomes applicable to Watt linkages. However, in the resulting algorithm for Watt linkages, no stretch rotation is necessary. The effects of branch points are discussed and explained with examples below.

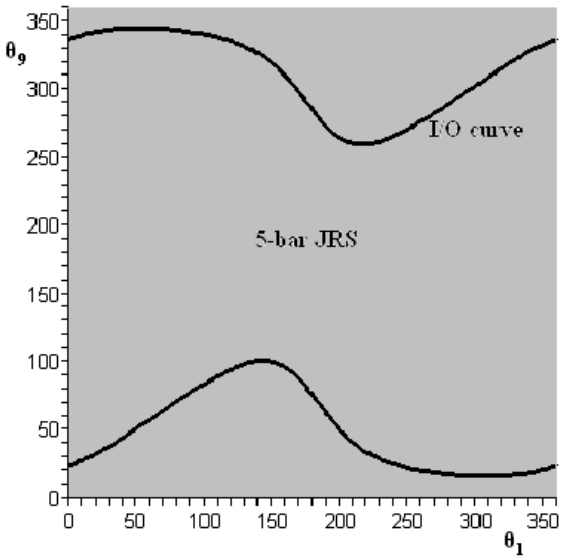

(a) Four branches without branch point

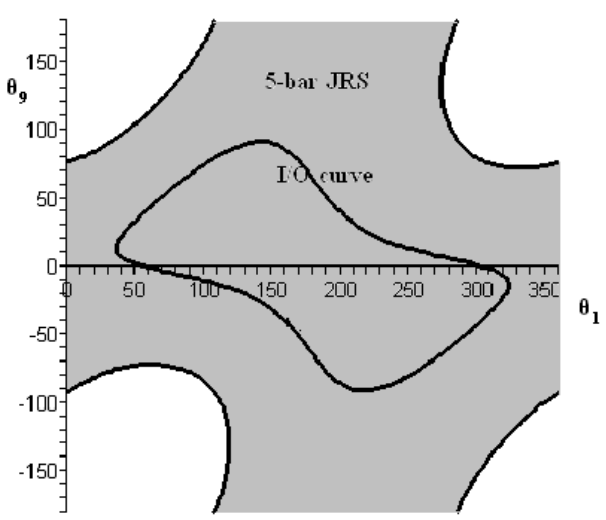

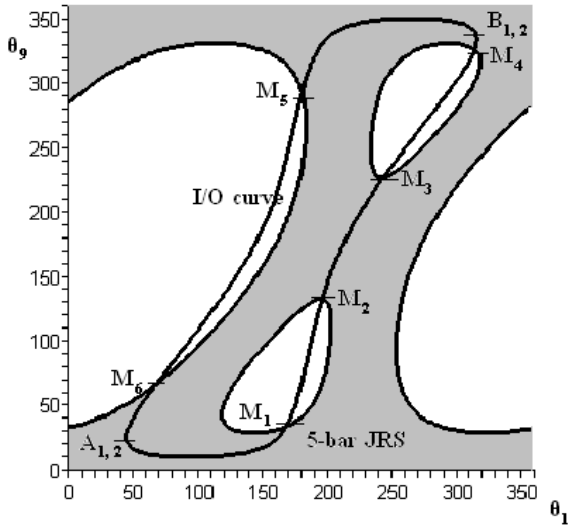

(b) Two branches without branch point (c) Three branches due to branch points

Figure 3.4 I/O curve and JRS

(1) No existence of branch point: the coupling between the four-bar loops in a Watt six-bar linkage (or between the four-bar and five-bar loops in the linkage after the stretch and rotation) does not affect the rotatability of the first four-bar loop. This may occur if no singular curve exists in the five-bar JRS (Fig. 3.4(a)), or if a singular curve does exist, but it does not intersect the I/O curve and therefore has no effect to the mobility of the four-bar loop (Fig. 3.4(b)).

In Fig. 3.4(a), the four-bar loop is a Class I chain and has two branches [3, 4] as depicted by the two I/O curves. The JRS of the five-bar loop has two overlapping sheets (Fig. 3.2(a)) and each sheet has one side [16]. Each I/O curve on each side of a JRS sheet constitutes a branch, leading to a total of four six-bar branches.

In Fig. 3.4(b), the five-bar loop is a Class II chain, which has only one branch. The JRS is a two-side sheet (Fig. 3.2(c)). The four-bar loop is a Class II chain, which has only one branch. The four-bar branch in both sides of the JRS sheet will form a total of two six-bar branches.

For a set of given Watt linkage configurations, the branch identification can be carried out in two steps.

a. Determine the branch of the first four-bar loop. A Class II chain has only one branch and has no branch problem. For a Class I four-bar loop, the branch can be identified with the branch (or sheet) identification criterion [3, 4, 16].

b. Determine the sub-branch of the second four-bar loop [3, 4, 16]. The common joint between the two four-bar loops may be considered as the input joint. Therefore, the sub-branch of the second four-bar loop can be identified by examining if the angle from FE to FG (Fig. 3.3(a)) is in the range of $(0, \pi)$ or $(\pi, 2\pi)$. One may also note that the two one-side JRS sheets may be regarded as an edgeless two-side JRS sheet.

A set of six-bar configurations are in the same branch if the configurations of the first four-bar loop are in the same branch and the configurations of the second four-bar loop are also in the same sub-branch. The number of branches may be two or four.

(2) Existence of branch points: at a branch point, the mobility of the first four-bar loop is partially blocked by the second four-bar loop (or the five-bar loop after the stretch rotation) (Fig. 3.4(c)). The coupling between the four-bar loops may affect the rotatability of each individual

four-bar loop. In the JRS, the segment of the I/O curve between neighboring branch points represents a branch of the linkage. For example, in Fig. 3.4(c), the three branches are represented by segments M_2M_3, M_4M_5, and M_6M_1. To determine if a set of six-bar configurations are in the same branch, the following procedure can be used.

a. Identify the branch of these configurations in the first four-bar loop. All configurations must be in the same four-bar branch.

b. Find the branch points in the four-bar branch identified in the previous step.

c. If no branch point exists in the identified four-bar branch, proceed the branch identification as described in step (b) as the case with no branch point. All configurations are in the same branch, if they are in the same first four-bar branch and also in the same sub-branch of the second four-bar loop.

d. If branch points exist in the identified four-bar branch, the desired configurations are in the same branch only if they are in the same four-bar branch and also correspond to points between neighboring branch points on the I/O curve.

Remark: The branch formation is explained via the stretch and rotation that converts a Watt six-bar to a Stephenson six-bar chain. However, the derived branch identification scheme requires no stretch and rotation, because of the inherent properties in Watt six-bar chains: (1) the branch points are the dead center positions of the second four-bar loop, which occur when joints E, F, and G (Fig. 3.3(a)) lie on a common straight line; (2) the sub-branch identification of the five-bar loop resulted from the stretch and rotation is the same as the sub-branch identification of the second-four-bar loop with the common joint between the two four-bar loops as the input.

Table 3.1 The geometric dimensions of Watt six-bar chains

	a_1	a_2	a_3	a_4	β	γ	b_1	b_2	b_3	b_4
Example 1	7	6	6	4	60^o	60^o	3	7	7	5
Example 2	6	6	7	8	60^o	60^o	7	3	7	5

Table 3.2 Linkage configurations of a Watt six-bar chain

Position	θ_1	θ_9	θ_3	U_1	θ_7	U_2
P_1	151^o	81^o	132^o	80^o	51^o	60^o
P_2	140^o	87^o	118^o	71^o	44^o	55^o
P_3	140^o	87^o	118^o	71^o	169^o	305^o
P_4	56^o	272^o	118^o	330^o	44^o	55^o

The above algorithm is demonstrated in the following examples. The dimensions of Watt six-bar chains are listed in Table 3.1. It is assumed that θ1 is the input angle (Fig. 3.3(a)).

Example 1:

The second four-bar is a Class I loop according to N-bar laws and b_1 is the only short link. U_2 is the angle measured from b_2 to b_3. Since b_2 and b_3 are long links, U_2 can reach neither 0^o nor 180^o. Thus dead center positions do not occur in the second four-bar loop. In other words, there is no branch point in this Watt six-bar linkage. Let P_1, P_2, P_3, and P_4 be four unique linkage configurations (Table 3.2). To determine which linkage configuration(s) is in the same branch with P_1, the following steps are taken.

a. The first four-bar is a Class I loop, which has two branches. a_4 is the short link; a_1, a_2, and a_3 are long links. The angle between any two long links, such as U_1, can be used to distinguish the two branches [3, 4]. Since P_1, P_2, and P_3 have $U_1 \in (0^o, 180^o)$ while P_4 has $U_1 \in (180^o, 360^o)$, P_1 and P_4 are in different branches of the first four-bar loop. P_4 is weeded out.

b. The angle measured from FE to FG (i.e. U_2) is used to determine the sub-branch of the second four-bar loop. Since P_1 and P_2 have $U_2 \in (0^o, 180^o)$ while P_3 has $U_2 \in (180^o, 360^o)$, P_1 and P_3 are in different sub-branches of the second four-bar loop. P_3 is weeded out.

Both P_1 and P_2 are in the same branch because their configurations of the first four-bar loop are in the same branch and their configurations of the second four-bar loop in the same sub-branch.

Example 2:

The first four-bar loop is a Class II chain while the second four-bar is a Class I loop and b_2 is the only short link. U_2 is the angle measured from b_2 to b_3 and U_2 may reach both 0^o and 180^o. Therefore, dead center positions may exist in the second four-bar loop. In other words, branch points do exist in this Watt six-bar linkage. Let P_1, P_2, P_3, P_4, P_5, and P_6 be six unique linkage configurations (Table 3.3). To determine which linkage configuration(s) is in the same branch with P_1, the following steps are taken.

a. Locate the dead center positions of the second four-bar loop, which occur when joints E, F, and G lie on a common straight line, i.e. $U_2 = 0^o$ or 180^o. Four dead center positions M_1, M_2, M_3, and M_4 are found and the corresponding linkage configurations are listed in Table 3.3. They are the branch points of this Watt six-bar linkage and they divide the four-bar I/O curve into four segments.
b. Locate the dead center positions of the first four-bar loop, which occur when joints B, C, and D lie on a common straight line (Fig. 3.3(a)). Since neither a_2 nor a_3 is the longest link, the angle measured from CB to CD can reach 180^o but not 0^o. Let $U_1 = 180^o$. Two dead center positions *A* and *B* are found (Fig. 3.5). However, the position at *A* is blocked

by the second four-bar loop. The four-bar dead center position at *B* corresponds to two six-bar linkage configurations B_1 and B_2, which are listed in Table 3.3.

c. The first four-bar is a Class II loop, which has only one branch. All linkage configurations including the branch points and dead center positions are in the same branch of the first four-bar loop.

d. On the I/O curve of the first four-bar loop, a branch is formed between adjacent branch points [1].

e. Linkage configurations P_1, P_2, P_3, P_4, P_5, and dead the center positions B_1, B_2 are points between M_1 and M_4 on the I/O curve (Fig. 3.5). Hence, segment M_1M_4 forms one branch. Since there is no continuity between branches, M_3M_2 is the other branch. The segments of M_1M_4 and M_3M_2 are blocked by the second four-bar loop.

f. Segments M_1B and BM_4 are joined at B to form the branch M_1M_4. Configurations in M_1B can be identified by $\theta_1 \in (-98^o, -87^o)$ and $U_1 \in (0^o, 180^o)$ while configurations in BM_4 by $\theta_1 \in (-98^o, -36^o)$ and $U_1 \in (180^o, 360^o)$ (Fig. 3.5, Table 3.3).

g. Configuration P_6 is in the branch of segment M_3M_2, which does not contain the dead center position A. The branch is identified by $\theta_1 \in (27^o, 79^o)$ and $U_1 \in (180^o, 360^o)$ (Fig. 3.5, Table 3.3).

Table 3.3 Linkage configurations of a Watt six-bar chain

Position	θ_1	θ_9	θ_3	U_1	θ_7	U_2
P_1	-92°	319°	250°	204°	134°	109°
P_2	-92°	319°	250°	204°	174°	251°
P_3	-92°	344°	228°	156°	134°	161°
P_4	-60°	274°	284°	250°	154°	54°
P_5	-60°	274°	284°	250°	204°	306°
P_6	40°	61°	246°	245°	141°	83°
B_1	-98°	335°	237°	180°	132°	135°
B_2	-98°	335°	237°	180°	158°	225°
M_1	-87°	346°	226°	147°	139°	180°
M_2	79°	14°	226°	313°	139°	180°
M_3	27°	117°	304°	340°	200°	0°
M_4	-36°	243°	304°	278°	200°	0°

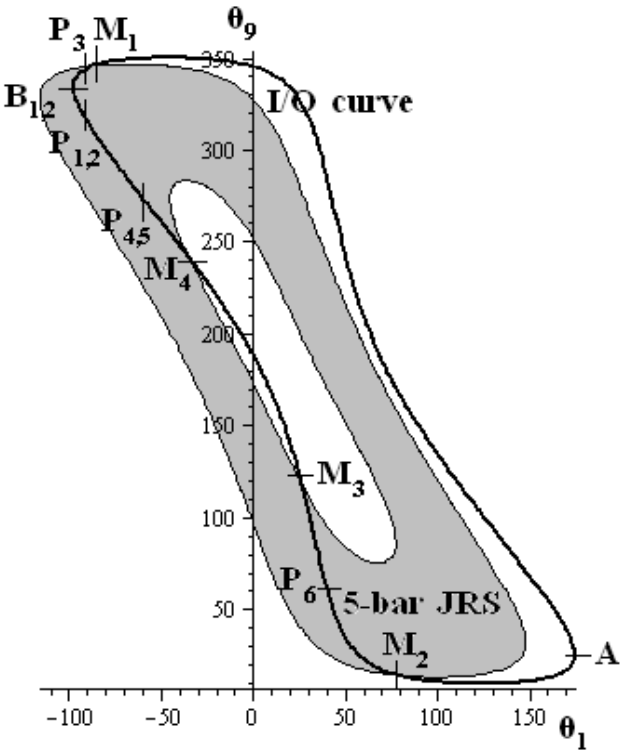

Figure 3.5 Branch points vs. tangent points in an RRCCR with parallel joint axes

3.3.3 Sub-branches

A branch may contain one or several sub-branches, divided by branch points and dead center positions. The choice of the input joint will affect the formation of the dead center positions in the first four-bar loop but not the branch points.

If all configurations are in the same branch, the linkage may reach all desired configurations continuously. If all configurations are also in the same sub-branch, the linkage will have the ability to reach all desired configurations without having to reach a dead center position or branch point, where the linkage may lose control. In a sub-branch, the input angle increases or decreases monotonously. Therefore the magnitude order of the input angle determines the order of reaching the desired configurations.

In Fig. 3.4(a), neither branch point nor dead center position exists in the linkage, hence each branch has only one sub-branch. The four-branches are identified by

$U_1 \in (0^o, 180^o)$ and $U_2 \in (0^o, 180^o)$;

$U_1 \in (0^o, 180^o)$ and $U_2 \in (180^o, 360^o)$;

$U_1 \in (180^o, 360^o)$ and $U_2 \in (0^o, 180^o)$;

$U_1 \in (180^o, 360^o)$ and $U_2 \in (180^o, 360^o)$.

In Fig. 3.4(b), there are two dead center positions, which divide each branch into two sub-branches. The JRS sheet has two sides. The I/O curve on each side corresponds to a branch. Hence, the two branches are identified by $U_2 \in (0^o, 180^o)$ and $U_2 \in (180^o, 360^o)$. In each branch, the two sub-branches are identified by $U_1 \in (0^o, 180^o)$ and $U_1 \in (180^o, 360^o)$.

In Fig. 3.4(c), each point on a branch (except the branch points) corresponds to two configurations [16]. Hence point A (as well as B) represents two dead center positions. M_i (i = 1,…, 6) and $A_{1,2}$ and $B_{1,2}$ are the dead center positions of the Watt linkage. These dead center positions divide a branch into sub-branches. Branch M_6M_1 has four sub-branches M_6A_1, M_1A_1, M_6A_2, M_1A_2; Branch M_4M_5 also has four sub-branches M_4B_1, M_5B_1, M_4B_2, M_5B_2; Branch points M_2M_3 has two sub-branches.

In example 2, the sub-branches in each of the two branches are identified as below.

The four sub-branches in M_1M_4 are

M_1B_1: $\{\theta_1 \in (-98^o, -87^o), U_1 \in (0^o, 180^o), U_2 \in (0^o, 180^o)\}$;

M_1B_2: $\{\theta_1 \in (-98^o, -87^o), U_1 \in (0^o, 180^o), U_2 \in (180^o, 360^o)\}$;

M_4B_1: $\{\theta_1 \in (-98^o, -36^o), U_1 \in (180^o, 360^o), U_2 \in (0^o, 180^o)\}$;

M_4B_2: $\{\theta_1 \in (-98^o, -36^o), U_1 \in (180^o, 360^o), U_2 \in (180^o, 360^o)\}$.

The two sub-branches in M_2M_3 are

$\{\theta_1 \in (27^o, 79^o), U_1 \in (180^o, 360^o), U_2 \in (0^o, 180^o)\}$;

$\{\theta_1 \in (27^o, 79^o), U_1 \in (180^o, 360^o), U_2 \in (180^o, 360^o)\}$.

One may easily conclude that configurations P_1 and P_4 are in sub-branch M_4B_1 and all other configurations are in different branch or sub-branch.

One may easily observe that in a branch formed between two branch points, if the number of dead center positions from the first four-bar loop is 0, 1, or 2, the number of sub-branches in the branch will be 2, 4, or 6, respectively. This is also true for Stephenson six-bar linkages.

Remark: In the above discussion, a hidden five-bar loop is introduced via the stretch and rotation of the second four-bar loop and the JRS of the five-bar loop is used to explain the formation of branches and sub-branches caused by the interaction between the four-bar loops. In practice, branch points are the dead center positions of the second four-bar loops. Hence stretch rotation is a convenient visual aid to understand the formation of branches and sub-branches and how Watt linkages and Stephenson linkages differ in mobility. In practice no stretch rotation has to be executed to conduct the mobility identification. Once the principle of mobility identification becomes known, the algorithm can be derived easily following the branch identification of Stephenson six-bar linkages [1].

3.3.4 Full Rotatability

The full rotatability of a linkage is input related. The full rotatability of a linkage should refer to a specific branch [20]. For a branch of a Watt six-bar linkage to have full rotatability, the following conditions must be satisfied.

a. The four-bar loop is a Class I chain and the short link of the four-bar loop must be the input or fixed link. In other words, no dead center position exists in the branch.
b. The I/O curve of the branch must stay within the JRS of the five-bar loop. In other words, no branch point exists in the branch.

In Fig. 3.4(a), no branch point or dead center position exists. Hence the linkage has full rotatability in all branches.

3.3.5 Watt Six-bar Chains with a Prismatic Joint

A prismatic joint may be regarded as a revolute joint located at infinity in the direction normal to the path of the slider. Hence, the N-bar mobility laws can be extended to govern the mobility of planar single-loop N-bar chains when prismatic joints are involved [21]. Let φ = AP (Fig. 3.6) represents the prismatic joint variable. The I/O curve between φ and a revolute joint variable, say θ, at A or C can be obtained from the first four-bar loop APCD. These I/O curves can be classified into three types (Fig. 3.7) [16]. Stretch rotation can be applied to the second four-bar loop DGFE and a joint rotation space in the φ-θ domain of the resulting five-bar loop can be established. Sample types of JRS are shown in Fig. 3.2(b) and (c). An almost identical mobility identification method can be obtained for such a Watt-type linkage (Fig. 3.6).

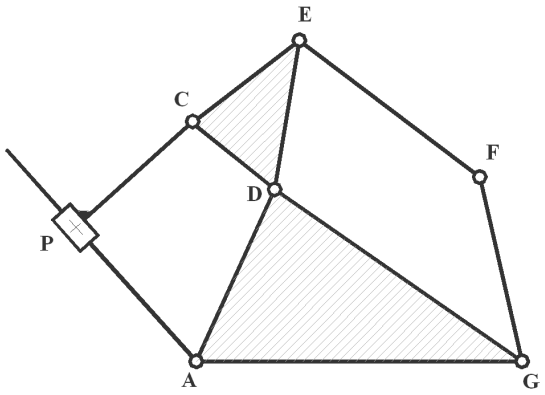

Figure 3.6 A Watt six-bar chain with one prismatic joint involved

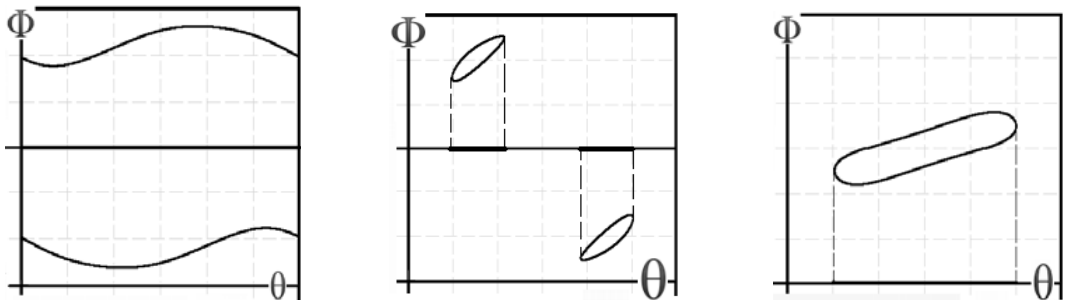

(a) CR-I (b) RR-I (c) RR-II

Figure 3.7 Three types of I/O curves with a prismatic joint variable

3.4 Conclusions

By using the stretch rotation to one of the four-bar loop, a Watt six-bar linkage is equivalent to a Stephenson six-bar linkage and the paper offers a simple explanation to the mobility formation of Watt six-bar linkages. The dead center positions of the second four-bar loop are the branch points. Although the formation of branch, sub-branch, and full rotatability of general Watt six-bar linkages is explained via the stretch and rotation of a four-bar loop, the resulting mobility criteria and algorithm requires no stretch and rotation and is easy to use. A Watt six-bar linkage may have up to four branches and each branch may have up to six sub-branches. The algorithm is suitable for automated mobility identification and is valid regardless whichever link is used as the input or fixed link.

REFERENCES

1. Ting, K.L. and Dou, X.H., 1996, “Classification and Branch Identification of Stephenson Six-Bar Chains,” *Mechanism and Machine Theory*, Volume 31, Issue 3, pp.283-295.
2. Grashof, F., 1983, *Theoretische Maschinenlehre*, Leipzig.
3. Ting, K.L., 1989, "Mobility Criteria of Single-Loop N-Bar Linkages," *Journal of Mechanisms, Transmissions, and Automation in Design*, pp. 504-507.
4. Ting, K.L. and Liu, Y.W., 1991, "Rotatability Laws for N-Bar Kinematic Chains and Their Proof," *ASME Journal of Mechanical Design*, Vol. 113, No. 1, pp. 32-39.
5. Ting, K.L., 1993, “Branch and dead position problems of N-bar linkages,” *American Society of Mechanical Engineers, Design Engineering Division*, (Publication), DE-Vol.65-2, Advances in Design Automation, pp.459-465.
6. Chase, T.R. and Mirth, J.A., 1993, "Circuit and branches of single Degree-of-Freedom Planar Linkages," *Journal of Mechanical Design*, Vol.115, No. 2, pp. 223-230.
7. Davis, H.P., Chase, T.R., and Mirth, J.A.., 1994, “Circuit analysis of Stephenson chain six-bar mechanisms,” *ASME Mechanism Synthesis and Analysis*, DE-vol.70, pp.349–358.
8. Ting, K.L., 1994, "Mobility criteria of geared five-bar linkages," *Mechanism and Machine Theory*, Vol.29, No.2, pp.251-264.
9. Foster, D.E. and Cipra, R.J., 1998, “Assembly configurations and branches of planar Single-Input-Dyadic mechanisms,” *ASME J. Mech. Des.*, 120(3), pp.381–386.
10. Foster, D.E. and Cipra, R.J., 2002, “An automatic method for finding the assembly configurations of planar Non-Single-Input-Dyadic mechanisms,” *ASME J. Mech. Des.*, 124(1), pp.58–67.
11. Guo, X.N. and Chu, J.K., 2004, “Mobility of Stephenson six-bar chains – Part I: circuit and circuit defect,” DETC 2004-57315, *Proceedings of ASME Design Engineering Technical Conferences and Computers and Information in Engineering Conference*, Salt Lake City, Utah.
12. Guo, X.N. and Chu, J.K., 2004, “Mobility of Stephenson six-bar chains – Part II: the motion order,” DETC 2004-57354, *Proceedings of ASME Design Engineering Technical Conferences and Computers and Information in Engineering Conference*, Salt Lake City, Utah.
13. Primrose, E.J.F., Freudenstein, F., and Roth, B., 1967, “Six-bar motion I. the Watt mechanism,” *Archive for Rational Mechanics and Analysis*, Vol. 24, pp. 22-41.
14. Mirth, J.A. and Chase, T.R., 1992, “Circuit rectification for four precision position synthesis of Stephenson six-bar linkages,” *ASME Mechanical Design and Synthesis*, DE-Vol.46, pp.359–366.
15. Mirth, J.A. and Chase, T.R., 1993, “Circuit analysis of Watt chain six-bar mechanisms,” *ASME, Mechanical Design*, pp.214–222.

16. Ting, K.L., 2008, "On the Input Joint Rotation Space and Mobility of Linkages," *Journal of Mechanical Design*, Vol.130, 092303-1-9.

17. Dijksman, E.A., 1976, *Motion Geometry of Mechanisms*, Cambridge University Press, Cambridge.

18. Ting, K. L., Xue C., Wang, J., and Currie, K. R., 2007, "General Mobility Identification and Rectification of Watt Six-Bar Linkages," *Proceedings of IDETC/CIE 2007 ASME Design Engineering Technical Conferences and Computers and Information in Engineering Conference*.

19. Yan, H.S., and Wu, L.L., 1989, "On the Dead center Positions of Planar Linkages Mechanisms," *ASME Journal of Mechanisms, Transmissions, and Automation in Design*, Vol.111, pp.40-46.

20. Ting, K.L., Wang, J., Xue, C. and Currie, K.R., 2008, "Full Rotatability of Stephenson Six-Bar and Geared Five-Bar Linkages," DETC 2008-49180, *Proceedings of the ASME 2008 International Design Engineering Technical Conferences & Computers and Information in Engineering Conference*, Brooklyn, NY.

21. Ting, K.L., Xue, C. Wang, J., and Currie, K.R., 2008, "Mobility Criteria of Planar Single-loop N-bar Chains with Prismatic Joints," DETC 2008-50075, *Proceedings of the ASME 2008 International Design Engineering Technical Conferences & Computers and Information in Engineering Conference*, Brooklyn, NY.

CHAPTER 4

ON THE VIRTUAL LOOPS AND VIRTUAL MULTILOOP LINKAGES

ABSTRACT

The concept of virtual loops is introduced to show that in view of joint rotatability, spatial mechanisms may be regarded as planar or spherical linkages containing one or more virtual loops. It is suggested that although the physical construction of a spatial linkage may bear little or no similarity to planar or spherical linkages, there is a striking similarity or compatibility in their intrinsic mobility characteristics and analysis. With the concept of virtual loops, all spatial linkages classified by Duffy [1] can be regarded as virtual planar or spherical linkages. Linkages in Duffy's group 1, 2, 3, and 4 may be treated as spherical linkages with one, two, three, and four virtual loops respectively. The concept of virtual loops is subtle, but significant. It establishes a unified view on planar, spherical, and spatial linkages and a useful model to view or even understand complex spatial linkages. The fact that all of Duffy's group 1 linkages and planar and spherical four-bar linkages are bimodal linkages is consistent with the proposed virtual loop concept. The dissertation presents a detailed account of how two types of spatial group 2 mechanisms can be modeled as Stephenson-type linkages where findings for planar Stephenson linkages can be used directly.

4.1 Introduction

Mobility identification is a common problem encountered in linkage analysis and synthesis. Mobility of linkages refers to the problems related to branch (or circuit [2-7]) defect, full rotatability, sub-branch (or singularities), and order of motion [8]. For many decades, the understanding of the mobility of conventional closed-loop linkages had been mostly restricted to planar and spherical four-bar linkages. Generally, for geometric properties found in planar linkages, similar properties can also be expected in spherical linkages. The mobility study of four-bar linkages may be traced back to the discovery of the Grashof criterion [9], which is commonly used to predict the full rotatability of planar four-bar linkages. The most significant advancement in linkage mobility research are the N-bar rotatability laws [10-13]. The N-bar rotatability laws offer the first simple, complete, and systematical explanation for the rotatability of any N-bar chain ($N \geq 3$) connected with revolute joints, in which the Grashof criterion becomes a very special case. The N-bar rotatability laws govern and predict the formation of branches, sub-branches, and full rotatability of any single loop planar and spherical N-bar chain.

The success in planar and spherical four-bar linkages was later extended to all bimodal linkages [14-19]. The equation relating the output and input of a bimodal linkage can always be expressed in quadratic form. Based on the discriminant function of the quadratic equation, an algorithm can be derived for the mobility identification of any bimodal linkages.

Mobility analysis becomes much more complex in multiple loop linkages, such as Stephenson and Watt six-bar linkages. In a single degree-of-freedom (DOF) multiloop linkage, the mobility is affected not only by each individual loop, but also by the interaction among loops. Based on the concept of Joint Rotation Space (JRS) [20, 21], Ting and his associates [8, 12, 22-

27] offered a simple and straightforward method for the branch identification of Stephenson and Watt six-bar chains without invoking coupler curves. A unified mobility identification and rectification methodology has been developed on planar six-bar linkages [28]. JRS represents the domain of the input variables of a linkage or a loop. Ting [21] detailed the concepts of JRS sheets and sides as well as branch points to offer geometric insights on how mobility between loops interact each other and thus the mobility formation of linkages.

JRS Sheet: The JRS of a linkage branch is called a JRS sheet. It represents the configuration space of a linkage branch in the input domain. Thus, the JRS of a Class I linkage contains two sheets and that of a Class II linkage contains only one sheet. There is no motion continuity between sheets, i.e. a linkage cannot be transformed between configurations in different JRS sheets.

Edge of a JRS sheet: The edge of a JRS sheet is the boundary curve of the JRS. Each point on the boundary curve of the JRS corresponds to a unique uncertainty singularity configuration of a linkage.

Side of a JRS sheet: The edge of a JRS sheet separates the sheet into sides. Each side of a JRS sheet represents the configuration space of a linkage sub-branch in the input domain. A point on one side of a JRS sheet corresponds to one and only one linkage configuration. Since a linkage can be programmed within one side of a JRS sheet without reaching the boundary where an uncertainty singularity occurs, each side of a JRS sheet represents a sub-branch or a singularity-free configuration space.

The sheets and sides of a JRS provide an intuitive model to explain the relationship among branches, sub-branches, and singularities. So far, JRS is the most effective method and a vital tool or model to understand the formation of branch and sub-branches of multiloop linkages.

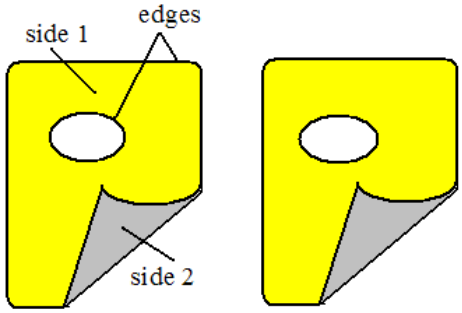

Figure 4.1 Two two-sided sheets

Table 4.1 Classification of spatial kinematic chains

Group	Number of links	Mechanism
1	4-7	R-3C, 2R-P-2C, 3R-2P-C, 4R-3P
2	5-7	3R- 2C, 4R-P-C, 5R-2P
3	6-7	5R- C, 6R-P
4	7	7R

However, the mobility study of spatial mechanisms is far from adequate. Realizing the large variety and the similarity shared by single DOF spatial mechanisms, Duffy [1, 29] classified their displacement analysis into four groups (Table 4.1). This elegant classification scheme is useful for a systematic mobility study on spatial mechanisms. Mobility study used to focus on a particular linkage type. Under this classification, a consistent mobility identification method on single DOF spatial mechanisms may be established.

4.2 Virtual Loop

Each spatial linkage connected with revolute or cylindrical joints has a spherical indicatrix [1], which is formed by bringing all joint axes to intersect at a common point. Using the D-H

notations [30, 31], the link and joint parameters of any spatial linkage can be defined by dual angles as

$$\hat{\alpha}_{ij} = \alpha_{ij} + \varepsilon a_{ij} \text{ and } \hat{\theta}_i = \theta_i + \varepsilon S_{ii} \qquad (4\text{-}1)$$

where $\varepsilon^2 = 0$, $\hat{\alpha}_{ij}$ is the twist angle between joint axes *i* and *j*, and $\hat{\theta}_i$ is the joint parameter at the joint axis *i*. If the dual part of all joint and link parameters are equal to zero, this spatial mechanism becomes a spherical linkage, which is the spherical indicatrix of the spatial mechanism. Fig. 4.2 shows an RCRCR mechanism and its corresponding spherical indicatrix. The spherical indicatrix may be regarded as a constraint imposed on the spatial mechanism by the angular displacements exclusively. Besides this constraint, on the orthogonal directions of the three dimensional space, three additional conditions are induced by the presence of joint offsets and skew distance between joint axes. All the equations, derived from the spherical indicatrix as well as the three additional constraint conditions, lead to a single-DOF spatial mechanism.

The mathematical formula of each constraint condition can be written in the form of

$$A\sin\theta_o + B\cos\theta_o + C = 0 \qquad (4\text{-}2)$$

where θ_o is the output variable and A, B, and C are functions of the input joint variable θ_i and three unknown angular and/or slider displacements. The first equation depicts the geometry of the spherical indicatrix and the other three the additional constraints. Like the loop-closure equations of a planar/spherical multiloop linkage, all equations, called fundamental equations of a spatial linkage, describe the essential geometry from which the mobility information of the linkage may be derived.

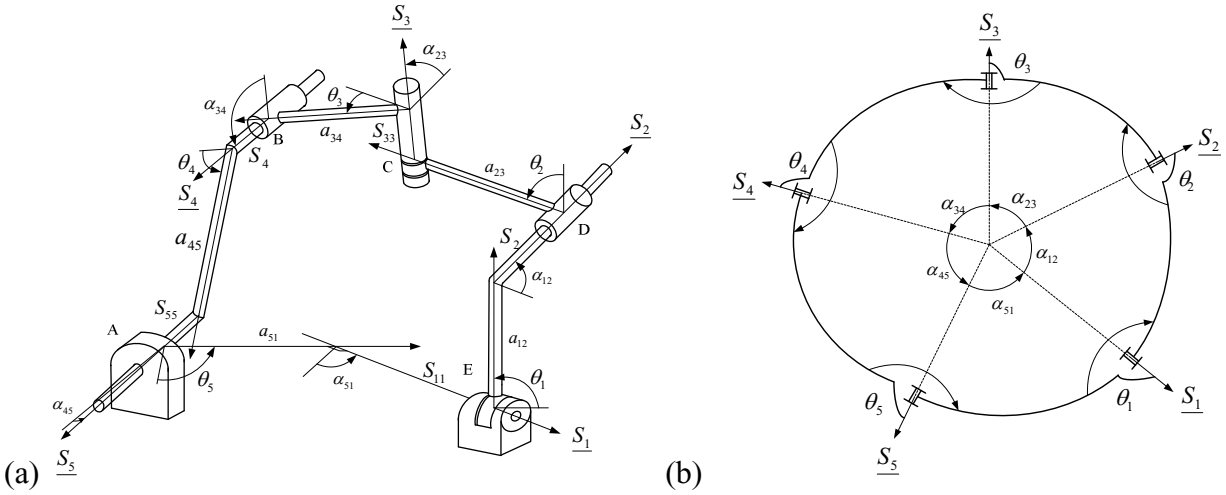

Figure 4.2 (a) An RCRCR mechanism and (b) the spherical indicatrix

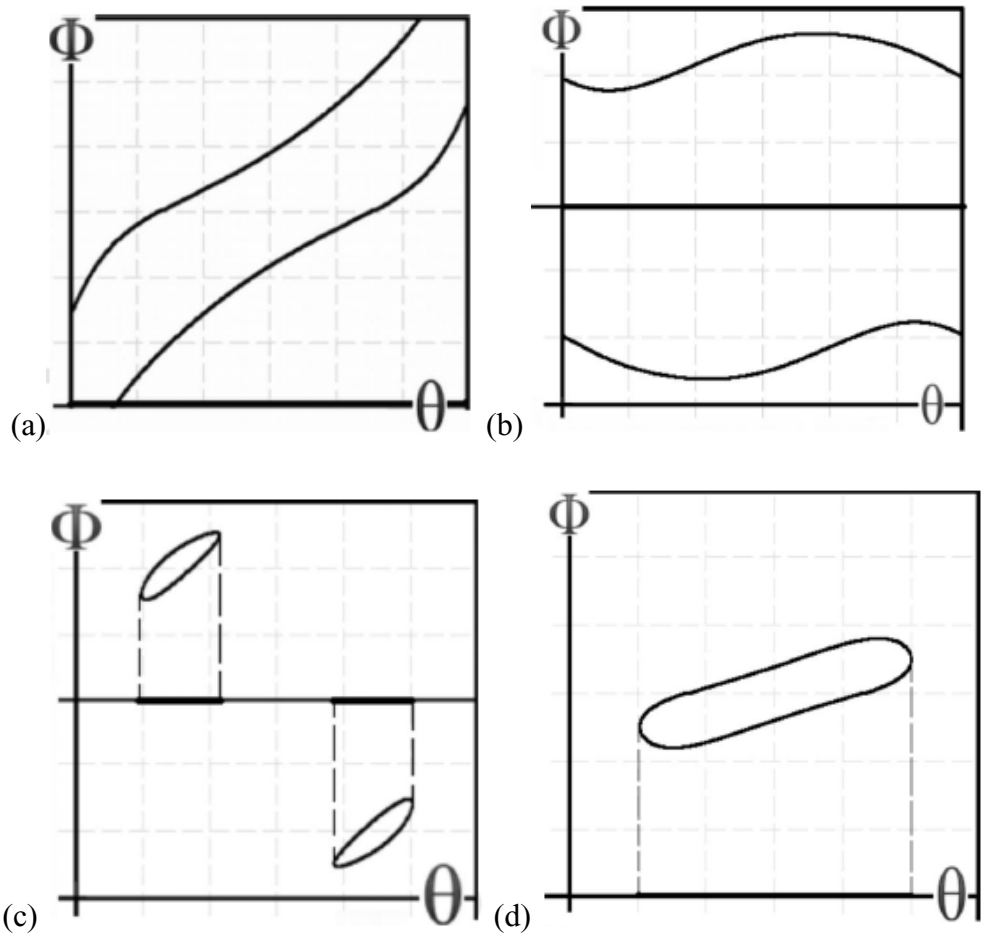

Figure 4.3 Types of I/O relationship of spatial group 1 linkages

(a) CC-I (b) CR-I (c) RR-I (d) RR-II

One may note that Eq. 4-2 is also the form of the loop-closure equation of any single loop planar or spherical linkage. Thus each fundamental equation may be regarded as a virtual loop, although this loop does not physically exist and no corresponding physical link length can be derived from it. Its mathematical form is called a virtual "loop-closure" equation. The concept of virtual loops is introduced by its mathematical form rather than its physical appearance.

4.2.1 Spatial Group 1 Linkages

Spatial group 1 linkages include RSSR, RRSS, RCCC, RSCR, RSCP, and 4R3P, where R, S, C, and P refer to the revolute, spherical, cylindrical, and prismatic joints used in the linkages. The discriminant method was widely used on RSSR, RRSS, and RCCC [15, 16, 32-35]. Like planar four-bar linkages, RSSR can be classified into three classes according to the possible number of branches [16]. The RRSS linkage is an inversion of the RSSR linkage, and the classification strategy for the two is essentially identical. Similar to planar or spherical four-bar loops, there exist four different types of I/O relationship totally in spatial group 1 linkages, namely crank-rocker (CR-I), crank-crank (CC-I), class I rocker-rocker (RR-I), and class II rocker-rocker (RR-II) [36].

Of group 1 linkages, the spherical indicatrix contains the input and output joint variables only, which is equivalent to a spherical four-bar linkage. Its corresponding fundamental equation determines the relationship between the input and output joint variables. Once the input and output joint variables are determined, they can be plugged into the other three fundamental equations to determine the unknown slider displacements. Since the linkage mobility can be derived from the input and output relationship, which is exclusively governed by the first

fundamental equation (from the spherical indicatrix), the other three fundamental equations may be regarded as redundant. Thus a spatial group 1 linkage is equivalent to and regarded as a single loop linkage.

Let $y = \tan\frac{\theta_o}{2}$ and $\cos\theta_o = \frac{1 - y^2}{1 + y^2}$, $\sin\theta_o = \frac{2y}{1 + y^2}$. Eq. 4-2 can be converted as

$$(C - B)y^2 + 2Ay + (C + B) = 0 \qquad (4\text{-}3)$$

The discriminant of the above quadratic equation is

$$\Delta' = A^2 - (C - B)(C + B) \qquad (4\text{-}4)$$

Singularity appears when the above discriminant is equal to zero, i.e.,

$$\Delta' = A^2 - (C - B)(C + B) = 0 \qquad (4\text{-}5)$$

From the viewpoint of mobility, a singular condition, representing the boundary of input domain, divides one sheet of JRS into two sides. One may find that the concept of JRS works well on virtual loops.

When an input joint variable is known, its corresponding output joint variable may be solved from Eq. 4-3. The derived two solutions show that one point in the JRS corresponds to two linkage configurations, and they are on different sides. Mathematically, Eqs. 4-6 and 4-7 represent points on each side of the JRS sheet, respectively. For any two known linkage configurations (except on the edge), they are on the same side if both of them meet the same equation (either Eq. 4-6 or 4-7); otherwise they are on different sides.

$$y_{1,2} = \frac{-A \pm \sqrt{(A^2 + B^2 - C^2)}}{C - B} \qquad (4\text{-}6,\ 4\text{-}7)$$

in which A, B, C are functions of the input joint variable.

Let $x = \tan\frac{\theta_i}{2}$ and $\cos\theta_i = \frac{1 - x^2}{1 + x^2}$, $\sin\theta_i = \frac{2x}{1 + x^2}$. Eq. 4-4 can be further converted to

$$\Delta' = Q_1 x^4 + Q_2 x^3 + Q_3 x^2 + Q_4 x + Q_5 \qquad (4\text{-}8)$$

where the coefficients Q_1, Q_2, Q_3, Q_4, and Q_5 are functions of the linkage structure parameters only. The discriminant of the above quartic equation is

$$\Delta = I^3 - 27J^2 \qquad (4\text{-}9)$$

where

$$I = Q_1 Q_5 - Q_2 Q_4 / 4 + Q_3^2 / 12$$

$$J = [72 Q_1 Q_3 Q_5 + 9 Q_2 Q_3 Q_4 - 27(Q_1 Q_4^2 + Q_5 Q_2^2) - 2 Q_3^3] / 432$$

Based on the sign of Δ of Eq. 4-9, the classification criterion can be derived for all spatial group 1 linkages as well as planar, spherical, and virtual four-bar loops [15].

- $\Delta > 0$, the formed virtual four-bar is Class I (Fig. 4-3(a), (b), and (c));
- $\Delta < 0$, the formed virtual four-bar is Class II (Fig. 4-3(d));
- $\Delta = 0$, the formed virtual four-bar is Class III.

The classification criterion derived from the discriminant function may be regarded as the algebraic form of the Grashof criterion [9].

4.2.2 Spatial Group 2 Linkages

A spatial group 2 linkage is referred to as a single DOF spatial linkage, which contains R, C, or P joints and has a total of five R and C joints [1]. Of a group 2 linkage, the spherical indicatrix contains the input, output, and one intermediate joint variables. The other three additional equations contain two unknown slider displacements besides the joint variables. Using the vector method introduced by Duffy [1], one of them can always be written as an equation without containing any unknown slider displacement, the second with one unknown slider displacement,

and the third with two unknown slider displacements. The input and output relationship can always be derived from the equation from the spherical indicatrix and the equation without containing any unknown slider displacement. Both of them are equivalent to virtual five-bar loops. The other two equations are redundant. Thus, a spatial group 2 linkage, consisting of two virtual five-bar loops, is equivalent to and regarded as a double loop linkage.

By varying the value of the intermediate joint variable (say θ_m), any virtual five-bar loop can be treated as a family of virtual four-bar loops. If all virtual four-bar loops of the family are Class I, then this virtual five-bar loop is Class I; otherwise it is Class II or III.

It is impossible to check all virtual four-bar loops of the family. The feasible process is to let Eq. 4-9 be equal to zero ($\Delta=0$) and see whether there exists any feasible solution of θ_m. If it does exist, so does the change point, and then this virtual five-bar loop is Class II or III. If no feasible solution of θ_m exists, then check one and only one virtual four-bar loop; if it is Class I, then the virtual five-bar loop is Class I, otherwise, it is Class II.

Since all fundamental equations for planar, spherical, and spatial linkages can be expressed in quadratic form, the above mobility criteria of virtual four-bar and five-bar loops may be extended to any virtual loops and be regarded as the generalization of the N-bar rotatability laws [10-13].

Table 4.2 Duffy's group 2 mechanisms

Number of links	Mechanism
Five	RCRCR, RRCRC, RCRRC, RCCRR, RRRCC
Six	RRRPCR, RRCPRR, RRRRPC, RPCRRR, RCRPRR, RRCRPR, RRRPRC, RCRRPR, RRPRRC
Seven	RRPRPRR, RPRRPRR, RPRRRPR, RRRRPPR, RRRPPRR

4.2.3 Spatial Group 3 and 4 Linkages

The concept of virtual loops is applicable to spatial groups 3 and 4 mechanisms as well. Every fundamental equation is equivalent to an individual virtual loop.

Concerning group 3 linkages, the spherical indicatrix contains the input, output, and two intermediate joint variables, which is equivalent to a spherical six-bar loop. The other three fundamental equations contain one unknown slider displacement besides the joint variables. Using the vector method introduced by Duffy [1], two of them can always be written as equations without containing any unknown slider displacement and the third with one unknown slider displacement. The equations without containing any unknown slider displacement lead to two additional constraint conditions to the three-DOF spherical indicatrix and therefore create the effect of two additional loops to the spherical indicatrix to form a single-DOF linkage. The input and output relationship can always be derived from the equation from the spherical indicatrix and the two equations without containing any unknown slider displacement. All of them are equivalent to virtual six-bar loops. The equation containing one unknown slider displacement is redundant. Thus, a spatial group 3 linkage, consisting of three virtual six-bar loops, is equivalent to and regarded as a three loop linkage.

Concerning group 4 linkages, the spherical indicatrix as well as the other three fundamental equations contain the input, output, and three intermediate joint variables, which are equivalent to four seven-bar loops. No equation is redundant. Thus a spatial group 4 linkage is equivalent to and regarded as a four loop linkage.

Generally, if the fundamental equation containing any unknown slider displacement is regarded as redundant, there exists one virtual four-bar loop in spatial group 1 linkages, two

virtual five-bar loops in group 2 linkages, three virtual six-bar loops in group 3 linkages, and four virtual seven-bar loops in group 4 linkages. When the offset is zero at the revolute joint between the cylindrical joints, a general RCRCR is degenerated into a special case, namely a simple RCRCR. A virtual loop may degenerate to a less complicated loop. For example, in a simple RCRCR, one of the virtual loops is a four-bar loop.

With the concept of virtual loops, a unified linkage classification scheme based on the number of (virtual) loops becomes apparent. All linkages can be classified into four groups according to the level and similarity of mobility or computation complexity rather than their physical appearance. Each spatial group 1, 2, 3, or 4 mechanism can be regarded as a virtual spherical linkage formed by one or more virtual loops. Such a unified classification scheme represents a very unique and desirable aspect of this paper. It suggests that mobility analysis of all linkages can be carried out in a unified and systematic manner based on the similarity of the mobility features rather than the specific or individual linkage structure. The fact that all of Duffy's group 1 linkages and planar and spherical four-bar linkages are bimodal linkages is consistent with the proposed virtual loop concept. The concept of virtual loops is perfectly applied in the following section where two types of spatial group 2 linkages are modeled as virtual Stephenson linkages.

4.3 Virtual Stephenson Linkage

Simple RCRCR and group 2 linkages with parallel joint axes are simplified versions of group 2 mechanisms. Each of them can be modeled as a virtual multiloop linkage consisting of a four-bar loop and a five-bar loop. Therefore, their mobility and branch conditions are completely

compatible to that of Stephenson six-bar linkages and may be regarded as virtual Stephenson linkages where findings for planar Stephenson linkages can be used directly. The concept of virtual loops offers the background for a unified mobility analysis for both ordinary and virtual Stephenson linkages.

4.3.1 Simple RCRCR

A simple RCRCR mechanism is shown schematically in Fig. 4.4. The axes of the joints R, C, R, C, and R are labeled 1, 2, 3, 4, and 5 in order. The input angular displacement is θ_1 and the output angular displacement θ_5. The remaining five variables are the angular displacements θ_2, θ_3, θ_4 and the slider displacements S_2 and S_4. By using the D-H notation [30, 31], $\alpha_{12} = 60^o$, $\alpha_{23} = 45^o$ $\alpha_{34} = 35^o$, $\alpha_{45} = 30^o$, and $\alpha_{51} = 10^o$ are the angles between the corresponding joint axes, $a_{12} = 25$, $a_{23} = 30$, $a_{34} = 40$, $a_{45} = 10$, and $a_{51} = 32$ are the distance between the corresponding joint axes, $S_{11} = 30$ and $S_{55} = 25$ are the offset along the corresponding R-joint axes, and $S_{33} = 0$, i.e., the offset is zero between the links connected by the revolute joint between the two C-joints.

According to Duffy's sine, sine-cosine, and cosine laws [1], the motion of a simple RCRCR mechanism is governed by two fundamental equations. One equation, which is induced by the presence of joint offsets and skew distance between joint axes (called cylindroid surface constraint in [36]), can be written as

$$\begin{aligned} &7.36\cos\theta_5\cos\theta_1 + 6.68\cos\theta_5\sin\theta_1 - 6.79\sin\theta_5\sin\theta_1 + 6.69\sin\theta_5\cos\theta_1 \\ &- 0.84\cos\theta_5 + 0.31\sin\theta_5 - 3.80\cos\theta_1 + 1.11\sin\theta_1 + 6.67 = 0 \end{aligned} \tag{4-10}$$

The other equation, which can be derived from the spherical indicatrix, is written as

$$10.51\cos\theta_5\cos\theta_1 - 10.68\sin\theta_5\sin\theta_1 + 1.07\cos\theta_5 + 3.21\cos\theta_1 + 3.77 = \cos\theta_3 \qquad (4\text{-}11)$$

One may observe that the above two equations can be written in the form of Eq. 2-2, so each of them may be treated as a loop-closure equation derived from a virtual loop and simple RCRCR may be modeled as a double loop linkage. Eq. 4-10 has two joint variables, θ_1 and θ_5, so it is equivalent to a four-bar loop. Eq. 4-11 has three joint variables, θ_1, θ_5, and θ_3, so it is equivalent to a five-bar loop. Of the two virtual loops, there are two common joint variables, θ_1 and θ_5. Similar characteristics can also be found in a Stephenson six-bar linkage. Therefore, a simple RCRCR can be regarded as a virtual Stephenson linkage consisting of a virtual four-bar loop induced by the presence of joint offsets and skew distance between joint axes and a virtual five-bar loop derived from the spherical indicatrix (Fig. 4.4).

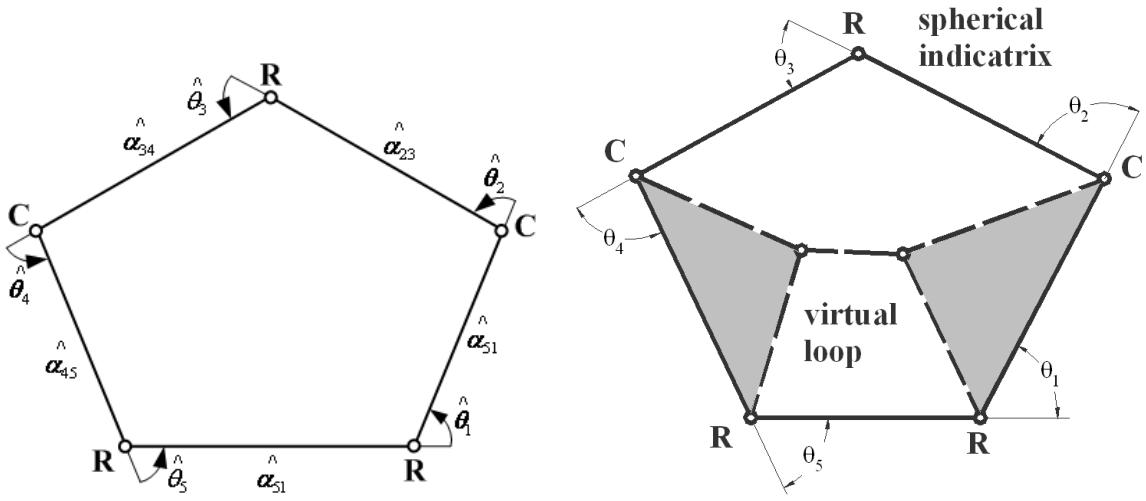

Figure 4.4 Analogy between a simple RCRCR and a virtual Stephenson linkage

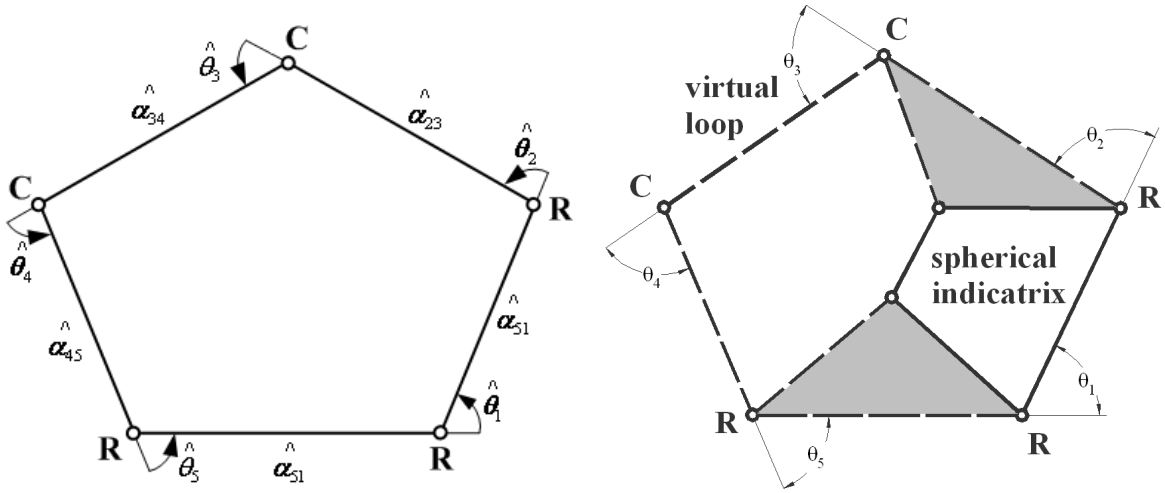

Figure 4.5 Analogy between an RRCCR ($\alpha_{45} = 0^{o}$) and a virtual Stephenson linkage

4.3.2 Spatial Group 2 with Parallel Joint Axes

An RRCCR with parallel joint axes (for convenience without losing generality, let $\alpha_{45} = 0^{o}$) is shown schematically in Figure 4.5. The axes of the joints R, R, C, C, and R are labeled 1, 2, 3, 4, and 5 in order. The input angular displacement is θ_1 and the output angular displacement θ_5. The remaining five variables are the angular displacements θ_2, θ_3, θ_4 and the slider displacements S_3 and S_4. By using the D-H notation [30, 31], $\alpha_{12} = 50^{o}$, $\alpha_{23} = 75^{o}$, $\alpha_{34} = 40^{o}$, and $\alpha_{51} = 55^{o}$ are the angles between the corresponding joint axes, $a_{12} = 14$, $a_{23} = 35$, $a_{34} = 38$, $a_{45} = 12$, and $a_{51} = 10$ are the distance between the corresponding joint axes, and $S_{11} = 15$, $S_{22} = 24$, and $S_{55} = 6$ are the offset along the corresponding R-joint axes.

According to Duffy's sine, sine-cosine, and cosine laws [1], the motion of a spatial group 2 linkage with parallel joint axes is governed by two fundamental equations. One equation, which is induced by the presence of joint offsets and skew distance between joint axes, can be written

as

$$(11.59\sin\theta_5\cos\theta_1 + 6.65\cos\theta_5\sin\theta_1 + 12.96\sin\theta_1 + 24.07\cos\theta_1 + 10.19)\sin\theta_2$$
$$+ (7.45\sin\theta_5\sin\theta_1 - 4.27\cos\theta_5\cos\theta_1 + 7.27\cos\theta_5 + 26.62\sin\theta_1 + 0.15\cos\theta_1 - 2.90)\cos\theta_2$$
$$+ (2.38\sin\theta_5\sin\theta_1 - 1.36\cos\theta_5\cos\theta_1 - 1.64\cos\theta_5 + 2.44\sin\theta_1 + 18.17\cos\theta_1 + 9.01) = 0$$

(4-12)

The other equation, which can be derived from the spherical indicatrix, is written as

$$7.91\sin\theta_1\sin\theta_2 + (-5.09\cos\theta_1 - 4.24)\cos\theta_2 + (-1.62\cos\theta_1 - 6.71) = 0 \qquad (4\text{-}13)$$

Likewise, one may observe that the above two equations can be written in the form of Eq. 4-2, Eq. 4-12 has three joint variables, θ_1, θ_2, and θ_5, so it is equivalent to a five-bar loop. Eq. 4-13 has two joint variables, θ_1 and θ_2, so it is equivalent to a four-bar loop. Of the two virtual loops, there are two common joint variables, θ_1 and θ_2. Similar characteristics can also be found in a Stephenson six-bar linkage. Therefore, a spatial group 2 linkage with parallel joint axes can be regarded as a virtual Stephenson linkage consisting of a virtual five-bar loop induced by the presence of joint offsets and skew distance between joint axes and a virtual four-bar loop derived from the spherical indicatrix (Fig. 4.5).

From the viewpoint of linkage mobility and displacement analysis, both simple RCRCR and spatial group 2 with parallel joint axes are completely compatible to Stephenson linkages. Their mobility can be obtained exactly in the same way for Stephenson six-bar linkages [8, 28].

4.4 Mobility Identification and Rectification of Virtual Stephenson Linkages

The difficulties concerning the mobility of Stephenson-type linkages mainly lie on the branches induced by the interaction between loops. The problem is even more complicated with the sub-branches when the input is given through a joint not in the four-bar loop.

4.4.1 Branch

The branch problem of a linkage is strictly affected by the kinematic chain and is irrelevant to the input or output condition [12, 22-28]. In a branch, an input value may correspond to more than one linkage configuration while in a sub-branch each input value corresponds to a unique linkage configuration. For a two-DOF five-bar linkage, Ting [21] refers the input domain of a branch as a sheet while that of a sub-branch as one side of the sheet and a sheet with a boundary has two sides. The concept of sheet and side of JRS offers an excellent model to explain and understand the interaction between loops in Stephenson six-bar linkages [8].

Branch points: They are the intersection points between curves of a four-bar loop and boundary curves of the JRS sheet of a five-bar loop. Therefore, they are the common solutions of the I/O displacement equation of the four-bar loop and the singular condition equation of the five-bar loop.

The concept of JRS offers clear geometric insight for mobility analysis. If no branch point exists, the branch condition can be easily identified by the branch of the four-bar loop and the side of the five-bar JRS sheet [21]. If branch points exist, the effects of branch points must also be taken into consideration in the branch formation [8]. The maximum number of branches that a Stephenson six-bar linkage may have is six [8].

Dead center position: The dead center position of a single-DOF planar linkage occurs when the input link reaches its rotation limit. At such positions, a linkage may be out of control momentarily and have zero mechanical advantage [38]. Dead center positions in a Stephenson linkage may result from the four-bar loop or the combination of the four-bar and five-bar loops depending on the choice of the input joint. The analysis of dead center positions can be separated

into two categories depending on whether the input is given through a joint in the four-bar or the five-bar loop.

On the I/O curve of the four-bar loop, the points with a vertical slope are called singular points. If the input is given through a joint in the four-bar loop, then the singular points and branch points [8] are the dead center positions of the Stephenson linkage. If the input is not given through a joint in the four-bar loop, then the singular or branch points discussed above will not be dead center positions. Ting and his associates [27] presented a simple method to find all dead center positions of any Stephenson six-bar linkage with the input joint not in the four-bar loop. The association of these dead center positions to each branch is also identified.

Generally, the I/O relationship between any pair of joint parameters can be expressed by a polynomial equation [27]. In any sub-branch, the input reaches an extreme value when the linkage is at a dead center position. Therefore, all of the dead center positions, disregarding whichever joint is used as the input joint, can be found by solving polynomial equations [27]. It may be noted that the existence of the dead center positions is strictly input related and is irrelevant to the choice of the output joint.

4.4.2 Sub-branch

A branch may be divided into sub-branches by the dead center positions. A branch may have one, two, or more sub-branches depending on the number of dead center positions in the branch. In a sub-branch, a one-to-one correspondence exists between the input angle and the linkage configuration; the input increases or decreases monotonously from one dead-center position to another. Such a one-to-one correspondence is the core issue in the sub-branch identification.

Since such a correspondence can be easily established with the input joint in the four-bar loop, the sub-branch identification with other input conditions can be accomplished via the above established correspondence.

4.4.3 Unified Methodology

A unified theory for the mobility analysis of planar six-bar linkages based on the concept of JRS has been completely established [28]. The principle is applicable to virtual Stephenson linkages as well. However, one point should be mentioned. In planar six-bar linkages (Fig. 4.6), the angles θ_{34} and θ_{78} are used for side identification of JRS. θ_{34} is the angle between links 3 and 4 ($\theta_{34} = \theta_4 - \theta_3$); θ_{78} is the angle between links 7 and 8 ($\theta_{78} = \theta_8 - \theta_7$). But in virtual Stephenson linkages, the mathematical equations 6 and 7 are used instead. In other words, the linkage configurations must meet the same mathematical equation if they are said to be on the same side.

In a virtual four-bar loop, the coefficients A, B, and C of Eq. 4-2 contain one input joint variable θ_i. To distinguish them against the coefficients of other virtual loops, they are written as

$$A = A_1 = p_1 \sin\theta_i + p_2 \cos\theta_i + p_3$$

$$B = B_1 = p_4 \sin\theta_i + p_5 \cos\theta_i + p_6$$

$$C = C_1 = p_7 \sin\theta_i + p_8 \cos\theta_i + p_9 \qquad (4\text{-}14)$$

in which $p_1, p_2, \ldots, p_9$ are functions of all joint and link parameters.

In a virtual five-bar loop, the coefficients A, B, and C of Eq. 4-2 contain one input joint variable θ_i and one intermediate joint variable θ_m. To distinguish them against the coefficients of other virtual loops, they are written as

$$A = A_2 = p_1 \sin\theta_i + p_2 \cos\theta_i + p_3$$

$$B = B_2 = p_4 \sin\theta_i + p_5 \cos\theta_i + p_6$$

$$C = C_2 = p_7 \sin\theta_i + p_8 \cos\theta_i + p_9 \qquad (4\text{-}15)$$

in which $p_1, p_2, \ldots, p_9$ are functions of the intermediate joint variable θ_m.

Likewise, to distinguish the singular conditions between a four-bar loop and a five-bar loop, Eqs. 4-6 and 4-7 are further written as follows.

Four-bar loop: $$y_{1,2} = \frac{-A_1 \pm \sqrt{(A_1^2 + B_1^2 - C_1^2)}}{C_1 - B_1} \qquad (4\text{-}16, 17)$$

Five-bar loop: $$y_{1,2} = \frac{-A_2 \pm \sqrt{(A_2^2 + B_2^2 - C_2^2)}}{C_2 - B_2} \qquad (4\text{-}18, 19)$$

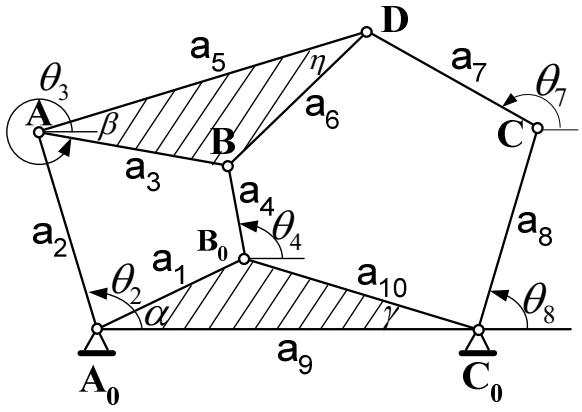

Figure 4.6 A Stephenson six-bar linkage

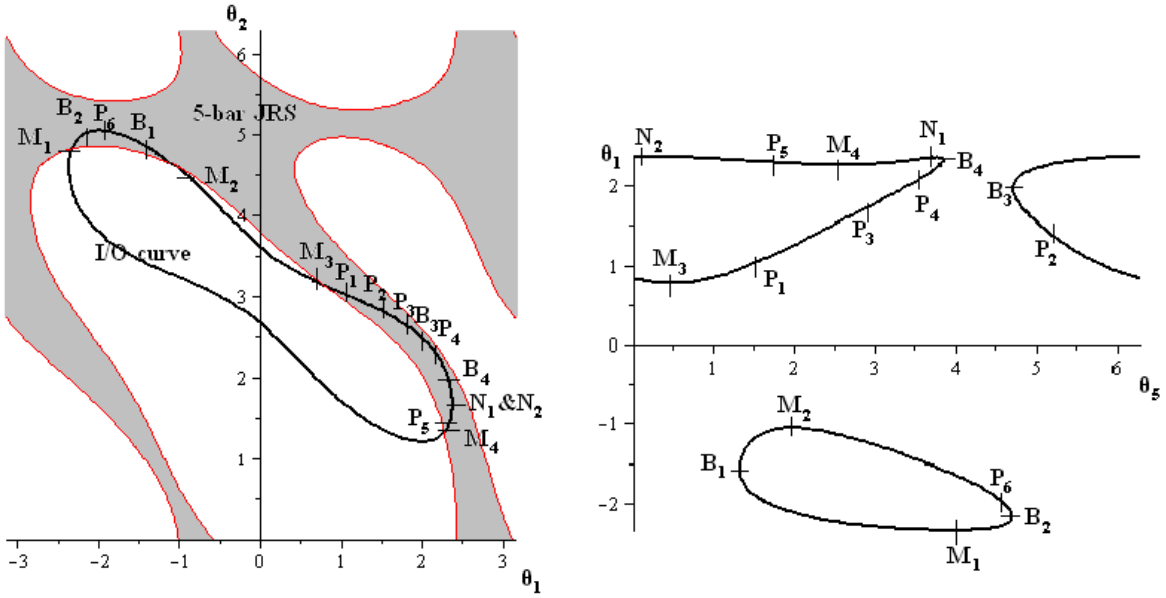

Figure 4.7 Branches of a virtual Stephenson linkage

(a) I/O curve (θ_2 vs. θ_1) in JRS (b) I/O curve of (θ_5 vs. θ_1)

4.4.4 Example

A group 2 mechanism (RRCCR) with parallel joint axes is used to illustrate the methodology. The same joint and link parameters in section 4.3.2 are used here.

From Eq. (4-13), $A_1 = 7.91\sin\theta_1$, $B_1 = -5.09\cos\theta_1 - 4.24$, $C_1 = -1.62\cos\theta_1 - 6.71$.

From Eq. (4-12),

$$A_2 = 11.59\sin\theta_5\cos\theta_1 + 6.65\cos\theta_5\sin\theta_1 + 12.96\sin\theta_1 + 24.07\cos\theta_1 + 10.19,$$

$$B_2 = 7.45\sin\theta_5\sin\theta_1 - 4.27\cos\theta_5\cos\theta_1 + 7.27\cos\theta_5 + 26.62\sin\theta_1 + 0.15\cos\theta_1 - 2.90,$$

$$C_2 = 2.38\sin\theta_5\sin\theta_1 - 1.36\cos\theta_5\cos\theta_1 - 1.64\cos\theta_5 + 2.44\sin\theta_1 + 18.17\cos\theta_1 + 9.01.$$

Table 4.3 shows the orientation angles of θ_1, θ_2, and θ_5 at all branch points, singular points, dead center positions, and six configurations, P_i, i = 1, 2, 3, …, 6. Fig. 4.7(a) shows the I/O curve between θ_1 and θ_2 and Fig. 4.7(b) shows the relationship between θ_5 and θ_1.

For the given set of linkage configurations, P_i, i = 1, 2, 3, …, 6,

a. Determine the branch condition of these configurations.
b. Determine the sub-branch condition of these configurations when θ_5 is the input angle.
c. Determine their order of motion.

Branch identification:

a. Find and locate all branch points [8] (M_1, M_2, M_3, and M_4 in Table 4.3(a)).
b. Find and locate all singular points [27] (N_1 and N_2 in Table 4.3(a)).
c. Find and locate all dead center positions (B_1, B_2, B_3, and B_4 in Table 4.3(a)) if θ_5 is to be the input angle.
d. Divide all configurations into two groups by the side identification criterion of four bar loop (Eqs. 4-16 and 4-17) (Table 4.3(a)).
e. In Table 4.3(a), sort the first group by the ascending (or descending) order of θ_1 and then the second group by the reverse order. Points between two neighboring branch points are grouped as one branch. Table 4.1(b) shows the two branches between M_1 and M_2, M_3 and M_4 (Fig. 4.7).

Sub-branch identification:

Now the branch is identified. If θ_1 is the input angle, all singular points and branch points are dead center positions, which divide a branch into sub-branches. In each branch, the sub-branches between neighboring dead center positions can be recognized by the side identification criteria of

four-bar loops (Eqs. 4-16 and 4-17) and/or five-bar loops (Eqs. 4-18 and 4-19) and the magnitude order of θ_1. For example, in Fig. 4.7(a), branch M_1M_2 has two sub-branches separated by the side identification criterion of a four-bar loop (Eqs. 4-16 and 4-17); branch M_3M_4 has four sub-branches separated by the side identification criteria of both a four-bar loop (Eqs. 4-16 and 4-17) and a five-bar loop (Eqs. 4-18 and 4-19). The example is shown in Table 4.4, which is obtained by sorting Table 4.3(b) as below.

a. In each branch, divide the configurations in Table 4.3(a) into two groups according to the side identification criterion of a four-bar loop (Eqs. 4-16 and 4-17), and then

b. Divide each group into two sub-groups according to the side identification criterion of a five-bar loop (Eqs. 4-18 and 4-19).

By now, each branch in Table 4.4 should have no more than four groups and any of these groups is a sub-branch. One may note that in Table 4.4, the sub-branches have been arranged in the order of occurrence in the motion cycle of the branch.

Table 4.3 Branch identification

(a) By checking the side identification criterion of a four-bar loop: equations 2-16 and 2-17, and sorting the order of θ_1 values; (b) by forming branch for every two branch points

Position	θ_1	θ_2	θ_5	four-bar loop	five-bar loop
M_1	-134	276	227	equation 17	equations 18 & 19
B_2	-124	288	269	equation 17	equation 18
P_6	-110	290	259	equation 17	equation 18
B_1	-90	283	77	equation 17	equation 19
M_2	-60	264	112	equation 17	equations 18 & 19
M_3	45	180	28	equation 17	equations 18 & 19
P_1	60	174	91	equation 17	equation 18
P_2	80	165	296	equation 17	equation 19
P_3	100	154	167	equation 17	equation 18
B_3	113	144	271	equation 17	equation 19
P_4	120	137	204	equation 17	equation 18
B_4	134	111	221	equation 17	equation 18
N_1	136	96	217	equations 16 & 17	equation 18
N_2	136	96	6	equations 16 & 17	equation 19
P_5	132	79	97	equation 16	equation 19
M_4	130	77	148	equation 16	equations 18 & 19

(a)

Position	θ_1	θ_2	θ_5	four-bar loop	five-bar loop
M_1	-134	276	227	equation 17	equations 18 & 19
B_2	-124	288	269	equation 17	equation 18
P_6	-110	290	259	equation 17	equation 18
B_1	-90	283	77	equation 17	equation 19
M_2	-60	264	112	equation 17	equations 18 & 19
M_3	45	180	28	equation 17	equations 18 & 19
P_1	60	174	91	equation 17	equation 18
P_2	80	165	296	equation 17	equation 19
P_3	100	154	167	equation 17	equation 18
B_3	113	144	271	equation 17	equation 19
P_4	120	137	204	equation 17	equation 18
B_4	134	111	221	equation 17	equation 18
N_1	136	96	217	equations 16 & 17	equation 18
N_2	136	96	6	equations 16 & 17	equation 19
P_5	132	79	97	equation 16	equation 19
M_4	130	77	148	equation 16	equations 18 & 19

(b)

Table 4.4 Sub-branches by θ_1

Position	θ_1	θ_2	θ_5	four-bar loop	five-bar loop
M_1	-134	276	227	equation 17	equations 18 & 19
B_2	-124	288	269	equation 17	equation 18
P_6	-110	290	259	equation 17	equation 18
B_1	-90	283	77	equation 17	equation 19
M_2	-60	264	112	equation 17	equations 18 & 19
M_3	45	180	28	equation 17	equations 18 & 19
P_1	60	174	91	equation 17	equation 18
P_3	100	154	167	equation 17	equation 18
P_4	120	137	204	equation 17	equation 18
B_4	134	111	221	equation 17	equation 18
N_1	136	96	217	equations 16 & 17	equation 18
P_5	132	79	97	equation 16	equation 19
M_4	130	77	148	equation 16	equations 18 & 19
P_2	80	165	296	equation 17	equation 19
B_3	113	144	271	equation 17	equation 19
N_2	136	96	6	equations 16 & 17	equation 19

Table 4.5 Order of motion

Position	θ_1	θ_2	θ_5	four-bar loop	five-bar loop
M_1	-134	276	227	equation 17	equations 18 & 19
B_2	-124	288	269	equation 17	equation 18
P_6	-110	290	259	equation 17	equation 18
M_2	-60	264	112	equation 17	equations 18 & 19
B_1	-90	283	77	equation 17	equation 19
M_3	45	180	28	equation 17	equations 18 & 19
P_1	60	174	91	equation 17	equation 18
P_3	100	154	167	equation 17	equation 18
P_4	120	137	204	equation 17	equation 18
B_4	134	111	221	equation 17	equation 18
N_1	136	96	217	equations 16 & 17	equation 18
M_4	130	77	148	equation 16	equations 18 & 19
P_5	132	79	97	equation 16	equation 19
N_2	136	96	6	equations 16 & 17	equation 19
B_3	113	144	271	equation 17	equation 19
P_2	80	165	296	equation 17	equation 19

Table 4.6 Sub-branches by θ_5

Position	θ_1	θ_2	θ_5	four-bar loop	five-bar loop
M_1	-134	276	227	equation 17	equations 18 & 19
B_2	-124	288	269	equation 17	equation 18
P_6	-110	290	259	equation 17	equation 18
M_2	-60	264	112	equation 17	equations 18 & 19
B_1	-90	283	77	equation 17	equation 19
P_2	80	165	296	equation 17	equation 19
M_3	45	180	28	equation 17	equations 18 & 19
P_1	60	174	91	equation 17	equation 18
P_3	100	154	167	equation 17	equation 18
P_4	120	137	204	equation 17	equation 18
B_4	134	111	221	equation 17	equation 18
N_1	136	96	217	equations 16 & 17	equation 18
M_4	130	77	148	equation 16	equations 18 & 19
P_5	132	79	97	equation 16	equation 19
N_2	136	96	6	equations 16 & 17	equation 19
B_3	113	144	271	equation 17	equation 19

Order of motion in a branch:

In each sub-branch the configurations appear in the descending or ascending order of the input values. In an identical branch, if the order of the input values reverses from a sub-branch to

the adjoining sub-branch, then the order of the appearance of the configurations throughout the entire branch cycle can be obtained.

Sort each sub-branch by the ascending or descending order of the θ_1 values. The θ_1 values in the adjoining sub-branch must ascend or descend in the opposite direction. For example, in branch M_3M_4, the sorting order reverses at the singular points N_1 and N_2 as well as the branch points M_3 and M_4. After sorting, all configurations in a branch will appear in the order listed in Table 4.5 throughout the entire branch cycle.

Sub-branch identification with input not given through the four-bar loop:

If the input is not given through a joint in the four-bar loop, the branch points and the singular points from the four-bar loop are generally not dead center positions. This situation occurs if the input is given through θ_5 (Fig. 4.5). In such a situation, all dead center positions B_1, B_2, B_3, and B_4 can be found [27] and included in Tables 4.3 to 4.5. The configurations between adjacent dead center positions are in the same sub-branch. In Table 4.5, one may reorganize the order of the appearance of the configurations by placing a dead center position as the starting position in each branch as shown in Table 4.6. It becomes obvious that the M_1M_2 branch cycle is completed in the order of (M_1, B_2, P_6, M_2, and B_1), in which B_2 and B_1 divide the branch into two sub-branches. Likewise, the M_3M_4 branch cycle proceeds in the order of (P_2, M_3, P_1, P_3, P_4, B_4, N_1, M_4, P_5, N_2, and B_3), in which B_4 and B_3 divide the branch into two sub-branches.

For any choice of the input joints, all dead center positions can be found [27]. By inserting the dead center positions in the list of the order of motion, such as the one in Table 4.6, the sub-branches in each branch and the order of motion in each sub-branch are obtained automatically. The above method is general and applicable to any number of sub-branches in a branch. It applies to both ordinary and virtual Stephenson linkages.

4.5 Conclusions

With the concept of virtual loops, spatial mechanisms can be regarded as multiloop planar or spherical linkages containing one or more virtual loops. It is suggested that although the physical construction of a spatial linkage may bear little or no similarity with planar or spherical linkages, there is striking similarity or compatibility in their intrinsic mobility characteristics and analysis. Under the concept of virtual loops, two types of spatial group 2 mechanisms can be modeled as Stephenson-type linkages where findings for planar Stephenson linkages can be used directly. The developed criteria on virtual loops may be regarded as the generalization of N-bar rotatability laws, which is suitable to treat all typical mobility issues of both ordinary and virtual Stephenson linkages. This dissertation establishes a unified view on planar, spherical, and spatial linkages and a useful model to view or even understand complex spatial linkages.

REFERENCES

1. Duffy, J., 1980, *Analysis of Mechanisms and Robot Manipulators*, New York, John Willey and Sons.
2. Mirth, J.A. and Chase, T.R., 1992, "Circuit Rectification for Four Precision Position Synthesis of Stephenson Six-bar Linkages," *ASME Mechanical Design and Synthesis*, DE-Vol.46, pp.359–366.
3. Chase, T.R. and Mirth, J.A., 1993, "Circuits and Branches of Single Degree-of-freedom Planar Linkages," *ASME J. of Mechanical Design*, Vol.115, pp.223–230.
4. Mirth, J.A. and Chase, T.R., 1993, "Circuit Analysis of Watt Chain Six-bar Mechanisms," *Journal of Mechanical Design, Transactions Of the ASME*, Vol.115, n 2, pp.214–222.
5. Davis, H.P., Chase, T.R. and Mirth, J.A., 1994, "Circuit Analysis of Stephenson Chain Six-bar Mechanisms," *ASME Mechanism Synthesis and Analysis*, DE-Vol.70, pp.349–358.
6. Davis, H.P. and Chase, T.R., 1994, "Stephenson Chain Branch Analysis: Four Generic Stationary Configurations and One New Linkage Polynomial," *ASME Mechanism Design and Synthesis*, DE-Vol.70, pp.359–367.
7. Mirth, J.A. and Chase, T.R., 1995, "Circuit Rectification for Four Precision Position Synthesis of Four-bar and Watt Six-bar Linkages," *Journal of Mechanical Design, Transactions of the ASME*, Vol.117, n 4, pp.612-619.
8. Ting, K.L. and Dou, X.H., 1996, "Classification and Branch Identification of Stephenson Six-bar Chains," *Mechanism and Machine Theory*, Vol.31, Issue 3, pp.283-295.
9. Grashof, F., 1983, *Theoretische Maschinenlehre*, Leipzig.
10. Ting, K.L., 1989, "Mobility Criteria of Single-loop N-Bar Linkages," *Journal of Mechanisms, Transmissions, and Automation in Design*, Vol.111, n4, pp.504-507.
11. Ting, K.L., and Liu, Y.W., 1991, "Rotatability Laws for N-Bar Kinematic Chains and Their Proof," *Journal of Mechanical Design*, Vol.113, No.1, pp.32-39.
12. Shyu, J.H. and Ting, K.L., 1994, "Invariant Link Rotatability of N-Bar Kinematic Chains," *Journal of Mechanical Design*, Vol.116, pp.343-347.
13. Ting, K.L., and Liu, Y.W., 1992, "On the Rotatability of Spherical N-Bar Chains," *Journal of Mechanical Design*, Vol. 116, No. 3, 1994, pp. 920-923.
14. Kazerounian, K.; Solecki, R., 1993, "Mobility Analysis of General Bi-modal Four Bar Linkages Based on Their Transmission Angle," *Mechanism & Machine Theory*, v 28, n 3, pp. 437-445.
15. Ting, K.L. and Dou, X.H., 1994, "Branch, Mobility Criteria, and Classification of RSSR and Other Bimodal Linkages," *ASME Mechanism Synthesis and Analysis*, DE-Vol.70, pp.303-310.

16. Su, H.J. Collins, C.L., and McCarthy, M., 2002, "Classification of RRSS linkages," *Mechanism and Machine Theory*, Vol. 37, pp.1413-1433.

17. Nolle, H., 1969, "Range of Motion Transfer by R-G-G-R Mechanisms," *Journal of Mechanisms*, 4, pp.145-157.

18. Gupta, K. C., and Tinubu, S. O., 1983, "Synthesis of Bimodal Generating Mechanisms without Branch Defect," *J. of Mechanisms, Transmissions, and Automation in Design*, Vol. 105, pp. 641-647.

19. Lee, D., Youm, Y., and Chung, W., 1996, "Mobility Analysis of Spatial 4- and 5- Link Mechanisms of the RS Class," *Mechanism and Machine Theory*, Vol. 31, pp.673-690.

20. Ting, K.L. and Shyu, J.H., 1992, "Joint Rotation Space of Five-bar Linkages," *American Society of Mechanical Engineers, Design Engineering Division (Publication), Mechanism Design and Synthesis*, DE-Vol.46, pp.93-101.

21. Ting, K.L., 2008, "On the Input Joint Rotation Space and Mobility of Linkages," *Journal of Mechanical Design*, Vol.130, 092303-1-9.

22. Ting, K.L., 1993, "Branch and Dead Position Problems of N-bar Linkages," *American Society of Mechanical Engineers, Design Engineering Division (Publication)*, DE-Vol.65-2, Advances in Design Automation, pp.459-465.

23. Ting, K.L., 1994, "Mobility Criteria of Geared Five-bar Linkages," *Mechanism and Machine Theory*, Vol.29, No.2, pp.251-264.

24. Dou, X.H. and Ting, K.L., 1996, "Branch Identification of Geared Five-bar Chains," *Journal of Mechanical Design, Transactions of the ASME*, Vol.118, No.3, pp.384-389.

25. Dou, X.H., 1996, *Mobility Analysis and Branch Identification of Multiloop and Spatial Linkages/Manipulators*, PhD Dissertation, Tennessee Technological University.

26. Ting, K. L., Xue C., Wang, J., and Currie, K. R., 2007, "General Mobility Identification and Rectification of Watt Six-Bar Linkages," *Proceedings of IDETC/CIE 2007 ASME Design Engineering Technical Conferences and Computers and Information in Engineering Conference*.

27. Ting, K.L., Wang, J., Xue, C., and Currie, K.R., 2008, "Full Rotatability of Stephenson Six-Bar and Geared Five-Bar Linkages," *Proceedings of IDETC/CIE 2008*, Brooklyn, NY.

28. Ting, K.L., Wang, J., and Xue, C., 2009, "Unified Mobility Identification and Rectification of Planar Six-Bar Linkages," *Proceedings of IDETC/CIE 2009*, San Diego, California..

29. Crane III, C.D. and Duffy, J., 2008, *Kinematic Analysis of Robot Manipulators*, New York, Cambridge University Press.

30. Denavit, J. and Hartenberg, R.S., 1964, *Kinematic Synthesis of Linkages*, New York, McGraw-Hill Book Company.

31. Vidyasagar, M. and Spong, M., 1989, *Robot Dynamics and Control*, New York, John Wiley and Sons.

32. Freudenstein, F., and Primrose, E.J.F., 1976, “On the Criteria for the Rotatability of the Cranks of a Skew Four-Bar Linkage,” *ASME Journal of Engineering for Industry*, pp. 1285-1288.

33. Gupta, K.C., 1978, “A General Theory for Synthesizing Crank-Type Four-Bar Function Generator With Transmission Angle Control,” *ASME Journal of Applied Mechanics*, Vol. 45, pp. 415-421.

34. Kohli, D., Cheng, J.C. and Tsai, K.Y., 1994, “Assimilability, Circuits, Branches, Locking Positions, and Rotatability of Input Links of Mechanisms with Four Closures,” *Journal of Mechanical Design, Transaction of ASME*, Vo1.116, pp.92-98.

35. Pamidi, P.R. and Freudenstein, F., 1975, “On the Motion of A Class of Five-Link, R–C–R–C–R, Spatial Mechanisms,” *ASME J. Eng. Ind.*, 97 (1), pp.334–339.

36. Midha, A., Zhao, Z., and Her, I. 1985, "Mobility Conditions for Planar Linkages Using Triangle Inequality and Graphical Interpretation," *Journal of Mechanisms, Transmissions, and Automation in Design*, Vol.107, No. 3, pp. 394-400.

37. Dou, X., and Ting, K.L., 1996, "Classification, Rotatability and Branch Identification of Simple RCRCR Mechanisms," *ASME Design Engineering technical Conferences and the Computer in Engineering*, paper No. 96-DETC/FAS-1363.

38. Yan, H.S., and Wu, L.L., 1989, “On the Dead-Center Positions of Planar Linkages Mechanisms,” *ASME Journal of Mechanisms, Transmissions, and Automation in Design*, Vol.111, pp.40-46.

CHAPTER 5

ON THE BRANCH FORMATION OF SPATIAL GROUP 2 LINKAGES[3]

ABSTRACT

A spatial linkage with the displacement governed by two fundamental equations can be regarded as a virtual double loop system. The mobility of the linkage is affected by the mobility of each individual "loop" as well as the interaction between the loops. The current use of branch points for branch identification is limited to linkages with simple topology, such as Stephenson-type linkages, which are simplified versions of group 2 mechanisms. However, in a general spatial group 2 linkage, both the fundamental equations are equivalent to virtual five-bar loops. Branch points in Stephenson-type linkages should be generalized to explain and define the interaction between two virtual five-bar loops. The concept of generalized branch points offers the explanation of how branches are formed in spatial group 2 linkages. This dissertation presents the theoretical background for the mobility analysis of complex spatial linkages.

[3] Accepted by the ASME 2009 International Design Engineering Technical Conferences & Computers and Information in Engineering Conference (IDETC/CIE), August 30 – September 2, 2009, San Diego, California, USA.

5.1 Introduction

For many decades, the understanding of the mobility of conventional closed-loop linkages had been mostly restricted to planar and spherical four-bar linkages. Generally, for geometric properties found in planar linkages, similar properties can also be expected in spherical linkages. The mobility study of four-bar linkages may be traced back to the discovery of the Grashof criterion [1], which is commonly used to predict the full rotatability of four-bar linkages. The most significant advancement in linkage mobility research are the N-bar rotatability laws [2-5]. The N-bar rotatability laws offer the first simple, complete, and systematical explanation for the rotatability of any N-bar chain ($N \geq 3$) connected with revolute joints, in which the Grashof criterion becomes a very special case. The N-bar rotatability laws govern and predict the formation of branches, sub-branches, and full rotatability of any single-loop planar and spherical N-bar chain. However, the mobility analysis becomes more complex for multiple loop linkages, where mobility is affected by not only each individual loop, but also the interaction among loops.

The concepts of joint rotation space (JRS) [6] and branch points [7] were first used to resolve the mobility problems of Stephenson six-bar linkages. They are simple and straightforward for the branch identification of Stephenson [7] and Watt six-bar chains [8] without invoking coupler curves. JRS represents the domain of the input variables of a linkage or a loop. Ting [9] detailed the concepts of JRS sheets and sides as well as branch points to offer geometric insights on how mobility between loops interact each other and thus the mobility formation of linkages. The sheets and sides of a JRS provide an intuitive model to explain the relationship among branches, sub-branches, and singularities. Each side of a JRS sheet represents a one-to-one correspondence between the input and the output and also an input domain free from any discontinuity and

singularity. So far, JRS is the most effective and vital tool or model to understand the formation of branch and sub-branches of multiloop linkages.

The concept of virtual loops [10] suggests that single loop spatial linkages may be regarded and treated as multiloop spherical linkages. Ting showed that a simple RCRCR mechanism and some spatial group 2 linkages with parallel joint axes are completely compatible to Stephenson six-bar linkages from the viewpoint of linkage mobility and displacement analysis [10]. Their mobility analysis can be conducted exactly in the same way for Stephenson six-bar linkages. However, simple RCRCR and spatial group 2 with parallel joint axes are linkages with simple topology; they are simplified versions of spatial group 2 linkages. A more general definition of branch points is sought to explain the branch formation of linkages.

5.2 Spherical Indicatrix and Virtual Loop

Each spatial linkage connected with revolute or cylindrical joints has a spherical indicatrix [11], which is formed by bringing all joint axes to intersect at a common point. Fig. 5.1 shows an RCRCR mechanism and its corresponding spherical indicatrix. The spherical indicatrix may be regarded as a constraint imposed on the spatial mechanism by the angular displacements. Besides this constraint, on the orthogonal directions of the three dimensional space, three additional conditions are induced by the presence of joint offsets and skew distance between joint axes. Mathematically all equations derived from the spherical indicatrix as well as the three additional constraint conditions lead to a single degree-of-freedom (DOF) spatial mechanism.

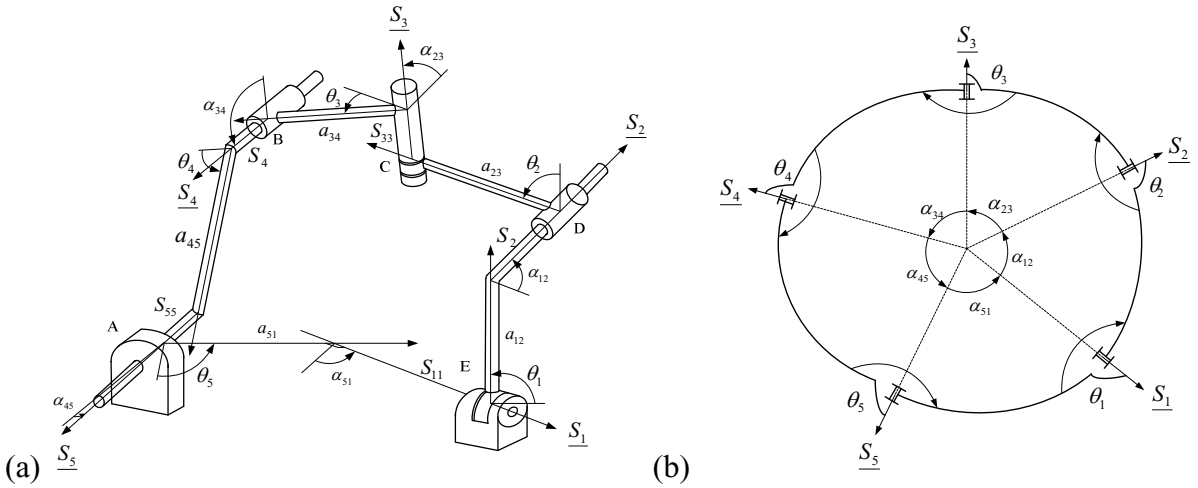

Figure 5.1 (a) An RCRCR mechanism and (b) the spherical indicatrix

The concept of virtual loops is introduced by its mathematical form rather than its physical appearance. With the concept of virtual loops, a unified linkage classification scheme based on the number of (virtual) loops becomes apparent. Each spatial group 1, 2, 3, or 4 mechanism can be regarded as a virtual spherical linkage formed by one or more virtual loops. The fact that all of Duffy's group 1 linkages and planar and spherical four-bar linkages are bimodal linkages and the fact that simple RCRCR and spatial group 2 with parallel joint axes are completely compatible with Stephenson six-bar linkages are consistent with the proposed virtual loop concept.

The geometry or mobility of a virtual loop in a virtual multiloop linkage is expressed by the fundamental equation (the virtual "loop-closure" equation), which can be written in the form of

$$A\sin\theta_o + B\cos\theta_o + C = 0 \qquad (5\text{-}1)$$

where θ_o is the output variable and A, B, and C are functions of the input joint variable θ_i.

5.2.1 N-bar Rotatability Laws and Mobility Criteria of Virtual Loops

The N-bar rotatability laws [2-5] govern and predict the mobility of single loop planar and spherical linkages. In the N-bar rotatability laws, the rotatability of a linkage is viewed from the entire chain rather than from a linkage that has a narrow scope limited by the fixed link. Therefore, the variety of mobility considerations due to different linkage inversions is eliminated; the joint rotatability in a chaotic N-bar chain suddenly becomes easy to understand. Ting classified single loop chains into three classes. A Class I chain has two branches while a Class II chain has only one branch. Therefore the branch problem does not exist in Class II chains. Class III is a transitional type between Class I and II chains.

The virtual "loop-closure" equation (Eq. 5-1) can be expressed in quadratic form. Any virtual four-bar loop can be classified into Class I, II, or III by using the discriminant function [10, 12]. By varying the value of the intermediate joint parameter, any virtual five-bar loop can be treated as a family of virtual four-bar loops. If all virtual four-bar loops of the family are Class I, then this virtual five-bar loop is Class I; otherwise it is Class II or III [10]. Since all fundamental equations for planar, spherical, and spatial linkages can be expressed in quadratic form, the mobility criteria of virtual loops may be regarded as the generalization of the N-bar rotatability laws.

5.2.2 Dead Center Positions

At a dead center position, the derivative of the output with respect to the input becomes infinite [13]; the input link reaches its rotation limit; and the linkage may be out of control

momentarily [14]. Generally, the input-output (I/O) relationship between any pair of joint parameters of a linkage can be expressed by a polynomial equation [15]. Therefore, all of the dead center positions of single-DOF linkages, disregarding whichever joint is used as the input joint, can be found by solving a polynomial equation [15].

Let $y = \tan\frac{\theta_o}{2}$ and $\cos\theta_o = \frac{1 - y^2}{1 + y^2}$, $\sin\theta_o = \frac{2y}{1 + y^2}$. Eq. 5-1 can be converted as

$$(C - B)y^2 + 2Ay + (C + B) = 0 \qquad (5\text{-}2)$$

At a dead center position, the input and output relationship equation should have equal roots for a given input. Thus, the discriminant of the above equation should vanish, which leads to a polynomial equation in terms of the input parameter only [16].

$$\Delta = A^2 - (C - B)(C + B) = 0 \qquad (5\text{-}3)$$

5.3 Spatial Group 2 Linkages

A spatial group 2 linkage is referred to as a single DOF spatial linkage, which contains R, C, or P joints (R, C, and P refer to the revolute, cylindrical, and prismatic joints used in the linkages) and has a total of five R and C joints [11]. Of a group 2 linkage, the first fundamental equation (say Eq. 5-1(a)) derived from the spherical indicatrix contains the input, output, and one intermediate joint variables, which is equivalent to a five-bar loop. The second fundamental equation (say Eq. 5-1(b)) leads to an additional constraint on the two-DOF spherical indicatrix and therefore creates the effect of an additional loop to the spherical indicatrix to form a single-DOF linkage. A spatial group 2 linkage, consisting of two virtual five-bar loops, is equivalent to and regarded as a double loop linkage.

The linkage mobility is governed by the two fundamental equations and how they influence each other. From the viewpoint of a virtual double loop linkage, since the mobility of each individual loop is governed by the N-bar rotatability laws [2-5] and/or the mobility criteria of virtual loops [10], the central issue in this dissertation is how the interaction between the loops affects the branch formation of the entire linkage.

Table 5.1 Duffy's group 2 mechanisms

Number of links	Mechanism
Five	RCRCR, RRCRC, RCRRC, RCCRR, RRRCC
Six	RRRPCR, RRCPRR, RRRRPC, RPCRRR, RCRPRR, RRCRPR, RRRPRC, RCRRPR, RRPRRC
Seven	RRPRPRR, RPRRPRR, RPRRRPR, RRRRPPR, RRRPPRR

5.3.1 JRS of Spatial Group 2 Linkages

The fundamental equation of any single loop planar/spherical linkage, virtual loop, or spatial group 1 linkage can be expressed in the form of Eq. 5-1 and later be converted as a quadratic equation (Eq. 5-2). The discriminant of this quadratic equation, $\Delta \geq 0$, describes the JRS of a group 1 linkage. $\Delta = 0$ is the singular condition representing the boundary of the input domain, which divides one sheet of JRS into two sides. When an input joint variable is known, the corresponding output joint variable can be solved from Eq. 5-2. The derived solutions represent linkage configurations on two sides of a JRS sheet. In other words, Eq. 5-4(a) is the mathematical expression of one side of a JRS and Eq. 5-4(b) of the other side.

$$y_{1,2} = \frac{-A \pm \sqrt{(A^2 + B^2 - C^2)}}{C - B} \qquad \text{(5-4ab)}$$

Fig. 5.2(a) shows the JRS of a single loop two-DOF linkage obtained through the discriminant function (θ_2 and θ_4 are the two input variables). A spatial group 2 linkage consists of two virtual five-bar loops and is equivalent to a double loop linkage. Each virtual loop has its own JRS. The JRS of any spatial group 2 linkage is the interaction between them (Fig. 5.2(b)).

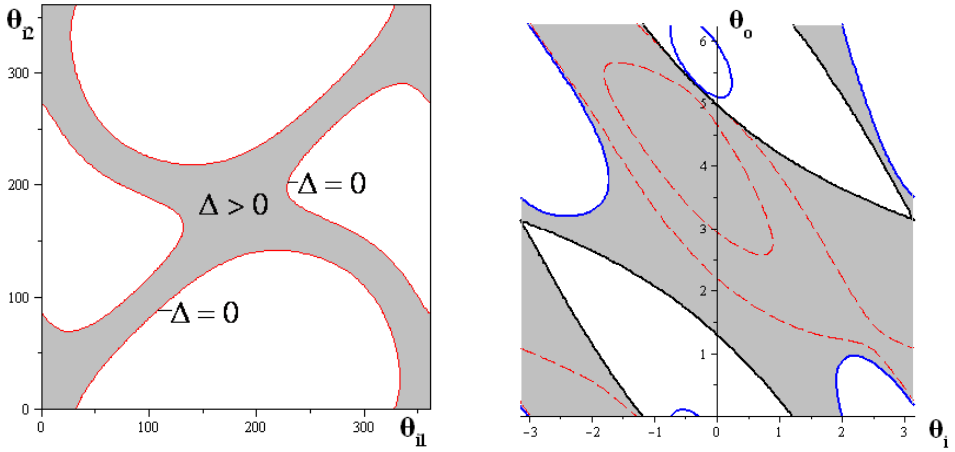

(a) single loop (b) double loops

Figure 5.2 JRS of a spatial group 2 linkage

5.3.2 Branch Points and Stephenson-Type Linkages

If Eq. 5-1(b) does not contain the intermediate joint parameter (say θ_5), it is a curve in the JRS of Eq. 5-1(a). This is the case with Stephenson six-bar linkages [7], Watt six-bar linkages [8], simple RCRCR [17], geared five-bar linkages [18], and some spatial group 2 linkages with parallel joint axes. They represent the simplified version of group 2 linkages, called Stephenson-type linkages [10], in which one of the fundamental equations represents a virtual four-bar loop and the other a virtual five-bar loop. Both loops have two common joint variables and the relationship between both variables is named as the I/O curve of the virtual four-bar loop. For the virtual five-bar loop, although it has two DOF, the JRS of the common joints as the virtual four-bar loop may be a bounded region [10]. The branch points are the intersections of the I/O curve of the virtual four-bar loop and the JRS boundary of the virtual five-bar loop. Since there is no difference in the mathematical treatment of a physical loop and a virtual loop, in the following discussion, the mobility conditions, such as branch, sub-branch, and joint rotatability can be explained and predicted unambiguously and automatically with the JRS properties and the branch points [9]. Branch points are the intersection points between the I/O curve and the JRS boundary curve. They represent how an I/O curve is blocked by the JRS of the five-bar loop to form branches [7]. Fig. 5.3 is a sample showing the mobility chart of a Stephenson-type linkage, where θ_3 and θ_4 are two common joint variables of the two real or virtual loops and branch points at 1 to 6 divide the I/O curve into three branches, 1-2, 3-4, and 5-6. The concept of branch points offers an explicit explanation and unambiguous prediction of the branch formation or continuity of all Stephenson-type linkages [7, 8, 10, 17, 18].

However, in a general spatial group 2 linkage, both the fundamental equations are equivalent to virtual five-bar loops. The I/O curve of a general spatial group 2 linkage is always contained in the JRS of each individual five-bar loop, so there is no intersection between the I/O curve and the JRS boundary curve. In other words, branch points in Stephenson-type linkages cannot explain and define the interaction between two virtual five-bar loops. The concept of branch points should be generalized to explain the branch formation of general group 2 linkages. Examining Fig. 5.3(b) with the concept of JRS sheets and sides [9], one may realize that each segment of the I/O curve actually represents two overlapping curves and each point, except the branch points, on the I/O curve represents two configurations. Since a branch point represents only one configuration, it is a double root between two curves. In other words, a branch point should be a tangent point between curves in a general group 2 linkage.

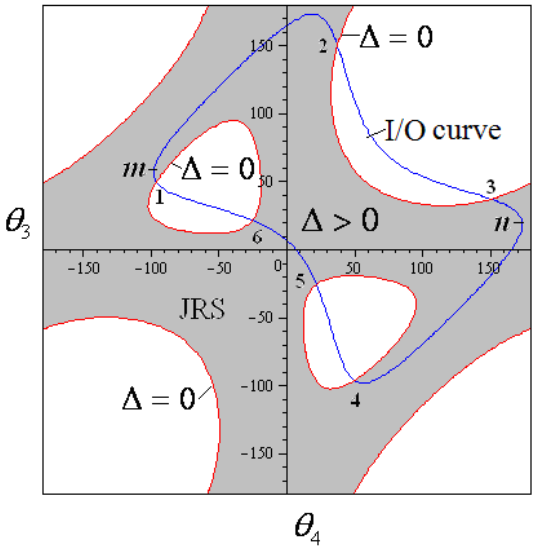

Figure 5.3 JRS, branches, and branch points of a Stephenson-type linkage

5.3.3 Tangent Points and Spatial Group 2 Linkages

Let θ_1 and θ_5 be the two common joint variables in Eq. 5-1 and θ_3 the output variable. Eq. 5-1 represents two surfaces in the input/output domain. The intersection of these two surfaces is the I/O curve, which describes the relationship between the input and output variables, say θ_1 and θ_3, respectively. Unlike group 1 linkages whose mobility can be derived from the input and output relationship, the I/O curves can be very complicated for group 2 linkages. Duffy used six curves depicting the variation of all joint variables with respect to the input parameter to express the true mobility or configuration variation of spatial linkages [11].

Any group 2 spatial linkage is governed by two fundamental equations. By varying the θ_5 value, Eq. 5-1(a) yields a family of curves representing the JRS of one virtual loop, so does Eq. 5-1(b). On the other hand, both fundamental equations represent a pair of curves if the value of θ_5 is given. For a given θ_5 value, if both curves do not intersect, no linkage configuration can be formed (Fig. 5.4(a)); if they intersect, the intersection points must be on the θ_1 vs. θ_3 curves, (also called I/O curve) of the linkage (Fig. 5.4(b) and (c)). The I/O curve is the locus of the intersection points of the curves corresponding to possible θ_5 values. As the value of θ_5 varies, the pair of curves representing Eq. 5-1 may evolve from non-intersecting to tangent and then to intersecting (Fig. 5.4). In other words, the linkage configuration may evolve from non-existence to existence (at the tangent point) and then to the formation of an entire branch.

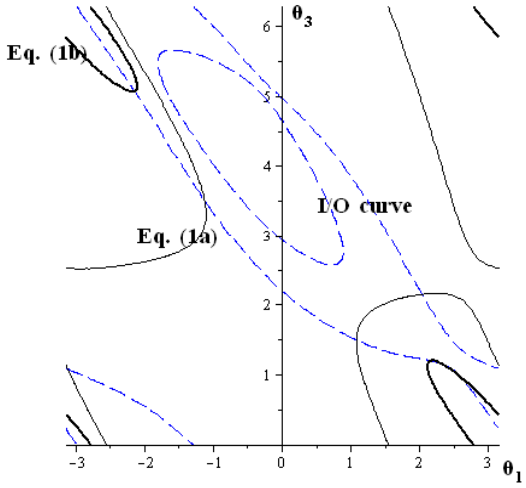

(a) no intersection point

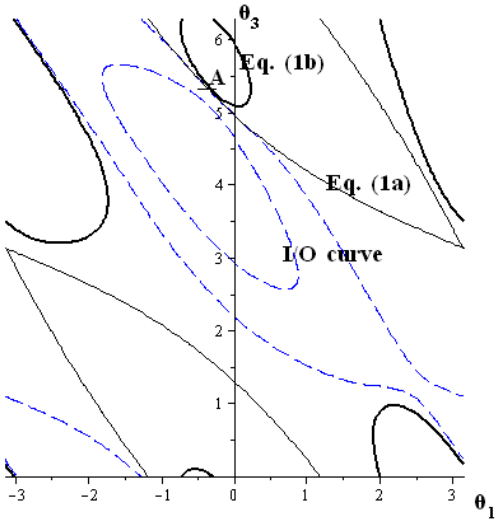

(b) one tangent point

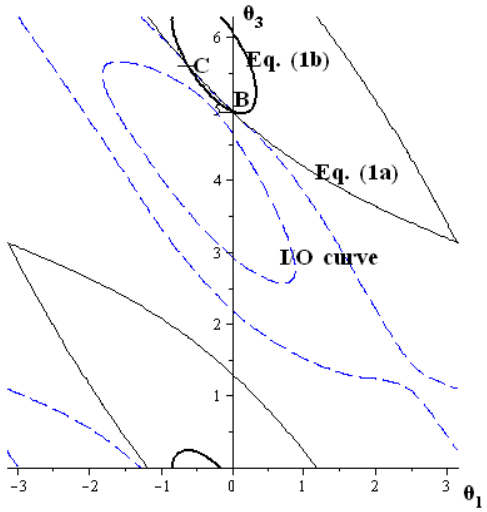

(c) two intersection points

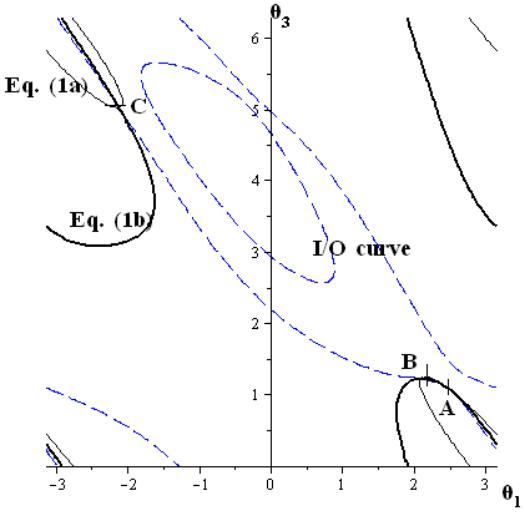

(d) one tangent and two intersection points

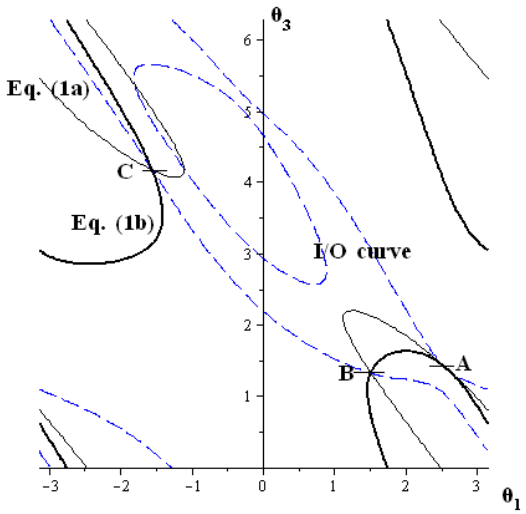

(e) one tangent and two intersection points

Figure 5.4 Formation of tangent points

The branch formation starts and ends at tangent points, therefore, tangent points contain the branch information of general group 2 linkages. They are the counterpart of branch points for Stephenson-type linkages. A tangent point may co-exist with other intersection points or even tangent point.

The input-output displacement equation, i.e. the I/O curve, can be obtained via both fundamental equations (Eq. 5-1(a) and (b)) by eliminating the intermediate variable θ_m.

$$f(\theta_i, \theta_o) = 0 \qquad (5\text{-}5)$$

where θ_i and θ_o are the input and output variables, respectively.

From the two fundamental equations, one may obtain

$$\frac{\partial(A_1 \sin\theta_o + B_1 \cos\theta_o + C_1)}{\partial\theta_i} = h_1 \,,\ \frac{\partial(A_1 \sin\theta_o + B_1 \cos\theta_o + C_1)}{\partial\theta_o} = h_2$$

$$\frac{\partial(A_2 \sin\theta_o + B_2 \cos\theta_o + C_2)}{\partial\theta_i} = h_3 \,,\ \frac{\partial(A_2 \sin\theta_o + B_2 \cos\theta_o + C_2)}{\partial\theta_o} = h_4$$

When the pair of curves become tangent to each other,

$$h_1 h_4 = h_2 h_3 \,. \qquad (5\text{-}6)$$

Because the tangent points are also on the I/O curve, the tangent points must satisfy Eqs. 5-5 and 5-6 simultaneously.

5.3.4 Property of Tangent Points

The branch formation starts and ends at tangent points, but not all tangent points are the branch starting or ending points in general group 2 linkages. Reading and interpreting the tangent points will be the pivotal and fundamental issues in the mobility analysis of spatial group 2

linkages. To be consistent with the Stephenson linkages, the tangent points, which are branch starting or ending points in general group 2 linkages, are called branch points.

For one tangent point, if one and only one pair of input and output joint variables (θ_i and θ_o), i.e., one solution, is derived when its intermediate joint parameter θ_m is substituted back to the two fundamental equations of the group 2 linkage, then the tangent point is definitely a branch point (Fig 5.4(b)). In other words, if one tangent point does not co-exist with other intersection points, it is a branch point.

For one tangent point, if more than one pair of input and output joint variables (θ_i and θ_o), i.e., more than one solution, are derived when its intermediate joint parameter θ_m is substituted back to the two fundamental equations of the group 2 linkage, then the tangent point co-exists with other intersection points. If the tangent point can reach at least one intersection point continuously, then this tangent point is not a branch point (Fig 5.4(d)); otherwise it is a branch point (Fig 5.4(e)).

As same as in Stephenson linkages, every two branch points will form a branch in spatial group 2 linkages.

5.4 Examples

In example 1, the branch points and tangent points of a Stephenson-type linkage (spatial group 2 linkage with parallel joint axes) are computed based on the concepts of branch points and tangent points to show the consistency of both concepts. Examples 2 and 3 show general group 2 mechanisms. Tangent points are computed and branch points are identified with the property of tangent points.

Example 1:

An RRCCR with parallel joint axes ($\alpha_{45} = 0^o$) is shown schematically in Figure 5.7(a). The axes of the joints R, R, C, C, and R are labeled 1, 2, 3, 4, and 5 in order. The input angular displacement is θ_1. The remaining six variables are the angular displacements θ_2, θ_3, θ_4, θ_5, and the slider displacements S_3 and S_4. By using the D-H notation [19, 20], $\alpha_{12} = 242^o$, $\alpha_{23} = 73^o$ $\alpha_{34} = 264^o$, $\alpha_{45} = 0^o$, and $\alpha_{51} = 286^o$ are the angles between the corresponding joint axes, $a_{12} = 12$, $a_{23} = 29.5$, $a_{34} = 15.8$, $a_{45} = 39$, and $a_{51} = 22$ are the distance between the corresponding joint axes, and S_{11} = 38, S_{22} = 24, and S_{55} = 53.5 are the offset along the corresponding R-joint axes.

The two fundamental equations derived by following Duffy's sine, sine-cosine, and cosine laws [11, 21] are

$$91.93\sin\theta_1\sin\theta_2 + (43.16\cos\theta_1 - 23.27)\cos\theta_2 + (24.81\cos\theta_1 - 6.67) = 0 \qquad \text{(5-7a)}$$

$$\begin{aligned}&(37.30\sin\theta_5\cos\theta_1 + 10.28\cos\theta_5\sin\theta_1 - 2.49\sin\theta_1 - 24.57\cos\theta_1 - 5.59)\sin\theta_2\\ &+(-17.5\sin\theta_5\sin\theta_1 + 4.83\cos\theta_5\cos\theta_1 + 31.65\cos\theta_5 - 5.66\sin\theta_1 + 10.19\cos\theta_1 + 21.69)\cos\theta_2\\ &+(-10.07\sin\theta_5\sin\theta_1 + 2.78\cos\theta_5\cos\theta_1 - 5.15\cos\theta_5 + 9.43\sin\theta_1 + 23.66\cos\theta_1 - 13.97) = 0\end{aligned} \qquad \text{(5-7b)}$$

Because of the parallelism between axes 4 and 5, Eq. 5-7(a) derived from the spherical indicatrix is a virtual four-bar loop while Eq. 5-7(b) is a virtual five-bar loop.

Branch points from the JRS method

Let $x = \tan\frac{\theta_5}{2}$ and $\cos\theta_5 = \frac{1 - x^2}{1 + x^2}$, $\sin\theta_5 = \frac{2x}{1 + x^2}$. Eq. 5-7(b) can be written in quadratic form as

$$
\begin{aligned}
&(5.36\cos\theta_2\cos\theta_1 - 12.77\sin\theta_2\sin\theta_1 - 24.57\sin\theta_2\cos\theta_1 - \\
&5.66\cos\theta_2\sin\theta_1 + 9.43\sin\theta_1 + 20.89\cos\theta_1 - 5.59\sin\theta_2 - 9.96\cos\theta_2 - 8.82)x^2 \\
&+ (74.60\sin\theta_2\cos\theta_1 - 35.02\cos\theta_2\sin\theta_1 - 20.14\sin\theta_1)x \\
&+ (15.02\cos\theta_2\cos\theta_1 + 7.78\sin\theta_2\sin\theta_1 - 24.57\sin\theta_2\cos\theta_1 - \\
&5.66\cos\theta_2\sin\theta_1 + 9.43\sin\theta_1 + 26.43\cos\theta_1 - 5.59\sin\theta_2 + 53.34\cos\theta_2 - 19.12) = 0
\end{aligned}
\tag{5-8}
$$

The singularity appears when the discriminant of the above quadratic equation is equal to zero.

$$
\begin{aligned}
&\Delta = (74.60\sin\theta_2\cos\theta_1 - 35.02\cos\theta_2\sin\theta_1 - 20.14\sin\theta_1)^2 \\
&- 4*(5.36\cos\theta_2\cos\theta_1 - 12.77\sin\theta_2\sin\theta_1 - 24.57\sin\theta_2\cos\theta_1 - \\
&5.66\cos\theta_2\sin\theta_1 + 9.43\sin\theta_1 + 20.89\cos\theta_1 - 5.59\sin\theta_2 - 9.96\cos\theta_2 - 8.82) \\
&*(15.02\cos\theta_2\cos\theta_1 + 7.78\sin\theta_2\sin\theta_1 - 24.57\sin\theta_2\cos\theta_1 - \\
&5.66\cos\theta_2\sin\theta_1 + 9.43\sin\theta_1 + 26.43\cos\theta_1 - 5.59\sin\theta_2 + 53.34\cos\theta_2 - 19.12) = 0
\end{aligned}
\tag{5-9}
$$

Eq. 5-9 represents the JRS boundary of the virtual five-bar loop. Let θ_2 be the output joint variable and θ_5 the intermediate joint variable. Then, Eq. 5-7(a) is the input-output displacement equation, representing the I/O curve of this linkage. Branch points (θ_1, θ_2), which are the intersections of the I/O curve and the JRS boundary of the five-bar loop, can be obtained by solving Eqs. 5-7(a) and 5-9 simultaneously. The corresponding θ_5 values can be determined from Eq. 5-7(b). In this example, six branch points, A_1, A_2, A_3, A_4, A_5, and A_6 (Fig. 5.5(a)) are obtained and listed in Table 5.2.

Tangent points from the tangent method

According to the proposed tangent point concept, Eq. 5-7(a) represents a family of curves and so does Eq. 5-7(b), though Eq. 5-7(a) degenerates to a curve. Let θ_5 be the output joint variable and θ_2 the intermediate joint variable. Eq. 5-7(a) and each curve in the family of curves of Eq. 5-7(b) form a pair of curves, which may intersect or tangent to each other if the θ_2 value is in the proper range of rotation.

Table 5.2 Branch points from the JRS method

	θ_1	θ_2	θ_5
A_1	2.39	-2.72	2.73
A_2	0.18	-1.65	1.39
A_3	-2.36	-0.99	1.19
A_4	0.82	-0.25	2.41
A_5	-2.79	2.46	-2.50
A_6	-0.82	3.08	-3.04

Table 5.3 Tangent points from the tangent method

	θ_1	θ_5	θ_2
A_1	2.39	2.73	-2.72
A_2	0.18	1.39	-1.65
A_3	-2.36	1.19	-0.99
A_4	0.82	2.41	-0.25
A_5	-2.79	-2.50	2.46
A_6	-0.82	-3.04	3.08
A_7	0.02	2.10	N/A
A_8	0.02	2.16	N/A
A_9	0.99	1.80	N/A
A_{10}	0.99	1.84	N/A
A_{11}	1.80	-2.45	N/A
A_{12}	1.80	-2.42	N/A
A_{13}	-0.74	2.88	N/A
A_{14}	-0.74	2.95	N/A

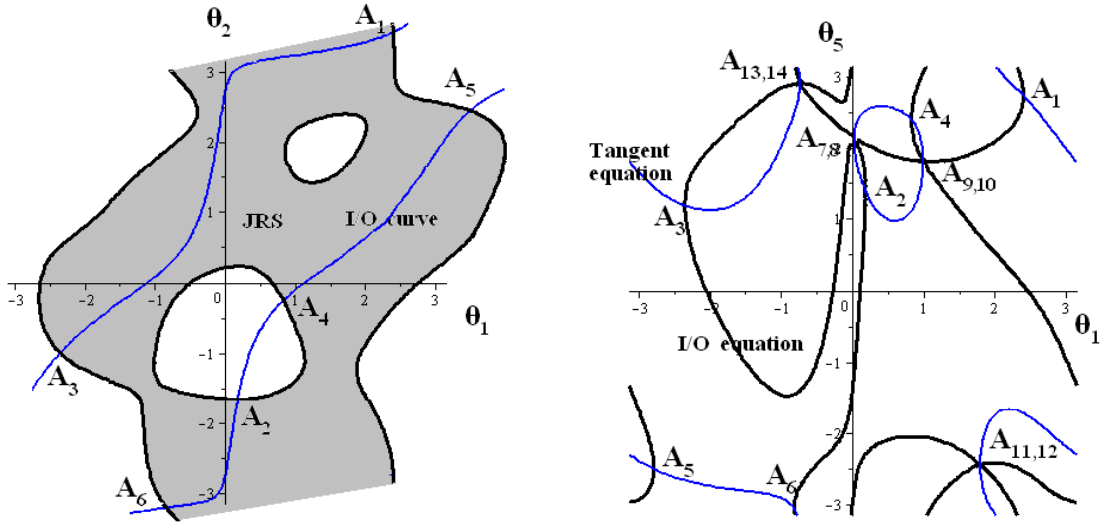

(a) branch points (b) tangent points

Figure 5.5 Branch points vs. tangent points in an RRCCR with parallel joint axes

Since Eq. 5-7(a) does not contain the output joint variable θ_5, its partial derivative with respect to θ_5, i.e. h_2, is equal to zero. When a pair of curves become tangent to each other, the partial derivative of Eq. 5-7(b) with respect to θ_5, i.e. h_4, must be equal to zero, too. This tangent equation combined with the input-output displacement equation will determine the tangent points (θ_1, θ_5) (see section 5.3.3) and the corresponding θ_2 values can be determined from Eq. 5-7. In this example, six tangent points, A_1, A_2, A_3, A_4, A_5, and A_6 (Fig. 5.5(b)) are found and listed in Table 5.3. Points A_7 through A_{14} in Table 5.3 are spurious solutions because their corresponding θ_2 values do not exist.

For each tangent point in this example, only one pair of input and output joint variables (θ_1 and θ_5), i.e., one solution, is derived when its intermediate joint parameter θ_2 is substituted back to the two fundamental equations (Eqs. 5-7(a) and 5-7(b)) of the group 2 linkage, thus all derived tangent points are branch points. The consistent results between Tables 5-2 and 5-3 demonstrate that tangent points are counterpart of branch points for Stephenson-type linkages. Every two branch points will form a branch. A total of six branch points in this example will form three branches: A_1 and A_3 form one branch; A_2 and A_6 form one branch; A_4 and A_5 form one branch

Example 2:

A general RCRCR mechanism is shown schematically in Figure 5.6(a). The axes of the joints R, C, R, C, and R are labeled 1, 2, 3, 4, and 5 in order. The input and output angular displacements are θ_1 and θ_5 while the intermediate angular displacement is denoted by θ_3. The remaining four variables are the angular displacements θ_2, θ_4 and the slider displacements S_2, S_4. By using the D-H notation [19, 20], $\alpha_{12} = 60^{\circ}$, $\alpha_{23} = 45^{\circ}$ $\alpha_{34} = 35^{\circ}$, $\alpha_{45} = 30^{\circ}$, and $\alpha_{51} = 10^{\circ}$ are the angles between the corresponding joint axes, $a_{12} = 25$, $a_{23} = 30$, $a_{34} = 40$,

$a_{45} = 10$, and $a_{51} = 32$, are the distance between the corresponding joint axes, and $S_{11} = 30$, $S_{33} = 25$, and $S_{55} = 8$ are the offset along the corresponding R-joint axes.

Fundamental equations: The two fundamental equations derived by following Duffy's sine, sine-cosine, and cosine laws [11, 21] are

$$\cos\theta_3 - 0.38 + 1.07\sin\theta_5 \sin\theta_1 - 0.32\cos\theta_1 - 1.05\cos\theta_1 \cos\theta_5 - 0.11\cos\theta_5 = 0 \quad \text{(5-10a)}$$

$$\begin{aligned}&\sin\theta_3 - 3.485\cos\theta_3 - 1.012 - 1.356\sin\theta_5 \sin\theta_1 + 2.442\cos\theta_1 + 1.098\cos\theta_1 \cos\theta_5 \\ &+ 0.666\cos\theta_5 - 1.618\sin\theta_5 \cos\theta_1 - 0.385\sin\theta_1 - 1.603\sin\theta_1 \cos\theta_5 - 0.034\sin\theta_5 = 0\end{aligned} \quad \text{(5-10b)}$$

Tangent points: Following the procedures introduced in section 5.3.3, a total of ten tangent points A_1, A_2, …, A_{10} (θ_1, θ_5) are found (Fig. 5.6(b)) and listed in Table 5-4. The corresponding intermediate joint parameter θ_3 values can be determined by solving Eq. 5-10(a) and (b) simultaneously.

By substituting the value of θ_3 at point A_5, A_6, A_9, or A_{10} back to the two fundamental equations, one and only one solution (θ_1, θ_5) is derived. A_5, A_6, A_9, and A_{10} are definitely branch points, because they do not co-exist with any other intersection points.

For the tangent point A_1, three pair of input and output joint variables (θ_1 and θ_5) are derived when its intermediate joint parameter θ_3 is substituted back to the two fundamental equations (Eq. 5-10(a) and (b)) of the group 2 linkage, in other words, the tangent point A_1 co-exists with other two intersection points. As the tangent point A_1 cannot reach the two intersection points continuously, A_1 is a branch point. Likewise, the tangent point A_2 is a branch point; tangent points A_3, A_4, A_7, and A_8 are not branch points.

Every two branch points will form a branch. A total of six branch points in this example will form three branches: A_5 and A_1 form one branch; A_{10} and A_2 form one branch; A_6 and A_9 form one branch (Fig. 5-6(b)).

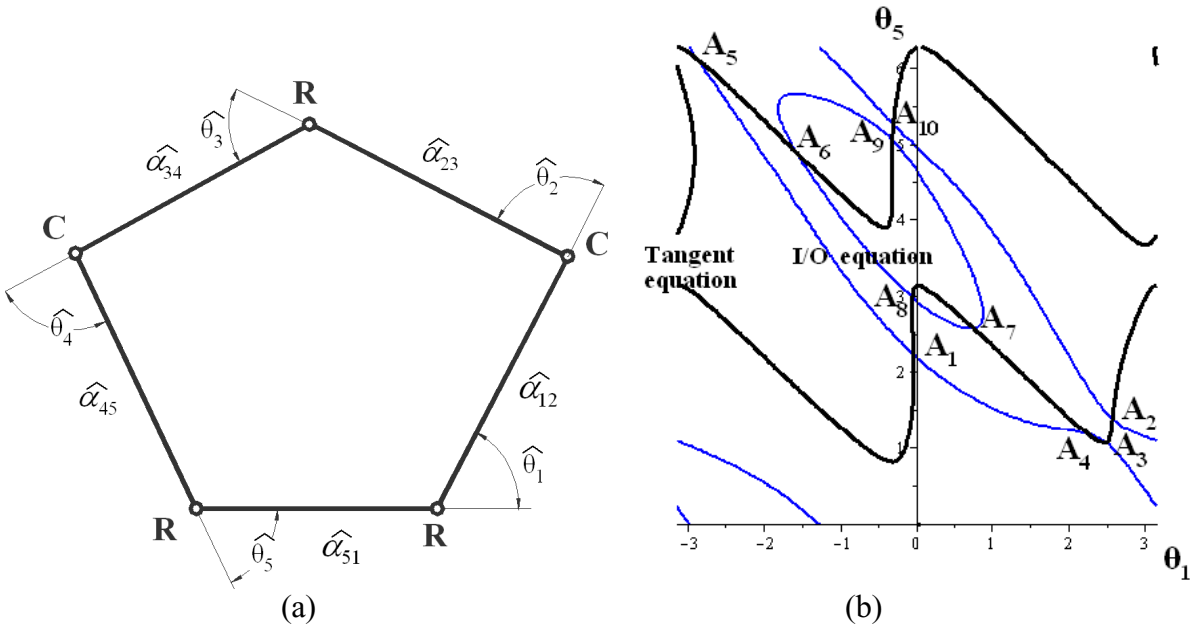

Figure 5.6 (a) General RCRCR mechanism (b) tangent points on I/O curve (θ_1 vs θ_5)

Table 5.4 Tangent points of a general RCRCR mechanism

	θ_1	θ_5	θ_3
A_1	-0.05	2.25	1.55
A_2	2.56	1.39	2.21
A_3	2.48	1.07	2.49
A_4	2.25	1.18	2.50
A_5	-2.87	6.13	2.63
A_6	-1.57	4.90	4.00
A_7	0.75	2.58	4.17
A_8	-0.07	3.00	4.26
A_9	-0.33	5.07	5.54
A_{10}	-0.32	5.27	6.16

Example 3:

The RRCCR mechanism is shown schematically in Figure 5.7(a). The axes of the joints R, R, C, C, and R are labeled 1, 2, 3, 4, and 5 in order. The input and output angular displacements are θ_1 and θ_5 while the intermediate angular displacement is denoted by θ_2. The remaining four variables are the angular displacements θ_3, θ_4 and the slider displacements S_3, S_4. By using the

D-H notation [19, 20], $\alpha_{12} = 60^{o}$, $\alpha_{23} = 45^{o}$ $\alpha_{34} = 35^{o}$, $\alpha_{45} = 30^{o}$, and $\alpha_{51} = 10^{o}$ are the angles between the corresponding joint axes, $a_{12} = 25$, $a_{23} = 30$, $a_{34} = 40$, $a_{45} = 10$, and $a_{51} = 32$ are the distance between the corresponding joint axes, and $S_{11} = 35$, $S_{22} = 15$, and $S_{55} = 0$ are the offset along the corresponding R-joint axes.

Fundamental equations: The two fundamental equations derived by following Duffy's sine, sine-cosine, and cosine laws [11, 21] are

$$\begin{aligned}&(35.3\sin\theta_5\cos\theta_1 + 34.8\cos\theta_5\sin\theta_1 + 10.6\sin\theta_1)\sin\theta_2\\&+ (17.7\sin\theta_5\sin\theta_1 - 17.4\cos\theta_5\cos\theta_1 + 5.32\cos\theta_5 - 5.32\cos\theta_1 - 52.2)\cos\theta_2\\&+ (30.6\sin\theta_5\sin\theta_1 - 30.2\cos\theta_5\cos\theta_1 - 3.07\cos\theta_5 - 9.21\cos\theta_1 - 51.8) = 0\end{aligned} \tag{5-11a}$$

$$\begin{aligned}&(-150.2\sin\theta_5\sin\theta_1 - 167.3\sin\theta_5\cos\theta_1 + 145.1\cos\theta_5\sin\theta_1 +\\&148.0\cos\theta_5\cos\theta_1 - 7.98\cos\theta_5 + 218.7\sin\theta_1 + 45.2\cos\theta_1 + 78.3)\sin\theta_2\\&+ (7.11\sin\theta_5\sin\theta_1 + 114.9\sin\theta_5\cos\theta_{15} + 113.2\cos\theta_5\sin\theta_1 +\\&2.83\cos\theta_5\cos\theta_1 + 129.3\cos\theta_5 + 34.6\sin\theta_1 - 8.63\cos\theta_1 - 172.4)\cos\theta_2\\&+ (5.37\sin\theta_5\sin\theta_1 + 107.2\sin\theta_5\cos\theta_1 + 105.5\cos\theta_5\sin\theta_1 +\\&11.7\cos\theta_5\cos\theta_1 - 38.5\cos\theta_5 + 32.2\sin\theta_1 - 147.5\cos\theta_1 - 26.0) = 0\end{aligned} \tag{5-11b}$$

Tangent points: A total of eight tangent points A_1, A_2, …, A_8 (θ_1, θ_5) are found (Fig. 3.5(b)) and listed in Table 5.5. The corresponding intermediate joint parameter θ_2 values can be determined by solving Eq. 5-11(a) and (b) simultaneously.

By substituting the value of θ_2 at point A_1, A_3, A_4, or A_6 back to the two fundamental equations, one and only one solution (θ_1, θ_5) is derived. A_1, A_3, A_4, and A_6 are definitely branch points, because they do not co-exist with any other intersection points.

For the tangent point A_2, three pair of input and output joint variables (θ_1 and θ_5) are derived when its intermediate joint parameter θ_2 is substituted back to the two fundamental equations (Eq. 5-11(a) and (b)) of the group 2 linkage, in other words, the tangent point A_2 co-exists with

other two intersection points. As the tangent point A_2 cannot reach the two intersection points continuously, A_2 is a branch point. Likewise, the tangent point A_5 is a branch point; tangent points A_7 and A_8 are not branch points.

Every two branch points will form a branch. A total of six branch points in this example will form three branches: A_1 and A_2 form one branch; A_3 and A_4 form one branch; A_5 and A_6 form one branch (Fig. 5-7(b)).

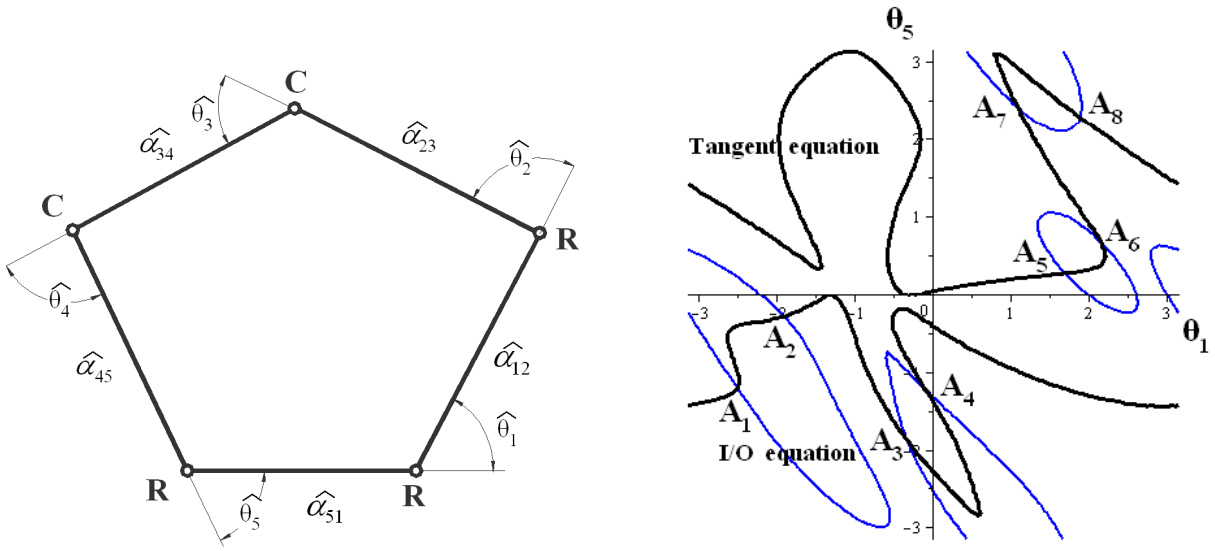

(a) (b)

Figure 5.7 (a) General RRCCR mechanism (b) tangent points on I/O curve (θ_1 vs θ_5)

Table 5.5 Tangent points of a general RRCCR mechanism

	θ_1	θ_5	θ_2
A_1	-2.50	-1.20	1.81
A_2	-1.91	-0.28	3.11
A_3	-0.34	-1.86	-1.79
A_4	-0.09	-1.22	-2.57
A_5	1.69	0.28	3.09
A_6	2.14	0.69	-2.80
A_7	1.08	2.43	-2.15
A_8	1.89	2.29	-1.84

5.5 Conclusions

The current use of branch points for branch identification is limited to Stephenson-type linkages, which are simplified versions of group 2 mechanisms. In this dissertation, tangent points, which can be directly derived from fundamental equations, are sought to explain the branch formation of linkages. As a matter of fact, tangent points are the counterpart of branch points for Stephenson-type linkages. The tangent method is general and can be applied on all group 2 linkages. The discovery of tangent points and the concept of generalized branch points will serve as the building blocks and foundation for the mobility analysis of spatial group 2 linkages and other more complex linkages.

REFERENCES

1. Grashof, F., 1983, *Theoretische Maschinenlehre*, Leipzig.
2. Ting, K.L., 1989, "Mobility Criteria of Single-Loop N-Bar Linkages," *Journal of Mechanisms, Transmissions, and Automation in Design*, pp. 504-507.
3. Ting, K.L. and Liu, Y.W., 1991, "Rotatability Laws for N-Bar Kinematic Chains and Their Proof," *ASME Journal of Mechanical Design*, Vol. 113, No. 1, pp. 32-39.
4. Shyu, J.H. and Ting, K.L., 1994, "Invariant Link Rotatability of N-Bar Kinematic Chains," *Journal of Mechanical Design*, Vol.116, pp.343-347.
5. Ting, K.L., and Liu, Y.W., 1992, "On the Rotatability of Spherical N-Bar Chains," *Journal of Mechanical Design*, Vol. 116, No. 3, 1994, pp. 920-923.
6. Ting, K.L. and Shyu, J.H., 1992, "Joint Rotation Space of Five-bar Linkages," *American Society of Mechanical Engineers, Design Engineering Division (Publication), Mechanism Design and Synthesis*, DE-Vol.46, pp.93-101.
7. Ting, K.L. and Dou, X.H., 1996, "Classification and Branch Identification of Stephenson Six-Bar Chains," *Mechanism and Machine Theory*, Volume 31, Issue 3, pp.283-295.
8. Ting, K. L., Xue C., Wang, J., and Currie, K. R., 2007, "General Mobility Identification and Rectification of Watt Six-Bar Linkages," *Proceedings of IDETC/CIE 2007 ASME Design Engineering Technical Conferences and Computers and Information in Engineering Conference*.
9. Ting, K.L., 2008, "On the Input Joint Rotation Space and Mobility of Linkages," *Journal of Mechanical Design*, Vol.130, 092303-1-9.
10. Ting, K.L., Xue C., Wang, J., and Currie, K.R., "On the Virtual Loops and Virtual Multiloop Linkages," (in preparation).
11. Duffy, J., 1980, *Analysis of Mechanisms and Robot Manipulators*, New York, John Willey and Sons.
12. Ting, K.L. and Dou, X.H., 1994, "Branch, Mobility Criteria, and Classification of RSSR and Other Bimodal Linkages," *ASME Mechanism Synthesis and analysis*, DE-Vol.70, pp.303-310.
13. Hunt, K.H., 1978, *Kinematic Geometry of Mechanisms*, Oxford University Press.
14. Yan, H.S., and Wu, L.L., 1989, "On the Dead-Center Positions of Planar Linkages Mechanisms," *ASME Journal of Mechanisms, Transmissions, and Automation in Design*, Vol.111, pp.40-46.
15. Ting, K.L., Wang, J., Xue, C. and Currie, K.R., 2008, "Full Rotatability of Stephenson Six-Bar and Geared Five-Bar Linkages," *Proceedings of IDETC/CIE 2008*, Brooklyn, NY.
16. Burnside, W.S. and Panton, A.W., 1886, *The Theory of Equations*, Longmans Green Co., London.

17. Dou, X. and Ting, K.L., 1996, “Classification, Rotatability, and Branch Identification of Simple RCRCR Mechanisms,” *ASME Design Engineering Technical Conference and the Computer in Engineering*, Paper No. 96-DETC/FAS-1363.

18. Dou, X. and Ting, K.L., 1996, “Branch identification of geared five-bar chains, Journal of Mechanical Design,” *Transactions of the ASME*, 118 (3), pp.384-389.

19. Denavit, J. and Hartenberg, R.S., 1964, *Kinematic Synthesis of Linkages*, New York, McGraw-Hill Book Company.

20. Vidyasagar, M. and Spong, M., 1989, *Robot Dynamics and Control*, New York, John Wiley and Sons.

21. Crane III, C.D. and Duffy, J., 2008, *Kinematic Analysis of Robot Manipulators*, New York, Cambridge University Press.

CHAPTER 6

ON THE MOBILITY OF SPATIAL GROUP 2 LINKAGES[4]

ABSTRACT

Spatial linkages are classified into four groups according to the number of fundamental equations or virtual loops that govern linkage displacement. The number of virtual loops represents the complexity of a spatial linkage as that of planar or spherical multiloop linkages. The concept of generalized branch points offers the explanation of how branches are formed in spatial group 2 linkages. In this dissertation, the mobility analysis is carried out based on the similarity of the mobility features rather than the specific or individual linkage structure. A branch rectification scheme is presented and demonstrated with examples.

[4] Accepted by the ASME 2009 International Design Engineering Technical Conferences & Computers and Information in Engineering Conference (IDETC/CIE), August 30–September 2, 2009, San Diego, California, USA.

6.1 Introduction

Linkage mobility refers to the problems concerning branch (or circuit [1-6]) defects, full rotatability, sub-branch (or singularities), and order of motion [7]. Linkages are often synthesized to assume the configurations at the desired discrete positions. When a linkage is synthesized, it is necessary to make sure that the linkage has adequate mobility for a continuous and smooth operation. Both the continuity and the smoothness problems may be addressed during the branch rectification process, although it is often a tedious and troublesome process.

For many decades, the understanding of the mobility of conventional closed-loop linkages had been mostly restricted to the Grashof criterion [8], which is used to determine the full rotatability of the input and output links of planar four-bar linkages. Generally, for geometric properties found in planar linkages, similar properties can also be expected in spherical linkages. The success in planar and spherical four-bar linkages was later extended to all bimodal linkages [9-13] and the determination of branch and sub-branches were taken into consideration. An important advancement in linkage mobility are the N-bar rotatability laws [14-17]. The N-bar rotatability laws offer the first simple, complete, and systematical explanation for the rotatability of any N-bar chain ($N \geq 3$) connected with revolute joints, in which the Grashof criterion becomes a very special case.

Table 6.1 Classification of spatial kinematic chains

Group	Number of links	Mechanism
1	4-7	R-3C, 2R-P-2C, 3R-2P-C, 4R-3P
2	5-7	3R- 2C, 4R-P-C, 5R-2P
3	6-7	5R- C, 6R-P
4	7	7R

However, the mobility study of spatial mechanisms is far from adequate. Realizing the large variety and the similarity shared by single degree-of-freedom (DOF) spatial mechanisms, Duffy [18, 19] classified their displacement analysis into four groups (Table 6.1). This elegant classification scheme is useful for a systematic mobility study of spatial mechanisms. The mobility study used to focus on a particular linkage type. Instead, under this classification, a consistent mobility identification method on single DOF closed-loop spatial mechanisms may be established.

Spatial group 1 linkages, including RSSR, RRSS, RCCC, RSCP, RSCR, and 4R3P, where R, S, C, and P refer to the revolute, spherical, cylindrical, and prismatic joints used in the linkages, draw much attention in the mobility research of spatial linkages. The RRSS linkage is an inversion of the RSSR linkage, and the classification strategy for the two is essentially identical. The geometric and algebraic properties of the coupler curves of the RSSR and RCCC mechanisms were presented in [20, 21]. The coupler curve equations were derived in [22] for the spherical four-bar and the RCCC mechanism. The discriminant method was widely used on RSSR, RRSS, and RCCC [10, 11, 23-25]. These linkages are known as bimodal linkages. Like planar four-bar linkages, RSSR can always be classified into three classes according to the possible number of branches [24].

Of group 1 mechanisms, the equations relating the output and input (the input-output displacement equations) can always be expressed in quadratic form, i.e. one input corresponds to two outputs only. However, the input-output displacement equations derived from group 2 mechanisms are usually expressed in high-degree polynomials, leading to more branches and a more complex mobility situation. For example, the polynomials are fourth degree for general RCRCR [26, 27] and eighth-degree for other general group 2 mechanisms [18]. The high-degree

polynomial also represents the existence of many limit points, which in turn makes the mobility analysis difficult [12].

When the offset is zero at the revolute joint between the cylindrical joints, a general RCRCR is degenerated into a special case, named as simple RCRCR. Pamidi and Freudenstein [28] presented conditions for determining the rotatability of input and output links of simple RCRCR mechanism, although the conditions are extremely complicated. The successful approach is displayed in [29], in which the simple RCRCR mechanism is regarded as a spherical 5R linkage with one cylindroid surface constraint formed by a virtual bimodal linkage. The mobility of spatial linkages with four branches was first attributed to Kohli et al [30]. By performing a full displacement analysis through the whole input cycle, they provided a general analytical treatment for determining the assemblability, the rotatability of input links, dead-center positions, and the number of branches. Based on the property of the solutions from the quartic equation, an algorithm was used to identify branches of general RCRCR [31]. A search technique was applied to find the assembly configurations (or branch) of RRRCC, RRCRC, RRRRCR, and RRRRRRR spatial mechanisms [32, 33]. The process is similar to the plot of an input-output displacement equation, which can be directly obtained under the closure equation derived by Duffy [18].

The discussion in this dissertation will focus on group 2 mechanisms. The concept of virtual loops [34] is used to highlight the mobility similarity to planar or spherical multiloop linkages. The concepts of joint rotation space (JRS) [35, 36] as well as the generalized branch points [37] are used to explain the branch formation of linkages. This dissertation presents the mobility analysis scheme of group 2 linkages, which may be regarded as advancement to the mobility analysis of complex linkages.

6.2 Important Concepts

Since some essential concepts described in this paper are either just or yet to be published, the following terminologies, concepts, and practices are explained and outlined below.

6.2.1 Spherical Indicatrix and Virtual Loop

Each spatial linkage connected with revolute or cylindrical joints has a spherical indicatrix [18], which is formed by bringing all joint axes to intersect at a common point. Fig. 6.1 shows an RCRCR mechanism and its corresponding spherical indicatrix. The concept of virtual loops [34] is introduced by its mathematical form rather than its physical appearance. With the concept of virtual loops, a unified linkage classification scheme based on the number of (virtual) loops becomes apparent. Each spatial group 1, 2, 3, or 4 mechanism can be regarded as a virtual spherical linkage formed by one or more virtual loops. The fact that all of Duffy's group 1 linkages and planar and spherical four-bar linkages are bimodal linkages and the fact that simple RCRCR mechanism and spatial group 2 with parallel joint axes are completely compatible with Stephenson six-bar linkages are consistent with the concept of virtual loops [34].

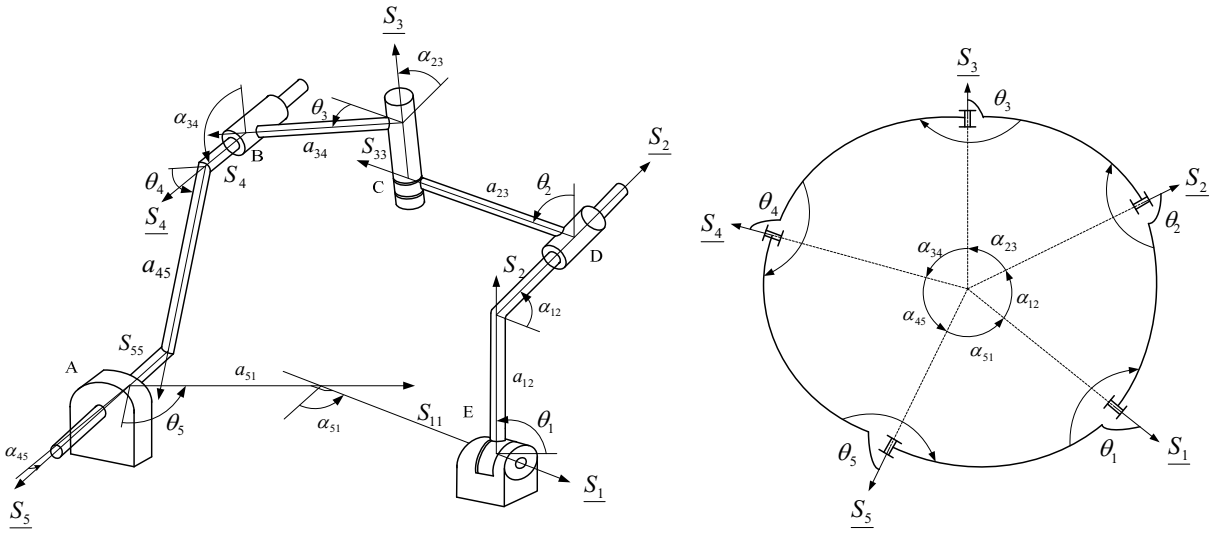

(a) (b)

Figure 6.1 (a) An RCRCR mechanism and (b) the spherical indicatrix

The geometry or mobility of a virtual loop in a virtual multiloop linkage is expressed by the fundamental equation (the virtual "loop-closure" equation), which can be written in the form of

$$A\sin\theta_o + B\cos\theta_o + C = 0 \qquad (6\text{-}1)$$

where θ_o is the output variable and A, B, and C are functions of the input joint variable θ_i.

6.2.2 N-bar Rotatability Laws and Mobility Criteria of Virtual Loops

The N-bar rotatability laws [14-17, 35] govern and predict the mobility of single loop planar and spherical linkages. In the N-bar rotatability laws, the rotatability of a linkage is viewed from the entire chain rather than from a linkage that has a narrow scope limited by the fixed link. Therefore, the variety of mobility considerations due to different linkage inversions is eliminated; the joint rotatability in a chaotic N-bar chain suddenly becomes easy to understand. Ting classified single loop chains into three classes. A Class I chain has two branches while a

Class II chain has only one branch. Therefore the branch problem does not exist in Class II chains. Class III is a transitional type between Class I and II chains.

The virtual "loop-closure" equation (Eq. 6-1) can be expressed in quadratic form. Any virtual four-bar loop can be classified into Class I, II, or III by using the discriminant function [10, 34]. By varying the value of the intermediate joint parameter, any virtual five-bar loop can be treated as a family of virtual four-bar loops. If all virtual four-bar loops of the family are Class I, then this virtual five-bar loop is Class I; otherwise it is Class II or III [34]. Since all fundamental equations for planar, spherical, and spatial linkages can be expressed in quadratic form, the mobility criteria of virtual loops may be regarded as the generalization of the N-bar rotatability laws.

6.2.3 Dead Center Positions

At a dead center position, the derivative of the output with respect to the input becomes infinite [38]; the input link reaches its rotation limit; and the linkage may be out of control momentarily [39]. Generally, the input-output (I/O) relationship between any pair of joint parameters of a linkage can be expressed by a polynomial equation [40]. Therefore, all of the dead center positions of single-DOF linkages, disregarding whichever joint is used as the input joint, can be found by solving a polynomial equation [40].

Let $y = \tan\frac{\theta_o}{2}$ and $\cos\theta_o = \frac{1 - y^2}{1 + y^2}$, $\sin\theta_o = \frac{2y}{1 + y^2}$. Eq. 6-1 can be converted as

$$(C - B)y^2 + 2Ay + (C + B) = 0 \qquad (6\text{-}2)$$

At a dead center position, the input and output relationship equation should have equal roots for a given input. Thus, the discriminant of the input and output equation (Eq. 6-2) should

vanish, which leads to a polynomial equation in terms of the input parameter only [41]. At a dead center position, the following equation must be satisfied,

$$\Delta = A^2 - (C - B)(C + B) = 0 \qquad (6\text{-}3)$$

6.2.4 Spatial Group 2 Mechanisms

A spatial group 2 linkage is referred to as a single DOF spatial linkage, which contains R, C, or P joints and has a total of five R and C joints [18]. The structures are different depending on the connecting sequences of R, C, and P joints. With different fixed link, the mechanisms with the same structure may have more inversions (Table 6-2).

Table 6.2 Duffy's group 2 mechanisms

Number of links	Mechanism
Five	RCRCR, RRCRC, RCRRC, RCCRR, RRRCC
Six	RRRPCR, RRCPRR, RRRRPC, RPCRRR, RCRPRR, RRCRPR, RRRPRC, RCRRPR, RRPRRC
Seven	RRPRPRR, RPRRPRR, RPRRRPR, RRRRPPR, RRRPPRR

Of a group 2 linkage, the first fundamental equation (say Eq. 6-1(a)) derived from the spherical indicatrix contains the input, output, and one intermediate joint variables, which is equivalent to a spherical five-bar loop. The second fundamental equation (say Eq. 6-1(b)) leads to an additional constraint on the two-DOF spherical indicatrix and therefore creates the effect of an additional loop to the spherical indicatrix to form a single-DOF linkage. A spatial group 2 linkage, consisting of two virtual five-bar loops, is equivalent to and regarded as a double loop linkage. Its linkage mobility is governed by the two fundamental equations and how they influence each other. The mobility of each individual loop is governed by the N-bar rotatability laws [14-17] and/or the mobility criteria of virtual loops [34]; JRS and branch/tangent points are used to explain how the interaction between the loops affects the branch formation of the entire linkage [37].

6.2.5 JRS, Branch Points, and Tangent Points

JRS [35, 36] represents the domain of the input variables of a linkage or a loop. The concepts of JRS and branch points were first used to resolve the mobility problems of Stephenson six-bar linkages [7]. Ting [35] further modeled JRS as sheets and sides and used branch points to offer a geometric explanation on how mobility between loops interact each other and thus the mobility formation of linkages. One may find that the concept of JRS works well with virtual loops.

The fundamental equation (Eq. 6-1) can be converted as a quadratic equation (Eq. 6-2). The discriminant of this quadratic equation, $\Delta \geq 0$, describes its JRS. $\Delta = 0$ is the singular condition representing the boundary of the input domain, which divides one sheet of JRS into two sides. When an input joint variable is known, the corresponding output joint variable can be solved

from Eq. 6-2. The derived solutions represent linkage configurations on two sides of a JRS sheet. In other words, Eq. 6-4(a) is the mathematical expression of one side of a JRS and Eq. 6-4(b) the other side.

$$y_{1,2} = \frac{-A \pm \sqrt{(A^2 + B^2 - C^2)}}{C - B} \qquad \text{(6-4ab)}$$

If Eq. 6-1(b) contains only the input and output joint parameters, as in the case of simple RCRCR or spatial group 2 linkages with parallel joint axes, it is a curve in the JRS of Eq. 6-1(a). This is the case with Stephenson-type linkages and represents the simplified version of group 2 linkages (Fig. 6.2). Branch points are the intersections of the I/O curve and the JRS boundary of the other loop. An input vs. output curve is cut into branches by branch points [7]. Since there is no difference in the mathematical treatment of a physical loop and a virtual loop, in the following discussion, the mobility conditions, such as branch, sub-branch, and joint rotatability can be explained and predicted unambiguously and automatically with the JRS properties and the branch points [35].

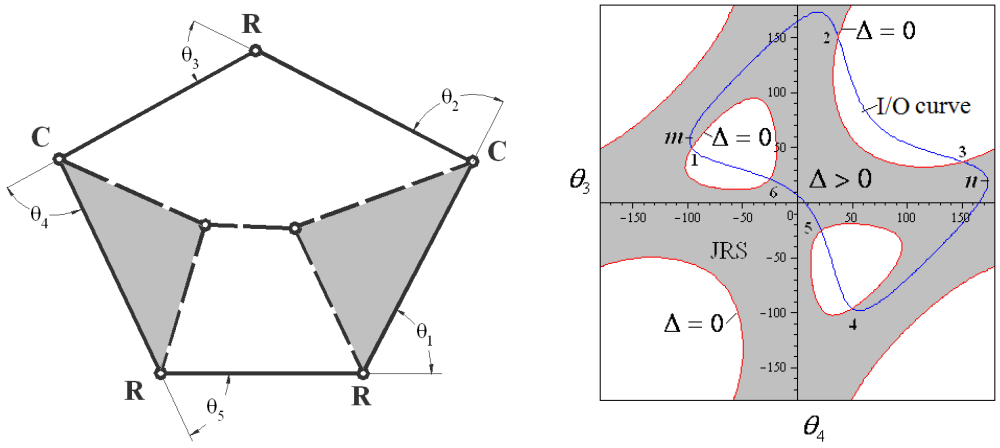

Figure 6.2 (a) Stephenson-type linkage and (b) JRS and branches

The current use of branch points for branch identification is limited to linkages with simple topology and singularity conditions, such as Stephenson-type linkages [7]. However, in a general spatial group 2 linkage, both the fundamental equations are equivalent to virtual five-bar loops. Branch points in Stephenson-type linkages cannot explain and define the interaction between two virtual five-bar loops. Branch points must be generalized in order to explain and predict the branch formation of general group 2 linkages.

As shown in Fig. 6.3, the linkage configuration may evolve from non-existence to existence (two curves are tangent to each other at one point named as tangent point) and then to the formation of an entire branch. Tangent points contain the branch information of general group 2 linkages; they are the counterpart of branch points for Stephenson linkages [34]. One tangent point may co-exist with other intersection points or even with tangent point.

The branch formation starts and ends at tangent points, but not all tangent points are the branch starting or ending points in general group 2 linkages. Reading and interpreting the tangent points will be the pivotal and fundamental issues in the mobility analysis of spatial group 2 linkages. To be consistent with the Stephenson linkages, the tangent points, which are branch starting or ending points in general group 2 linkages, are called branch points.

For one tangent point, if one and only one pair of input and output joint variables (θ_i and θ_o), i.e. one solution, is derived when its intermediate joint parameter θ_m is substituted back to the two fundamental equations of the group 2 linkage, then the tangent point is definitely a branch point (Fig 6.3(b)). In other words, if one tangent point does not co-exist with other intersection points, it is a branch point.

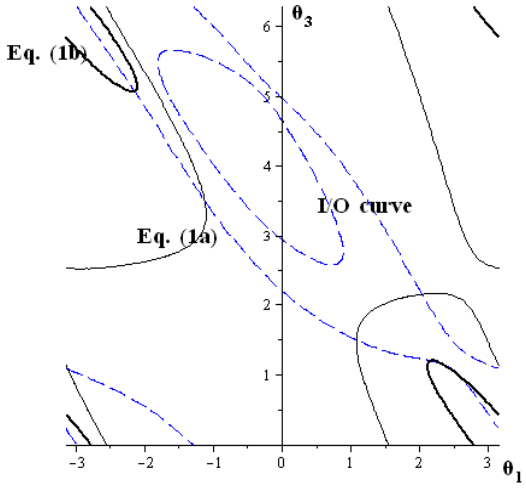

(a) no intersection point

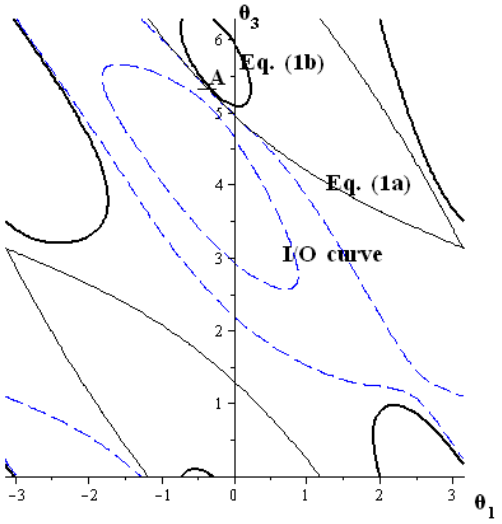

(b) one tangent point

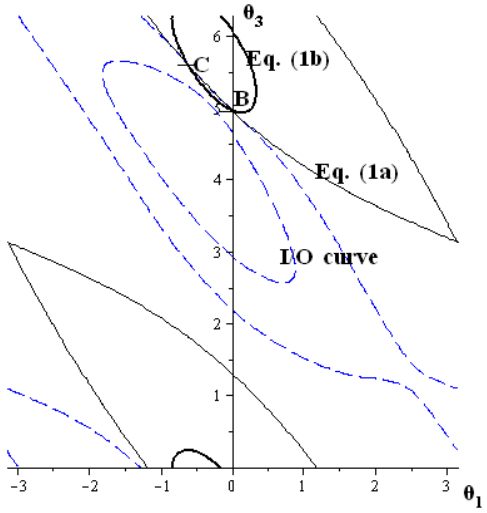

(c) two intersection points

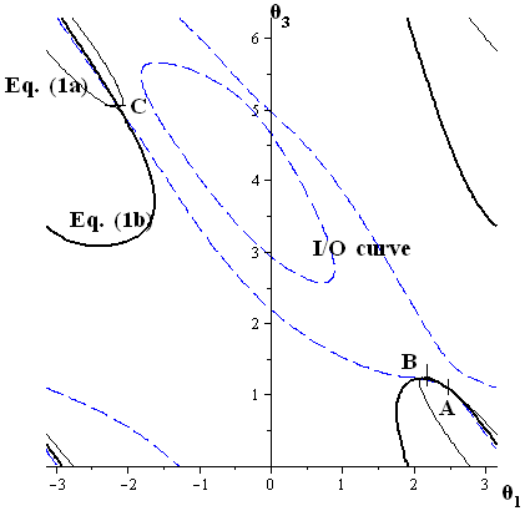

(d) one tangent and two intersection points

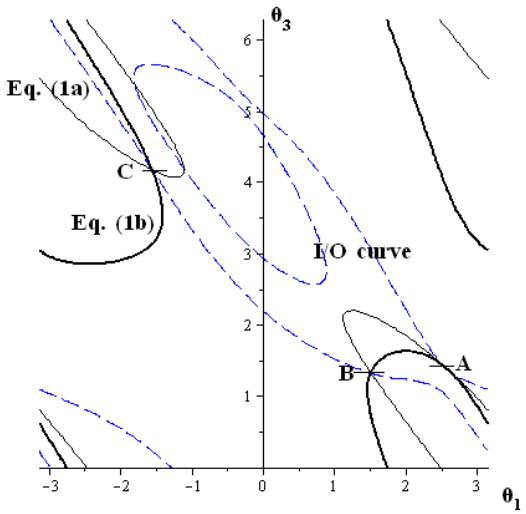

(e) one tangent and two intersection points

Figure 6.3 Formation of tangent points

For one tangent point, if more than one pair of input and output joint variables (θ_i and θ_o), i.e. more than one solution, are derived when its intermediate joint parameter θ_m is substituted back to the two fundamental equations of the group 2 linkage, then the tangent point co-exists with other intersection points. If the tangent point can reach at least one intersection point continuously, then this tangent point is not a branch point (Fig 6.3(d)); otherwise it is a branch point (Fig 6.3(e)).

As same as in Stephenson linkages, every two branch points will form a branch in spatial group 2 linkages.

6.3 Mobility analysis of Spatial Group 2 Mechanisms

The mobility of a spatial group 2 linkage is governed by the fundamental equations representing two virtual five-bar loops, and how they influence each other. Eq. 6-1 represents two surfaces in the input/output domain. The intersection of these two surfaces is the I/O curve, which describes the relationship between the input and output variables, say θ_1 and θ_3, respectively. Unlike group 1 linkages, whose mobility can be derived from the input and output relationship, the I/O curves can be very complicated for group 2 linkages. Duffy [18] used six curves depicting the variation of all joint variables with respect to the input parameter to express the true mobility or configuration variation of spatial linkages. Since a linkage is controlled by the input exclusively, a methodology based on the input domain is highly desired.

The mobility of each individual loop can be identified with the N-bar rotatability laws [14-17] and/or mobility criteria of virtual loops [34]; the generalized branch points are used to explain how the interaction between loops affects the branch formation of the entire linkage.

Assuming the generalized branch points of a group 2 linkage are derived, a mobility analysis scheme can be developed. In each step, if a branch defect is detected, the linkage will be weeded out immediately. The scheme is outlined below.

- Identify the branch of each individual virtual five-bar loop, respectively. This can be done easily with the N-bar rotatability laws [14-17] and/or the mobility criteria of virtual loops [34]. If any virtual loop is Class I, then the generalized branch points will be separated into different groups. If dead center positions exist, they will be separated too.
- Further separate the branch points and dead center positions with the use of JRS side identification criterion.
- In each group, every two branch points will form a branch in spatial group 2 linkages.
- Identify sub-branch, joint rotatability, and other mobility condition relevant to the choice of the input joint.

It is important to recognize that branch formation and the continuity of motion between positions is irrelevant to the choice of the input joint. The detail mobility analysis process will be demonstrated with examples.

Example 1:

The RCRCR mechanism is shown schematically in Figure 6.4(a). The axes of the joints R, C, R, C, and R are labeled as 1, 2, 3, 4, and 5, respectively. The input and output angular displacements are θ_1 and θ_5 while the intermediate angular displacement is denoted by θ_3. The remaining four variables are the angular displacements θ_2, θ_4 and the slider displacements S_2 and S_4. By using the D-H notation [42, 43], $\alpha_{12} = 60^{\circ}$, $\alpha_{23} = 45^{\circ}$ $\alpha_{34} = 35^{\circ}$, $\alpha_{45} = 30^{\circ}$, and $\alpha_{51} = 10^{\circ}$ are the angles between the corresponding joint axes, $a_{12} = 25$, $a_{23} = 30$, $a_{34} = 40$,

$a_{45} = 10$, and $a_{51} = 32$, are the distance between the corresponding joint axes, and $S_{11} = 30$, $S_{33} = 25$, and $S_{55} = 8$ are the offset along the corresponding R-joint axes.

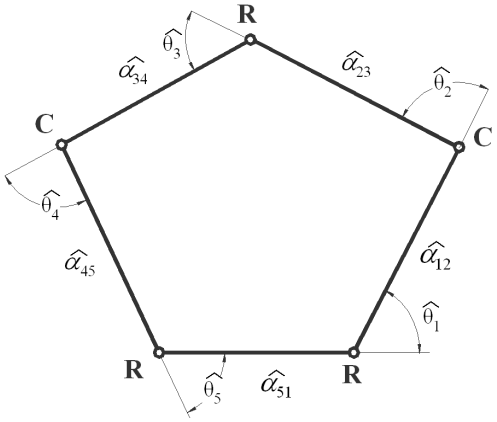

(a) A general RCRCR mechanism

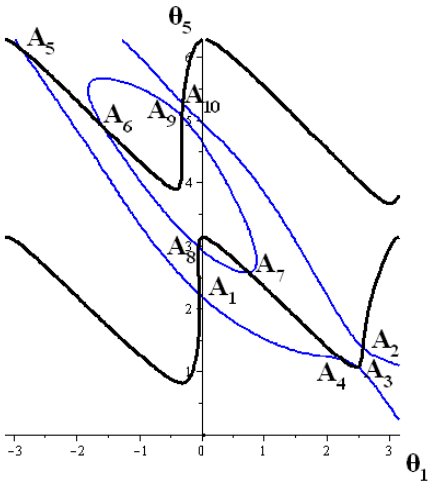

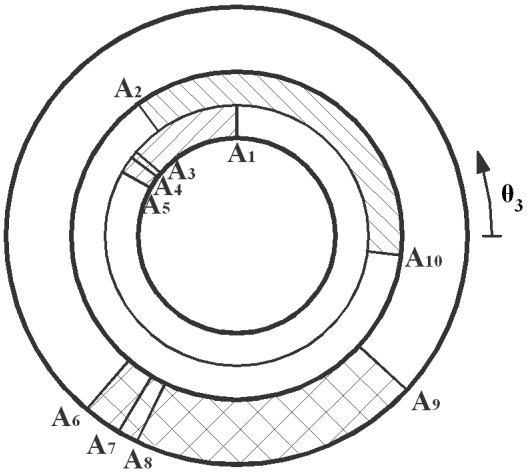

(b) Tangent points on I/O curve (θ_1 vs θ_5) (c) Location of tangent points on the circle of θ_3

Figure 6.4 Mobility analysis of an RCRCR mechanism

Table 6.3 Tangent points of a general RCRCR mechanism

	θ_1	θ_5	θ_3	Property
A_1	-0.05	2.25	1.55	branch point
A_2	2.56	1.39	2.21	branch point
A_3	2.48	1.07	2.49	
A_4	2.25	1.18	2.50	
A_5	-2.87	6.13	2.63	branch point
A_6	-1.57	4.90	4.00	branch point
A_7	0.75	2.58	4.17	
A_8	-0.07	3.00	4.26	
A_9	-0.33	5.07	5.54	branch point
A_{10}	-0.32	5.27	6.16	branch point

Fundamental equations: The two fundamental equations derived by following Duffy's sine, sine-cosine, and cosine laws [18, 19] are

$$\cos\theta_3 - 0.38 + 1.07\sin\theta_5\sin\theta_1 - 0.32\cos\theta_1 - 1.05\cos\theta_1\cos\theta_5 - 0.11\cos\theta_5 = 0 \qquad \text{(6-5a)}$$

$$\begin{aligned}&\sin\theta_3 - 3.485\cos\theta_3 - 1.012 - 1.356\sin\theta_5\sin\theta_1 + 2.442\cos\theta_1 + 1.098\cos\theta_1\cos\theta_5 \\ &+ 0.666\cos\theta_5 - 1.618\sin\theta_5\cos\theta_1 - 0.385\sin\theta_1 - 1.603\sin\theta_1\cos\theta_5 - 0.034\sin\theta_5 = 0\end{aligned} \qquad \text{(6-5b)}$$

Tangent points: A total of ten tangent points A_1, A_2, …, A_{10} (θ_1, θ_5) are found and listed in Table 6.3. The corresponding intermediate joint parameter θ_3 values can be determined by solving Eq. 6-5(a) and (b) simultaneously. Among them, A_1, A_2, A_5, A_6, A_9, and A_{10} are generalized branch points (Fig. 6.4(b)).

The branch rectification procedures are outlined as follows.

Identify the branch of the first virtual five-bar loop (spherical indicatrix): it is a Class II loop, therefore no branch defect exists according to the N-bar rotatability laws [14-17] or the mobility criteria of virtual loops [34].

Identify the branch of the second virtual five-bar loop: it is a Class II loop too and no branch defect exists according to the mobility criteria of virtual loops [34].

By solving the polynomial equation converted from the input/output displacement, two dead center positions are identified [40].

In the second virtual five-bar loop (Eq. 6-5(b)), $A_2 = 1, B_2 = -3.485$,

$C_2 = -1.012 - 1.356\sin\theta_5\sin\theta_1 + 2.442\cos\theta_1 + 1.098\cos\theta_1\cos\theta_5 + 0.666\cos\theta_5$
$-1.618\sin\theta_5\cos\theta_1 - 0.385\sin\theta_1 - 1.603\sin\theta_1\cos\theta_5 - 0.034\sin\theta_5$. Its JRS sides can be expressed mathematically as follows.

$$y_{1,2} = \frac{-A_2 \pm \sqrt{(A_2^2 + B_2^2 - C_2^2)}}{C_2 - B_2} \qquad \text{(6-6ab)}$$

Eq. 6-6(a) represents one JRS side and Eq. 6-6(b) the other JRS side. This side identification criterion will separate the branch points and the dead center positions into different groups: A_6 and A_9 as well as the two dead center positions are on one JRS side; A_1, A_2, A_5, and A_{10} are on the other JRS side.

Branches will be formed between every two branch points. In short, this general RCRCR mechanism has a total of three branches: A_6 and A_9 form one branch; A_1 and A_5 form one branch; A_2 and A_{10} form one branch (Fig. 6.4(c)).

Branch rectification may be done via simply locating all branch points and the linkage configurations on the circle by the intermediate joint parameter θ_3. For example, if the θ_3 value of a linkage configuration is located between A_6 and A_9 on the circle, then this configuration is on the branch formed by A_6 and A_9.

When the θ_3 value of a linkage configuration is located on the overlap segment between branch points A_1 and A_2, the side identification criterion on the first virtual loop can be applied to solve the overlap problem. In the first virtual five-bar loop (Eq. 6-5(a)), $A_1 = 0$, $B_1 = 1$, $C_1 = -0.38 + 1.07\sin\theta_5 \sin\theta_1 - 0.32\cos\theta_1 - 1.05\cos\theta_1 \cos\theta_5 - 0.11\cos\theta_5$. Its JRS sides can be expressed mathematically as follows.

$$y_{1,2} = \frac{-A_1 \pm \sqrt{(A_1^2 + B_1^2 - C_1^2)}}{C_1 - B_1} \qquad \text{(6-7ab)}$$

Eq. 6-7(a) represents one JRS side where branch point A_1 is located and Eq. 6-7(b) the other JRS side where branch point A_2 is located. If the linkage configuration meets Eq. 6-7(a), then it is on the branch formed by A_1 and A_5; if the linkage configuration meets Eq. 6-7(b), then it is on the branch formed by A_2 and A_{10}.

By checking the θ_3 value of a linkage configuration, we have the following observations.

- $\theta_3 \in (0, 1.55)$, on the branch A_2-A_{10};
- $\theta_3 \in [1.55, 2.21]$ and side identification criterion of the virtual loop (Eq. 6-7(a) or (b)), on the branch A_1-A_5 or A_2-A_{10};
- $\theta_3 \in (2.21, 2.63]$, on the branch A_1-A_5;
- $\theta_3 \in (2.63, 4.00)$, no linkage assembly;
- $\theta_3 \in [4.00, 5.54]$, on the branch A_6-A_9;
- $\theta_3 \in (5.54, 6.16)$, no linkage assembly;
- $\theta_3 \in [6.16, 6.28]$, on the branch A_2-A_{10}.

Identify the singularity, sub-branch, joint rotatability, and other mobility condition relevant to the choice of the input joint:

A branch may be divided into sub-branches by the dead center positions. By inserting the dead center positions in their corresponding branches, the sub-branch problem can be solved. A branch may have one, two, or more sub-branches depending on the number of dead center positions in the branch. In a sub-branch, a one-to-one correspondence exists between the input angle and the linkage configuration and the input increases or decreases monotonously from one dead-center position to another. Such a one-to-one correspondence is the core issue in the sub-branch identification. Therefore, once a sub-branch is identified unambiguously, the order of the motion or the order of reaching all linkage configurations can be identified by the ascending or descending order of the input values.

In this example, the two dead center positions divide the branch A_6-A_9 into two sub-branches. Since there is no dead center position on the branches A_1-A_5 and A_2-A_{10}, they have full rotatability and each branch has only one sub-branch.

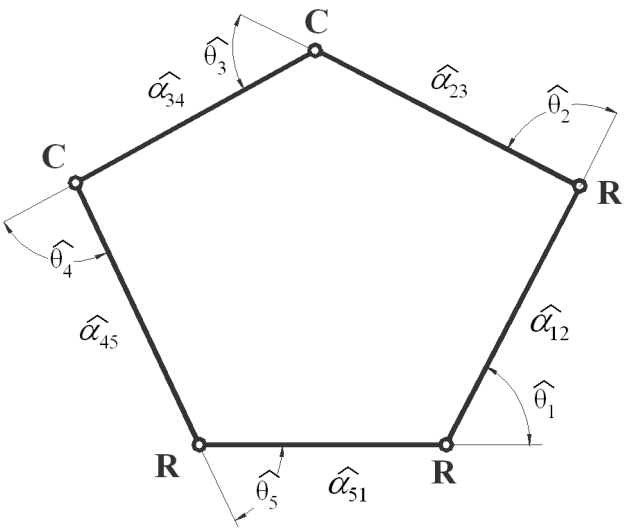

(a) A general RRCCR mechanism

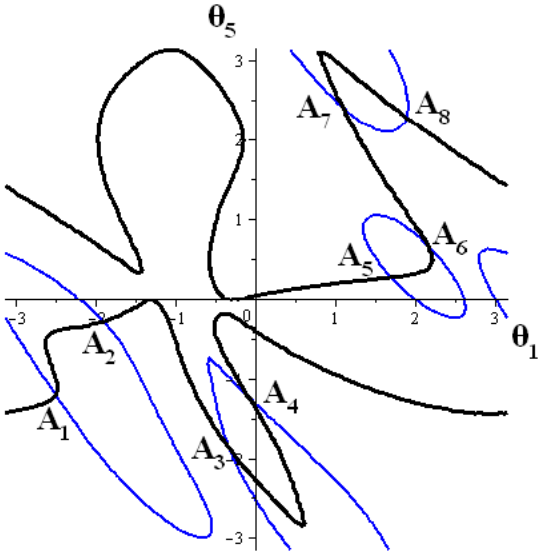

(b) Tangent points on I/O curve (θ_1 vs θ_5)

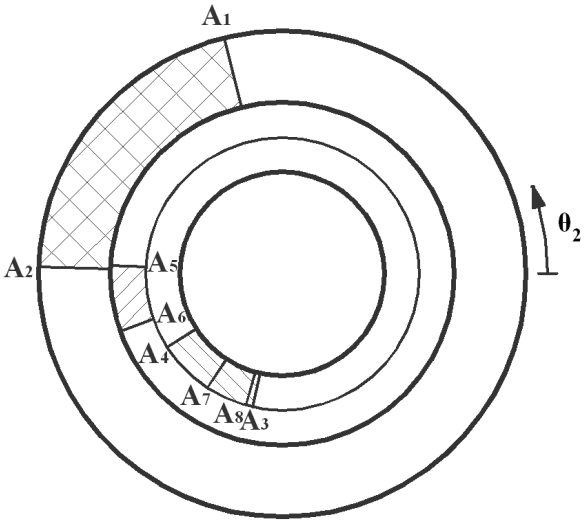

(c) Location of tangent points on the circle of θ_2

Figure 6.5 Mobility analysis of an RRCCR mechanism

Table 6.4Tangent points of a general RRCCR

	θ_1	θ_5	θ_2	Property
A_1	-2.50	-1.20	1.81	branch point
A_2	-1.91	-0.28	3.11	branch point
A_3	-0.34	-1.86	4.49	branch point
A_4	-0.09	-1.22	3.71	branch point
A_5	1.69	0.28	3.09	branch point
A_6	2.14	0.69	3.48	branch point
A_7	1.08	2.43	4.13	
A_8	1.89	2.29	4.44	

Example 2:

The RRCCR mechanism is shown schematically in Figure 6.5(a). The axes of the joints R, R, C, C, and R are labeled as 1, 2, 3, 4, and 5, respectively. The input and output angular displacements are θ_1 and θ_5 while the intermediate angular displacement is denoted by θ_2. The remaining four variables are the angular displacements θ_3, θ_4 and the slider displacements S_3 and S_4. By using the D-H notation [42, 43], $\alpha_{12} = 60^o$, $\alpha_{23} = 45^o$ $\alpha_{34} = 35^o$, $\alpha_{45} = 30^o$, and $\alpha_{51} = 10^o$ are the angles between the corresponding joint axes, $a_{12} = 25$, $a_{23} = 30$, $a_{34} = 40$, $a_{45} = 10$, and $a_{51} = 32$ are the distance between the corresponding joint axes, and $S_{11} = 35$, $S_{22} = 15$, and $S_{55} = 0$ are the offset along the corresponding R-joint axes.

Fundamental equations: The two fundamental equations derived by following Duffy's sine, sine-cosine, and cosine laws [18, 19] are

$$\begin{aligned}&(35.3\sin\theta_5\cos\theta_1 + 34.8\cos\theta_5\sin\theta_1 + 10.6\sin\theta_1)\sin\theta_2\\&+(17.7\sin\theta_5\sin\theta_1 - 17.4\cos\theta_5\cos\theta_1 + 5.32\cos\theta_5 - 5.32\cos\theta_1 - 52.2)\cos\theta_2\\&+(30.6\sin\theta_5\sin\theta_1 - 30.2\cos\theta_5\cos\theta_1 - 3.07\cos\theta_5 - 9.21\cos\theta_1 - 51.8) = 0\end{aligned} \quad \text{(6-8a)}$$

$$\begin{aligned}&(-150.2\sin\theta_5\sin\theta_1 - 167.3\sin\theta_5\cos\theta_1 + 145.1\cos\theta_5\sin\theta_1 +\\&148.0\cos\theta_5\cos\theta_1 - 7.98\cos\theta_5 + 218.7\sin\theta_1 + 45.2\cos\theta_1 + 78.3)\sin\theta_2\\&+(7.11\sin\theta_5\sin\theta_1 + 114.9\sin\theta_5\cos\theta_{15} + 113.2\cos\theta_5\sin\theta_1 +\\&2.83\cos\theta_5\cos\theta_1 + 129.3\cos\theta_5 + 34.6\sin\theta_1 - 8.63\cos\theta_1 - 172.4)\cos\theta_2\\&+(5.37\sin\theta_5\sin\theta_1 + 107.2\sin\theta_5\cos\theta_1 + 105.5\cos\theta_5\sin\theta_1 +\\&11.7\cos\theta_5\cos\theta_1 - 38.5\cos\theta_5 + 32.2\sin\theta_1 - 147.5\cos\theta_1 - 26.0) = 0\end{aligned} \quad \text{(6-8b)}$$

Tangent points: A total of eight tangent points A_1, A_2, …, A_8 (θ_1, θ_5) are found and listed in Table 6-4. The corresponding intermediate joint parameter θ_2 values can be determined by solving Eq. 6-8(a) and (b) simultaneously. Among them, A_1, A_2, A_3, A_4, A_5, and A_6 are generalized branch points.

The branch rectification procedures are outlined as follows.

Identify the branch of the first virtual five-bar loop (spherical indicatrix): it is a Class II loop, therefore no branch defect exists according to the N-bar rotatability laws [14-17] or the mobility criteria of virtual loops [34].

Identify the branch of the second virtual five-bar loop: it is a Class II loop too and no branch defect exists according to the mobility criteria of virtual loops [34].

In the second virtual five-bar loop (Eq. 6-8(b)), the side identification criterion is applied to separate the branch points into different groups: A_1 and A_2 are on one JRS side; A_3, A_4, A_5, and A_6 are on the other JRS side.

Branches will be formed between every two branch points. This general RRCCR mechanism has a total of three branches: A_1 and A_2 form one branch; A_3 and A_4 form one branch; A_5 and A_6 form one branch (Fig. 6.5(c)).

By checking the θ_2 value of a linkage configuration, we have the following observations.

- $\theta_2 \in (0, 1.81)$, no linkage assembly;
- $\theta_2 \in [1.81, 3.09)$, on the branch A_1-A_2;
- $\theta_2 \in [3.09, 3.11]$ and side identification criterion of the virtual loop, on the branch A_1-A_2 or A_5-A_6;
- $\theta_2 \in (3.11, 3.48]$, on the branch A_5-A_6;
- $\theta_2 \in (3.48, 3.71)$, no linkage assembly;
- $\theta_2 \in [3.71, 4.49]$, on the branch A_3-A_4;
- $\theta_2 \in (4.49, 6.28)$, no linkage assembly.

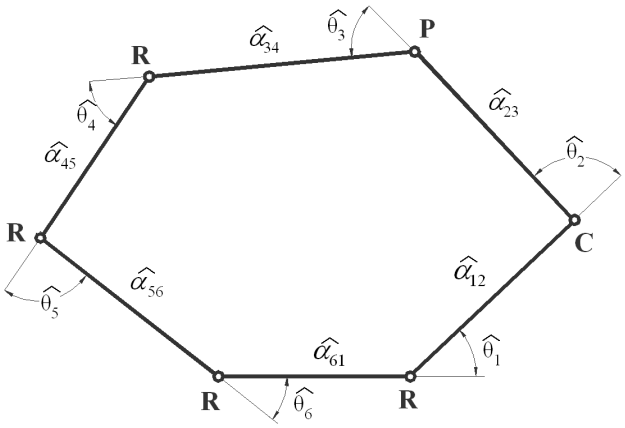

(a) An RRRPCR mechanism

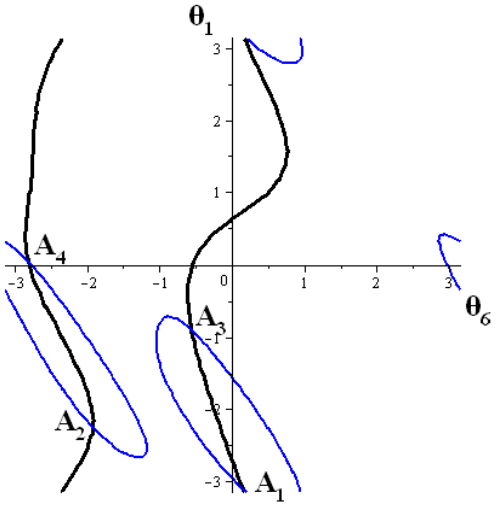

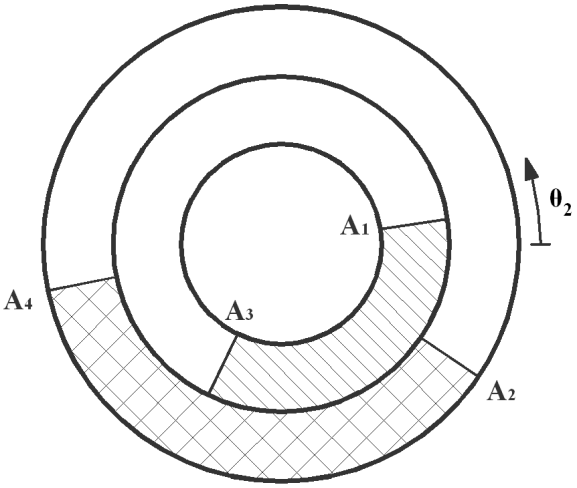

(b) Tangent points on I/O curve (θ_6 vs θ_1) (c) Location of tangent points on the circle of θ_2

Figure 6.6 Mobility analysis of an RRRPCR mechanism

Table 6.5 Tangent points of a RRRPCR mechanism

	θ_6	θ_1	θ_2	Property
A_1	0.16	-3.11	0.15	branch point
A_2	-1.94	-2.25	5.68	branch point
A_3	-0.56	-0.89	4.26	branch point
A_4	-2.82	0.05	3.34	branch point

Example 3:

The RRRPCR mechanism is shown schematically in Figure 6.6(a). The axes of the joints R, C, P, R, R, and R are labeled as 1, 2, 3, 4, 5, and 6, respectively. The input and output angular displacements are θ_6 and θ_1 while the intermediate angular displacement is denoted by θ_2. The

remaining four variables are the angular displacements θ_4, θ_5 and the slider displacements S_2 and S_3. By using the D-H notation [42, 43], $\alpha_{12} = 30^o$, $\alpha_{23} = 35^o$ $\alpha_{34} = 30^o$, $\alpha_{45} = 45^o$, $\alpha_{56} = 60^o$, and $\alpha_{61} = 10^o$ are the angles between the corresponding joint axes, $a_{12} = 10$, $a_{23} = 40$, $a_{34} = 20$, $a_{45} = 30$, $a_{56} = 25$, and $a_{61} = 32$ are the distance between the corresponding joint axes, $\theta_{33} = 90^o$ is angular displacement on P-joint, and $S_{11} = 10$, $S_{44} = 10$, $S_{55} = 15$, and $S_{66} = 30$ are the offset along the corresponding R-joint axes.

The two fundamental equations in the form of Eq. 6-1 can be derived by following Duffy's sine, sine-cosine, and cosine laws [18, 19]. The corresponding coefficients are listed as follows:

$$A_1 = (-3.75\sin\theta_1 + 4.30\cos\theta_1)\sin\theta_6 + (4.24\sin\theta_1 + 3.69\cos\theta_1 - 0.38)\cos\theta_6 + (0.43\sin\theta_1 + 0.38\cos\theta_1 + 1.23)$$

$$B_1 = (3.73\sin\theta_1 + 4.33\cos\theta_1)\sin\theta_6 + (4.26\sin\theta_1 - 3.67\cos\theta_1 + 0.37)\cos\theta_6 + (0.43\sin\theta_1 - 0.37\cos\theta_1 - 1.22)$$

$$C_1 = 3.07\sin\theta_1\sin\theta_6 - (3.03\cos\theta_1 + 0.92)\cos\theta_6 - (0.31\cos\theta_1 + 4.05)$$

$$A_2 = (-11.25\sin\theta_1 + 4.74\cos\theta_1 + 2.17)\sin\theta_6 + (4.02\sin\theta_1 + 11.08\cos\theta_1 + 1.13)\cos\theta_6 + (-25.10\sin\theta_1 + 5.64\cos\theta_1 + 23.47)$$

$$B_2 = (-2.05\sin\theta_1 + 12.99\cos\theta_1)\sin\theta_6 + (12.79\sin\theta_1 + 2.77\cos\theta_1 + 2.26)\cos\theta_6 + (6.51\sin\theta_1 + 29.74\cos\theta_1 + 2.59)$$

$$C_2 = -9.13\sin\theta_1\sin\theta_6 + (8.99\cos\theta_1 + 2.74)\cos\theta_6 + (0.91\cos\theta_1 + 36.01) \qquad (6\text{-}9)$$

Tangent points: A total of four tangent points A_1, A_2, …, A_4 (θ_6, θ_1) are found and listed in Table 6-5. The corresponding intermediate joint parameter θ_2 values can be determined by solving the two fundamental equations simultaneously. All tangent points A_1, A_2, A_3, and A_4 are generalized branch points.

The branch rectification procedures are outlined as follows.

Identify the branch of the first virtual five-bar loop (spherical indicatrix): it is a Class II loop, therefore no branch defect exists according to the N-bar rotatability laws [14-17] or the mobility criteria of virtual loops [34].

Identify the branch of the second virtual five-bar loop: it is a Class II loop too and no branch defect exists according to the mobility criteria of virtual loops [34].

In the second virtual five-bar loop, the side identification criterion is applied to separate the branch points into different groups: A_1 and A_3 are on one JRS side; A_2 and A_4 are on the other JRS side.

Branches will be formed between every two branch points. This RRRPCR mechanism has a total of two branches: A_1 and A_3 form one branch; A_2 and A_4 form one branch (Fig. 6.6(c)).

By checking the θ_2 value of a linkage configuration, we have the following observations.

- $\theta_2 \in (0, 0.15]$, on the branch A_1-A_3;
- $\theta_2 \in (0.15, 3.34)$, no linkage assembly;
- $\theta_2 \in [3.34, 4.26)$, on the branch A_3-A_4;
- $\theta_2 \in [4.26, 5.68]$ and side identification criterion of the virtual loop, on the branch A_1-A_3 or A_2-A_4;
- $\theta_2 \in (5.68, 6.28]$, on the branch A_1-A_3.

6.4 Conclusions

With the increased number of links or joints, the complexity of the linkage increases drastically. The concept of virtual loops is used to highlight the mobility similarity or compatibility of planar and spherical multiloop linkages. The generalized branch points offer

explicit explanation of branch formation. In this dissertation, the mobility analysis scheme of group 2 linkages is carried out in a systematic manner based on the similarity of the mobility features rather than the specific or individual linkage structure.

REFERENCES

1. Mirth, J.A. and Chase, T.R., 1992, “Circuit Rectification for Four Precision Position Synthesis of Stephenson Six-bar Linkages,” *ASME Mechanical Design and Synthesis*, DE-Vol.46, pp.359–366.
2. Chase, T.R. and Mirth, J.A., 1993, “Circuits and Branches of Single Degree-of-freedom Planar Linkages,” *ASME J. of Mechanical Design*, Vol.115, pp.223–230.
3. Mirth, J.A. and Chase, T.R., 1993, “Circuit Analysis of Watt Chain Six-bar Mechanisms,” *Journal of Mechanical Design, Transactions Of the ASME*, Vol.115, n 2, pp.214–222.
4. Davis, H.P., Chase, T.R. and Mirth, J.A., 1994, “Circuit Analysis of Stephenson Chain Six-bar Mechanisms,” *ASME Mechanism Synthesis and Analysis*, DE-Vol.70, pp.349–358.
5. Davis, H.P. and Chase, T.R., 1994, “Stephenson Chain Branch Analysis: Four Generic Stationary Configurations and One New Linkage Polynomial,” *ASME Mechanism Design and Synthesis*, DE-Vol.70, pp.359–367.
6. Mirth, J.A. and Chase, T.R., 1995, “Circuit Rectification for Four Precision Position Synthesis of Four-bar and Watt Six-bar Linkages,” *Journal of Mechanical Design, Transactions of the ASME*, Vol.117, n 4, pp.612-619.
7. Ting, K.L. and Dou, X.H., 1996, “Classification and Branch Identification of Stephenson Six-Bar Chains,” *Mechanism and Machine Theory*, Volume 31, Issue 3, pp.283-295.
8. Grashof, F., 1983, *Theoretische Maschinenlehre*, Leipzig.
9. Nolle, H., 1969, “Range of Motion Transfer by R-G-G-R Mechanisms,” *Journal of Mechanisms*, 4, pp.145-157.
10. Ting, K.L. and Dou, X.H., 1994, "Branch, Mobility Criteria, and Classification of RSSR and Other Bimodal Linkages," *ASME Mechanism Synthesis and analysis*, DE-Vol.70, pp.303-310.
11. Su, H.J. Collins, C.L., and McCarthy, M., 2002, “Classification of RRSS linkages,” *Mechanism and Machine Theory*, Vol. 37, pp.1413-1433.
12. Lee, D., Youm, Y., and Chung, W., 1996, “Mobility Analysis of Spatial 4- and 5- Link Mechanisms of the RS Class,” *Mechanism and Machine Theory*, Vol. 31, pp.673-690.
13. Gupta, K. C., and Tinubu, S. O., 1983, “Synthesis of Bimodal Generating Mechanisms without Branch Defect,” *J. of Mechanisms, Transmissions, and Automation in Design*, Vol. 105, pp. 641-647.
14. Ting, K.L., 1989, "Mobility Criteria of Single-Loop N-Bar Linkages," *Journal of Mechanisms, Transmissions, and Automation in Design*, pp. 504-507.
15. Ting, K.L. and Liu, Y.W., 1991, "Rotatability Laws for N-Bar Kinematic Chains and Their Proof," *ASME Journal of Mechanical Design*, Vol. 113, No. 1, pp. 32-39.
16. Shyu, J.H. and Ting, K.L., 1994, “Invariant Link Rotatability of N-Bar Kinematic Chains,” *Journal of Mechanical Design*, Vol.116, pp.343-347.

17. Ting, K.L., and Liu, Y.W., 1992, "On the Rotatability of Spherical N-Bar Chains," *Journal of Mechanical Design*, Vol. 116, No. 3, 1994, pp. 920-923.

18. Duffy, J., 1980, *Analysis of Mechanisms and Robot Manipulators*, New York, John Willey and Sons.

19. Crane III, C.D. and Duffy, J., 2008, *Kinematic Analysis of Robot Manipulators*, New York, Cambridge University Press.

20. Primrose, E.J.F. and Freudenstein, F., 1969, "Spatial Motions I: Point Paths of Mechanisms with Four or Fewer Links," *ASME Journal of Engineering for Industry*, Series B 91 (1), pp.103-113.

21. Marble, S.D. and Pennock, G.R., 2000, "Algebraic-Geometric Properties of the Coupler Curves of the RCCC Spatial Four-Bar Mechanism," *Mechanism and Machine Theory*, 35, pp.675-693.

22. Worle, H., 1962, "Untersuchungen uber Kippelkurven Viergliedriger Raumlicher Kurbelgetriebe," *Konstruktion*, 14 (10), pp.390-392.

23. Nolle, H., 1969, "Range of Motion Transfer by R–G–G–R Mechanisms," *Journal of Mechanisms*, 4, pp.145–157.

24. Williams, R.L.II and Reinholtz, C.F., 1987, "Mechanism Link Rotatability and Limit Position Analysis Using Polynomial Discriminants," *ASME Journal of Mechanisms, Transmissions, and Automation in Design*, 109 (2), pp.178–182.

25. Murray, A.P. and Larochelle, P.M., 1998, "A Classification Scheme for Planar 4R, Spherical 4R, and Spatial RCCC Linkages to Facilitate Computer Animation," *Proceedings of the 1998 ASME Design Engineering Technical Conferences: Mechanisms Conference*, Atlanta, GA.

26. Duffy J., 1969, *A Derivation of Dual Displacement Equations for Five, Six and Seven Link Spatial Mechanisms Using Spherical Trigonometry* (3 parts), Liverpool Polytechnic.

27. Yang, A.T., 1969, "Displacement Analysis of Spatial Five-Link Mechanisms Using 13 × 3 Matrices with Dual Number Elements," *Trans. ASME, J. Engng Ind.*, 191B.

28. Pamidi, P.R. and Freudenstein, F., 1975, "On the Motion of A Class of Five-Link, R–C–R–C–R, Spatial Mechanisms," *ASME J. Eng. Ind.*, 97 (1), pp.334–339.

29. Dou, X. and Ting, K.L., 1996, "Classification, Rotatability, and Branch Identification of Simple RCRCR Mechanisms," *ASME Design Engineering Technical Conference and the Computer in Engineering*, Paper No. 96-DETC/FAS-1363.

30. Kohli, D., Cheng, J.C. and Tsai, K.Y., 1994, "Assimilability, Circuits, Branches, Locking Positions, and Rotatability of Input Links of Mechanisms with Four Closures," *Journal of Mechanical Design, Transaction of ASME*, Vo1.116, pp.92-98.

31. Guo, X.N., 2003, *Research on Structural and Kinematic Characteristics and Parameterized Solid Kinematic Simulation of Linkages*, Ph.D dissertation, Xi'an University of Technology.

32. Foster, D.E., and Cipra, R.J., 1998, "Assembly Configurations of Spatial Single-Loop Mechanisms with Revolute, Cylindrical, and Prismatic Joints," *Proceedings of the 1998 ASME Design Engineering Technical Conferences*, Atlanta, GA, September 13-16, Paper No. MECH-5897.

33. Foster, D.E., and Cipra, R.J., 2000, "Assembly Configurations of Spatial RRRCC, RRCRC, RRRRCR, and RRRRRRR Mechanisms," *Proceedings of the 2000 ASME Design Engineering Technical Conferences and Computers and Information in Engineering Conference*, Baltimore, Maryland, September 10-13, 2000, Paper No. MECH-14051.

34. Ting, K.L., Xue C., Wang, J., and Currie, K.R., "On the Virtual Loops and Virtual Multiloop Linkages," (in preparation).

35. Ting, K.L., 2008, "On the Input Joint Rotation Space and Mobility of Linkages," *Journal of Mechanical Design*, Vol.130, 092303-1-9.

36. Ting, K.L. and Shyu, J.H., 1992, "Joint Rotation Space of Five-bar Linkages," *American Society of Mechanical Engineers, Design Engineering Division (Publication), Mechanism Design and Synthesis*, DE-Vol.46, pp.93-101.

37. Xue C., Ting, K.L., Wang, J., and Currie, K.R., 2009, "On the Branch Formation of Spatial Group 2 Linkages," *Proceedings of IDETC/CIE 2009*, San Diego, California.

38. Hunt, K.H., 1978, *Kinematic Geometry of Mechanisms*, Oxford University Press.

39. Yan, H.S., and Wu, L.L., 1989, "On the Dead-Center Positions of Planar Linkages Mechanisms," *ASME Journal of Mechanisms, Transmissions, and Automation in Design*, Vol.111, pp.40-46.

40. Ting, K.L., Wang, J., Xue, C. and Currie, K.R., 2008, "Full Rotatability of Stephenson Six-Bar and Geared Five-Bar Linkages," *Proceedings of IDETC/CIE 2008*, Brooklyn, NY.

41. Burnside, W.S. and Panton, A.W., 1886, *The Theory of Equations*, London, Longmans Green Co.

42. Denavit, J. and Hartenberg, R.S., 1964, *Kinematic Synthesis of Linkages*, New York, McGraw-Hill Book Company.

43. Vidyasagar, M. and Spong, M., 1989, *Robot Dynamics and Control*, New York, John Wiley and Sons.

CHAPTER 7

ON THE JOINT ROTATION SPACE OF MULTILOOP LINKAGES

ABSTRACT

Joint rotation space (JRS) is an important concept of mobility analysis of complex linkages. However, the current concept and practice of JRS is based on the N-bar rotatability laws for single loop linkages. In this chapter, JRS is extended to multiloop linkages, including spatial linkages. Besides sheets and sides, a new element, bulk, is introduced to complete the concept of JRS. The JRS of any multiloop linkage reflects the interaction among all individual loops. Bulk, the new added component in JRS, will be helpful for the explanation and prediction of the branch formation of any complex linkage, particularly spatial linkages.

7.1 Introduction

The joint rotation space (JRS) [1-3] of a linkage represents the maximum possible input domain or the entire configuration space of the linkage. Each possible linkage configuration corresponds to a point in the input domain. But each point in the input domain may correspond to more than one linkage configuration. To control a linkage to reach a specific linkage configuration, it is important to understand its JRS.

The current concept and practice of JRS is based on the N-bar rotatability laws [4-6] for single loop linkages. One may envision the general mobility criteria as the algebraic form of the N-bar rotatability laws. The input and output relationship of any four-bar bimodal linkage has the form of

$$A\sin\theta_o + B\cos\theta_o + C = 0 \qquad (7\text{-}1)$$

where θ_o is the output variable and A, B, and C are functions of the input variable. By using $x = \tan(\theta_o/2)$, the above equation can be written as a quadratic equation, from which the discriminant function (Δ) can be obtained and the algebraic form of the Grashof criterion [7] can be derived.

The fundamental equation of any single loop planar/spherical linkage, virtual loop [8], or spatial group 1 linkage can be expressed in the form of Eq. 7-1 with A, B, and C as functions of all input parameters. Thus, the discriminant function can be obtained and then the JRS as well as the unified mobility criteria in the algebraic form can be established. Fig. 7.1 shows the JRS of a two-DOF linkage obtained through the discriminant function (θ_{i1} and θ_{i2} are the two input variables).

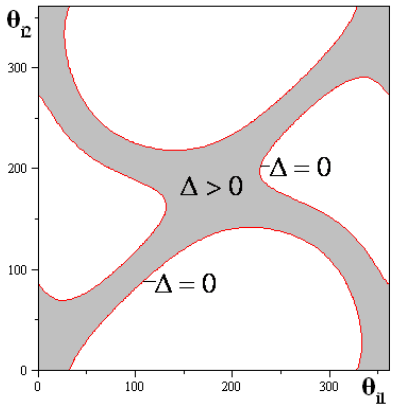

Figure 7.1 JRS of a single loop 2-DOF linkage

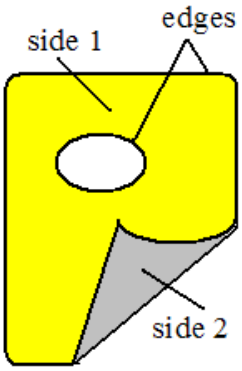

Figure 7.2 A two-sided sheet

The sheets and sides of a JRS provide an intuitive model to explain the relationship among branches, sub-branches, and singularities and establish not only a one-to-one correspondence between the input and the output but also an input domain free from any mobility defect [1-3].

JRS Sheet: The JRS of a linkage branch is called a JRS sheet. It represents the configuration space of a linkage branch in the input domain. There is no motion continuity between sheets, i.e. a linkage cannot be transformed between configurations corresponding to points on different JRS sheets (Fig. 7.2).

Edge of a JRS sheet: The edge of a JRS sheet is the boundary curve of the JRS (Fig. 7.2). Each point on the boundary curve of the JRS corresponds to a unique uncertainty singularity configuration of a linkage.

Side of a JRS sheet: The edge of a JRS sheet separates the sheet into sides (Fig. 7.2). Each side of a JRS sheet represents the configuration space of a linkage sub-branch in the input domain. A point on one side of a JRS sheet corresponds to one and only one linkage configuration. Since a linkage can be programmed within one side of a JRS sheet without reaching the boundary where an uncertainty singularity occurs, each side of a JRS sheet represents a (uncertainty) singularity-free configuration space.

7.2 JRS of Multiloop Linkages

The practice of JRS was first used in predicting the full input rotatability of geared linkages [9] and subsequently the mobility rectification of Stephenson six-bar [10] and geared five-bar linkages [11]. The research of JRS on multiple loop linkages did not start until recently. Fig. 7.3(b) shows a 7-bar parallel manipulator with the mobility chart [12]. With the use of the virtual loop concept [8], single loop spatial linkages can be treated as multiloop spherical linkages containing one or more virtual loops. In this chapter, a new component, bulk, is introduced to explain the formation of JRS in multiloop linkages, including spatial linkages.

The JRS of any multiloop linkage is affected by not only each individual loop but also the interaction among loops. There are three branches in the Stephenson six-bar linkage shown in Fig. 7.3(a), so it has three sheets. However, we may come up with different conclusion if this linkage is treated as a single loop and the corresponding principle is applied. In a single-DOF

linkage, there exists one input only, so the projection of I/O curves on the input (horizontal) axis is called the input domain or sheet of JRS [3]. In Fig. 7.3(a), if the I/O curves are projected onto the input (θ_3) axis, one may have the following observations: only two independent segments on the input axis are leading to two sheets; this is not correct. To avoid this misreading, the JRS of multiloop linkages is defined as the domain of all input variables of each individual loop. A Stephenson six-bar linkage consists of two individual loops. One of them is a five-bar loop with two input joint variables, so the JRS of Stephenson six-bar linkages must be presented and read in the domain of these two joint variables. The bulk is caused by the interaction between loops. For any double loop linkages, the number of bulks may be one, two, or four.

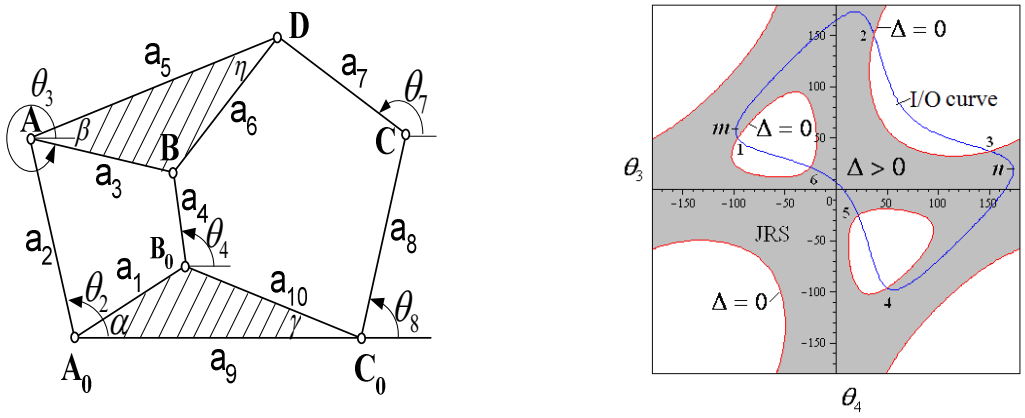

(a) Stephenson six-bar linkage

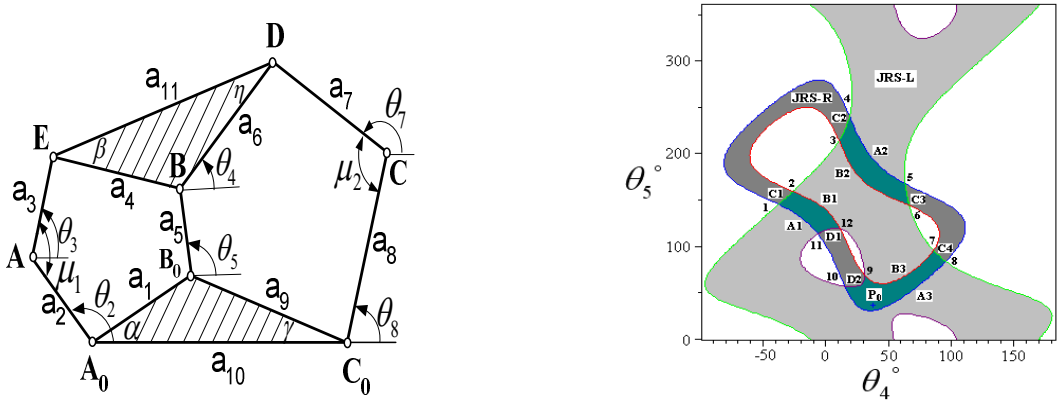

(b) Planar seven-bar linkage

Figure 7.3 JRS and branches of two loop linkages

The bulk of JRS represents the configuration space of a group of branches (or sheets) in the common input domain of all single loops. For configurations in the same bulk, they may or may not be on the same branch. For those not in the same bulk, they are definitely on different branches. The concept of bulk and its property is helpful to the mobility analysis of multiloop linkages, including spatial linkages.

In Fig. 7.3(a), both loops of the Stephenson six-bar linkage are Class II, so the result of their interaction is one bulk. Its JRS are divided into three separate areas (or curve segment for this one DOF example), so this bulk has three sheets. In Fig. 7.3(b), both loops of the 7-bar parallel manipulator are Class II, so the result of their interaction is one bulk. Its JRS are divided into three separate areas representing three sheets in this bulk of JRS.

7.3 Spatial Group 2 Linkages

The purpose of this chapter is to study the JRS of spatial group 2 linkages, particularly two-DOF. Any spatial group 2 linkage, physically or virtually, is governed by two fundamental equations in the form of

$$A_i \sin\theta_o + B_i \cos\theta_o + C_i = 0\,,\ (i = 1, 2) \qquad (7\text{-}2)$$

where θ_o is the output variable and A_i, B_i, and C_i (i = 1, 2) are functions of the common input joint variables and an intermediate joint variable. The two fundamental equations depict two virtual loops of a spatial linkage. One is derived from the spherical indicatrix; the other is induced by the presence of joint offsets and skew distance between joint axes. The JRS of any group 2 linkage is affected by not only each individual virtual loop but also the interaction between them.

The research on JRS of two-DOF group 2 linkages is both for practical and theoretical reasons. First of all, group 2 linkages are commonly used as parallel manipulators. They may also form a basic cell of a more complex linkage. For example, 2R-3C is a physical linkage, which can be used independently as a mechanism or a basic cell of a more complex linkage. Secondly, each pair of fundamental equations in a group 3 linkage is virtually equivalent to a two-DOF group 2 linkage; the property of its JRS is necessary for the mobility study of group 3 linkages.

The discriminant method can be used to derive the JRS bulk of any spatial group 2 linkage. Each loop may be regarded as a group 1 linkage; the discriminant function $\Delta \geq 0$ describes the JRS of a group 1 linkage. Two fundamental equations of a spatial group 2 linkage correspond to two discriminant functions and generate two independent JRS accordingly. Their intersection is the JRS bulk of this group 2 linkage. According to the mobility criteria of single loop linkage, each loop can be easily identified as Class I or II. If both loops are Class I, then there will be four bulks. If only one loop is Class I, then the number of JRS bulks is two. If neither loop is Class I, then there is only one bulk. The discriminant method is simple and straightforward; it applies to any multiloop linkage.

Besides the discriminant method, the discrete method is another approach to derive the JRS bulk of two-DOF group 2 linkages in which there are two input joint variables (say θ_1 and θ_2, respectively) and one output joint variable (say θ_6), and one intermediate joint variable (say θ_3). If the output joint variable (θ_6) is held constant, then Eq. 7-2 becomes the form of 3R-2C mechanism, which is one-DOF group 2 linkage. The JRS bulk of this one-DOF group 2 linkage can be easily derived via the discriminant functions. By varying the θ_6 value, Eq. 7-2 yields a

family of one-DOF group 2 linkages and the corresponding JRS bulks can also be derived. By connecting them in order, the JRS bulk is formed of the two-DOF group 2 linkage.

The discrete method can also be used to derive the JRS sheet of two-DOF group 2 linkages. If the output joint variable (θ_6) is held constant, then Eq. 7-2 becomes the form of 3R-2C mechanism, which is one-DOF group 2 linkage. The mobility relationship of the two input joint variables (θ_1 and θ_2) may be derived. By varying the θ_6 value, Eq. 7-2 yields a family of one-DOF group 2 linkages and the corresponding mobility relationship of the two input joint variables can be derived and connected in order to form the JRS sheet(s) of this two-DOF group 2 linkage.

7.4 Examples

The JRS of one-DOF group 2 linkage

Example 1: The RCRCR mechanism is shown schematically in Fig. 7.4(a). The axes of the joints R, C, R, C, and R are labeled 1, 2, 3, 4, and 5, respectively. The input and output angular displacements are θ_1 and θ_5 while the intermediate angular displacement is denoted by θ_3. The remaining four variables are the angular displacements θ_2, θ_4 and the displacements S_2 and S_4. By using the D-H notation [13, 14], $\alpha_{12} = 60^{\circ}$, $\alpha_{23} = 45^{\circ}$ $\alpha_{34} = 35^{\circ}$, $\alpha_{45} = 30^{\circ}$, and $\alpha_{51} = 10^{\circ}$ are the angles between the corresponding joint axes, $a_{12} = 25$, $a_{23} = 30$, $a_{34} = 40$, $a_{45} = 10$, and $a_{51} = 32$, are the distance between the corresponding joint axes, and $S_{11} = 30$, $S_{33} = 25$, and $S_{55} = 8$ are the offset along the corresponding R-joint axes.

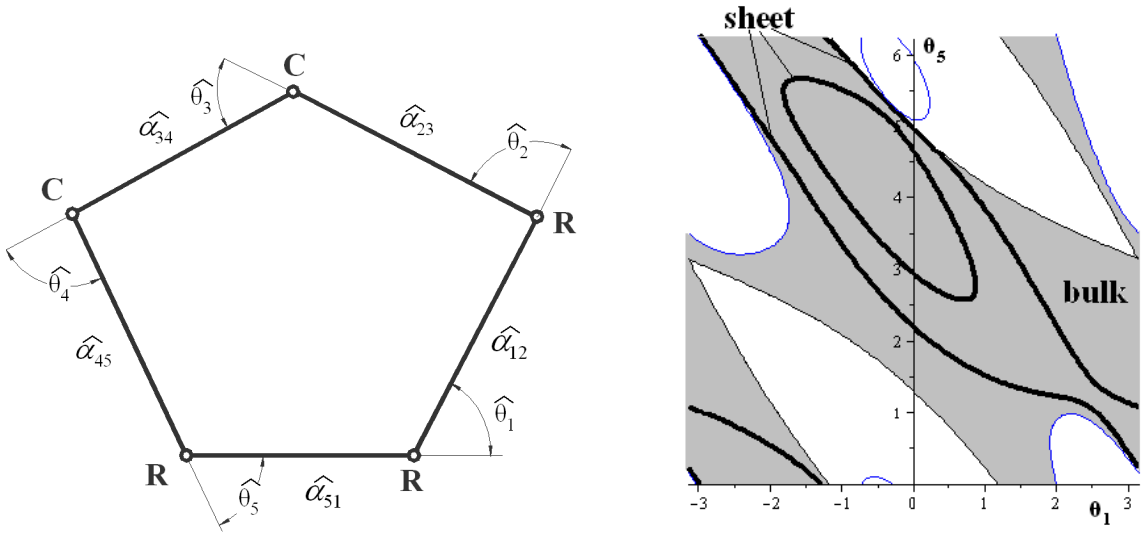

(a) RCRCR mechanism (b) JRS bulk and sheet

Figure 7.4 One-DOF group 2 linkage

The two loop-closure equations derived by following Duffy's sine, sine-cosine, and cosine laws [15, 16] are

$$\cos\theta_3 - 0.38 + 1.07\sin\theta_5\sin\theta_1 - 0.32\cos\theta_1 - 1.05\cos\theta_1\cos\theta_5 - 0.11\cos\theta_5 = 0 \tag{7-3}$$

$$\sin\theta_3 - 3.485\cos\theta_3 - 1.012 - 1.356\sin\theta_5\sin\theta_1 + 2.442\cos\theta_1 + 1.098\cos\theta_1\cos\theta_5 + 0.666\cos\theta_5 - 1.618\sin\theta_5\cos\theta_1 - 0.385\sin\theta_1 - 1.603\sin\theta_1\cos\theta_5 - 0.034\sin\theta_5 = 0 \tag{7-4}$$

The corresponding discriminant functions and the input/output displacement equation can be derived and plotted in Fig. 7.4(b). Since both loops are Class II based on the mobility criteria of single loop, there is only one JRS bulk. As shown in Fig. 7.4(b), there are three sheets (branches) in this one-DOF group 2 linkage.

The JRS of two-DOF group 2 linkage

Example 2: In example 1, let S_{33} be a variable (R_3 is replaced with C_3), then the linkage becomes RCCCR, which is a two-DOF group 2 linkage. The two loop-closure equations can be

derived by following Duffy's sine, sine-cosine, and cosine laws [15, 16]. The first loop-closure equation (7-3) remains unchanged, while the second one contains one more variable S_{33} is listed as follows:

$$\begin{aligned} &0.406\,S_{33}\sin\theta_3 - 35.34\cos\theta_3 - 10.27 - 13.75\sin\theta_5\sin\theta_1 + 24.76\cos\theta_1 \\ &+ 11.13\cos\theta_1\cos\theta_5 + 6.75\cos\theta_5 - 16.40\sin\theta_5\cos\theta_1 \\ &- 3.91\sin\theta_1 - 16.26\sin\theta_1\cos\theta_5 - 0.35\sin\theta_5 = 0 \end{aligned} \tag{7-5}$$

The second loop-closure equation corresponds to a six-bar virtual loop. From example 1 we know when S_{33} =25, the six-bar is degenerated into a Class II five-bar loop, thus this six-bar loop is Class II according to the mobility criteria. The first loop-closure equation corresponds to a Class II five-bar loop, so their intersection will lead to one bulk only in this RCCCR linkage.

The JRS sheet of this RCCCR linkage is derived with the discrete method. When S_{33} is held constant, this linkage becomes RCRCR, and the mobility relationship between the two input joint variables (θ_1 and θ_5) may be obtained. By varying the S_{33} value, Eqs. 7-3 and 7-5 yield a family of one-DOF group 2 linkages and the corresponding mobility relationship of the joint variables θ_1 and θ_5 may be derived and connected to form the JRS sheet of this two-DOF group 2 linkage. There is only one sheet (branch) in this example as shown in Fig. 7.5(b).

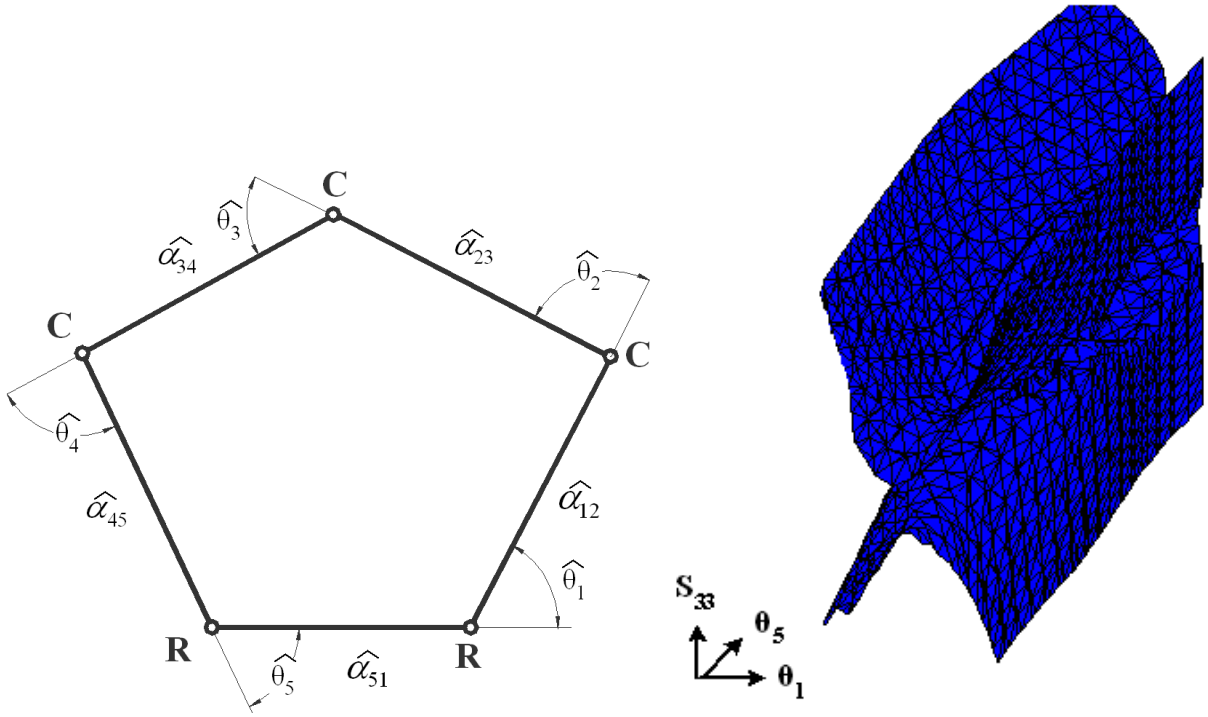

(a) RCCCR mechanism (b) JRS sheet

Figure 7.5 Two-DOF group 2 linkage

Example 3: The RRRRCR mechanism is shown schematically in Fig. 7.6(a). The axes of the joints R, R, R, R, C, and R are labeled 1, 2, 3, 4, 5, and 6, respectively. The input and output angular displacements are θ_1 and θ_6 while the intermediate angular displacements are denoted by θ_2 and θ_3. The remaining three variables are the angular displacements θ_4, θ_5, and the displacement S_4. By using the D-H notation [13, 14], $\alpha_{12} = 90^\circ$, $\alpha_{23} = 90^\circ$ $\alpha_{34} = 90^\circ$, $\alpha_{45} = 90^\circ$, $\alpha_{56} = 90^\circ$, and $\alpha_{61} = 90^\circ$ are the angles between the corresponding joint axes, $a_{12} = 2$, $a_{23} = 0$, $a_{34} = 8$, $a_{45} = 2$, $a_{56} = 2$, and $a_{61} = 3$ are the distance between the corresponding joint axes, and $S_{11} = 8$, $S_{22} = 3$, $S_{33} = 0$, $S_{44} = 0$, and $S_{66} = 2$ are the offset along the corresponding R-joint axes.

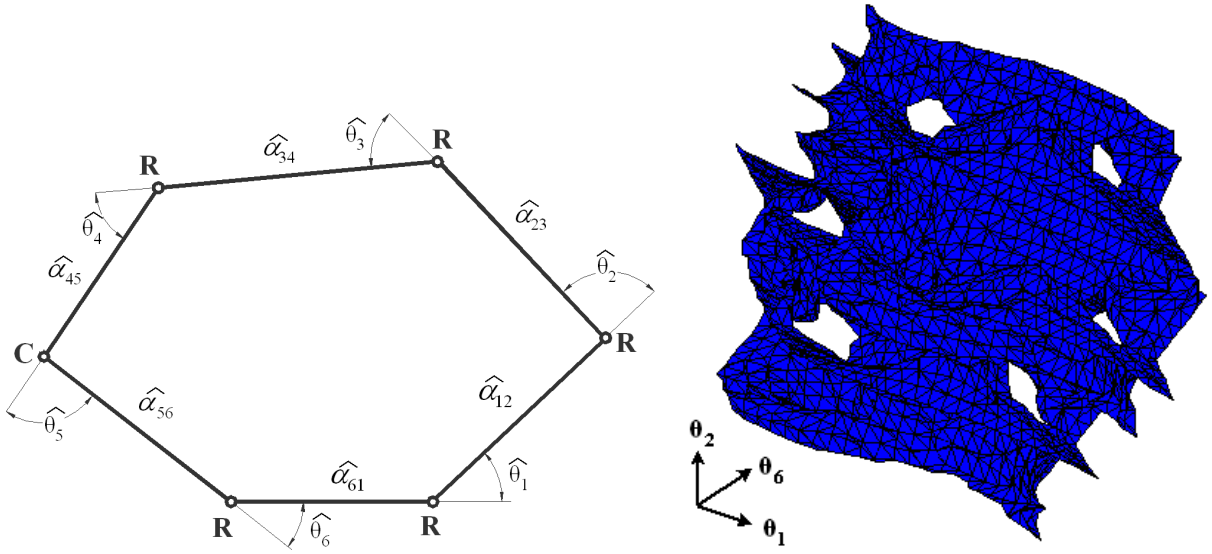

(a) RRRRCR mechanism (b) JRS sheet

Figure 7.6 Virtual two-DOF group 2 linkage

By following Duffy's sine, sine-cosine, and cosine laws [15, 16], there are three loop-closure equations equivalent to three virtual loops. Each pair of fundamental equations is virtually equivalent to a two-DOF group 2 linkage. Two fundamental equations are listed as follows:

$$(\sin\theta_6\cos\theta_1\cos\theta_2-\cos\theta_6\sin\theta_2)\sin\theta_3-\sin\theta_6\sin\theta_1\cos\theta_3=0 \qquad (7\text{-}6)$$

$$\begin{aligned}&(8\cos\theta_6\cos\theta_1-2\cos\theta_2\sin\theta_1)\sin\theta_3\\&+(8\sin\theta_6\sin\theta_2+8\cos\theta_6\cos\theta_2\cos\theta_1-2\cos\theta_1)\cos\theta_3\\&+(8\sin\theta_6+3\sin\theta_1\cos\theta_6+3\cos\theta_6+2\cos\theta_1\cos\theta_6+2)=0\end{aligned} \qquad (7\text{-}7)$$

Since both loops are Class II based on the mobility criteria of single loop, there is only one JRS bulk. The discrete method is used to derive the JRS sheet of this virtual two-DOF group 2 linkage. By varying the θ_6 value, Eqs. 7-6 and 7-7 yield a family of one-DOF group 2 linkages and the corresponding mobility relationship of the joint variables θ_1 and θ_2 may be derived and

connected to form the JRS sheet of this virtual two-DOF group 2 linkage. There is only one sheet (branch) in this example.

7.5 Conclusions

The JRS of multiloop linkages represents the domain of all common input variables of each individual loop. The JRS of any multiloop linkage, including spatial linkages, is affected by not only each individual loop but also by the interaction among loops. The addition of bulk into JRS completes the concept. The discriminant function and the discrete methods are introduced to obtain the JRS bulks and sheets. Several examples are presented to explain the form of JRS bulks and sheets of spatial one-DOF and (virtual) two-DOF group 2 linkages. The extension of JRS to multiloop linkages is helpful for the explanation and prediction of the branch formation of complex linkages, particularly spatial linkages.

REFERENCES

1. Ting, K.L. and Shyu, J.H., 1992, "Joint Rotation Space of Five-bar Linkages," *American Society of Mechanical Engineers, Design Engineering Division (Publication), Mechanism Design and Synthesis*, DE-Vol.46, pp.93-101.
2. Ting, K. L., 2007, "Joint Rotation Space and Mobility of Linkages," *Proceedings of IDETC/CIE 2007 ASME Design Engineering Technical Conferences and Computers and Information in Engineering Conference*.
3. Ting, K.L., 2008, "On the Input Joint Rotation Space and Mobility of Linkages," *Journal of Mechanical Design*, Vol.130, 092303-1-9.
4. Ting, K.L., 1989, "Mobility Criteria of Single-Loop N-Bar Linkages," *Journal of Mechanisms, Transmissions, and Automation in Design*, pp. 504-507.
5. Ting, K.L. and Liu, Y.W., 1991, "Rotatability Laws for N-Bar Kinematic Chains and Their Proof," *ASME Journal of Mechanical Design*, Vol. 113, No. 1, pp. 32-39.
6. Shyu, J.H. and Ting, K.L., 1994, "Invariant Link Rotatability of N-Bar Kinematic Chains," *Journal of Mechanical Design*, Vol.116, pp.343-347.
7. Grashof, F., 1983, *Theoretische Maschinenlehre*, Leipzig.
8. Dou, X. and Ting, K.L., 1996, "Classification, Rotatability, and Branch Identification of Simple RCRCR Mechanisms," *ASME Design Engineering Technical Conference and the Computer in Engineering*, Paper No. 96-DETC/FAS-1363.
9. Ting, K.L., 1994, "Mobility Criteria of Geared Five-Bar Linkages," *Mechanism and Machine Theory*, Vol.29, No.2, pp.251-264.
10. Ting, K.L., and Dou, X., 1996, "Classification and Branch Identification of Stephenson Six-bar Chains," *Mechanism and Machine Theory*, Vol. 31, No. 3, pp 283-295.
11. Dou, X.H. and Ting, K.L., 1996, "Branch Identification of Geared Five-Bar Chains," *Journal of Mechanical Design*, Vol.118, No.3, pp.384-389.
12. Wang, J., Ting, K. L., Xue C., and Currie, K. R., 2009, "General Mobility Analysis of Two-DOF Planar Seven-Bar Linkages," *Proceedings of IDETC/CIE 2009*, San Diego, California.
13. Denavit, J. and Hartenberg, R.S., 1964, *Kinematic Synthesis of Linkages*, New York, McGraw-Hill Book Company.
14. Vidyasagar, M. and Spong, M., 1989, *Robot Dynamics and Control*, New York, John Wiley and Sons.
15. Duffy, J., 1980, *Analysis of Mechanisms and Robot Manipulators*, New York, John Willey and Sons.
16. Crane III, C.D. and Duffy, J., 2008, *Kinematic Analysis of Robot Manipulators*, New York, Cambridge University Press.

CHAPTER 8

CONCLUSIONS

In this dissertation, the geometry attribute hidden behind spatial linkages has been investigated. The successfully developed concepts will form the foundation and backbone to support the mobility analysis of more complex linkages or manipulators. The often endless blind or trial and error search may be done intelligently.

8.1 Significance, Contribution, and Unique Features of this Research

8.1.1 Extension of the N-Bar Rotatability Laws

The N-bar rotatability laws are extended to N-bar chains containing prismatic joints. The effects of long and short links, full rotatability, linkage classification, and the formation of branches and sub-branches are discussed. The extension provides a consistent method to understand all aspects of linkage rotatability disregarding the existence of prismatic joints. In this dissertation, a Watt six-bar linkage is converted and equivalent to a Stephenson six-bar linkage. The equivalency offers a simple and clear visual explanation on the formation of branches and sub-branches and how Watt and Stephenson linkages differ in mobility. Although the formation of branch, sub-branch, and full rotatability of general Watt six-bar linkages is explained via the stretch rotation of a four-bar loop, the resulting mobility criteria and algorithm in this dissertation requires no stretch and rotation and is easy to use. The algorithm is suitable

for automated mobility identification and is valid regardless whichever link is used as the input or fixed link and whether prismatic joints are contained or not.

8.1.2 Concepts of Virtual Loops and Virtual Linkages

The concept of virtual loops is presented to describe the essential geometry behind spatial linkages in this dissertation. The similarities are demonstrated between a virtual loop and a physical loop (known as planar or spherical loop). Each group 1, 2, 3, or 4 spatial linkage can be regarded as a virtual spherical linkage formed by one or more virtual loops. The links among spatial linkages are discovered: each pair of fundamental equations in a group 4 linkage is virtually equivalent to a three-DOF group 2 linkage; each pair of fundamental equations in a group 3 linkage is virtually equivalent to a two-DOF group 2 linkage. The fact that all Duffy's group 1 linkages and planar and spherical four-bar linkages are bimodal linkages is consistent to the proposed virtual loop concept. From the viewpoint of linkage mobility and displacement analysis, simple RCRCR and group 2 linkages with parallel joint axes are virtually equivalent to Stephenson six-bar linkages. A unified mobility identification and rectification is offered for both ordinary and virtual Stephenson linkages in this dissertation. From one virtual loop to virtual Stephenson linkages and then to any virtual multiloop spherical linkages, a big picture of spatial linkages is presented. The concept of virtual loops is subtle but significant. It establishes a unified view on planar, spherical, and spatial linkages and a useful model to view or even understand complex spatial linkages.

8.1.3 Branch Formation of Spatial Linkages

The current use of branch point for branch identification is limited to linkages with simple topology and singularity conditions, such as Stephenson-type linkages, which are simplified versions of group 2 mechanisms. In this dissertation, tangent points, the counterpart of branch points for Stephenson-type linkages, are sought to explain the formation of branches. The discovery of tangent points and the generalization of branch points offer an explicit explanation and prediction of the branch formation of spatial group 2 linkage.

8.1.4 Extension of JRS to Multiloop Linkages

Joint rotation space (JRS) is an important concept on mobility analysis of complex linkages. It represents the domain of all common input variables of each individual (virtual) loop. In a multiple DOF linkage, the JRS is like a map for one to program the linkage in the input domain. The JRS of any multiloop linkage, including spatial linkages, is affected by not only each individual loop but also the interaction among loops. However, the current concept and practice of JRS is based on the N-bar rotatability laws for single loop linkages. In this dissertation, the extension of JRS is sought to account for the mobility of multiple loop (including virtual loop), single- and two-DOF systems. The addition of bulk into JRS completes the concept and is helpful for the explanation and prediction of the branch formation of any complex linkage, particularly spatial linkages.

8.2 Future Work

The mobility of spatial group 2 linkages is governed by two fundamental equations and how they influence each other. The generalized JRS and branch points may lead to the fundamental theory in treating the interaction between loops. The mobility theory of general group 2 linkages will be explored to develop an automated mobility analysis scheme. Mobility rectification is a bottleneck in complex linkage synthesis and programming. The research results of this dissertation may support computer-aided mobility rectification to remove this bottleneck. The mobility of complex linkages may be predicted in a simple and decisive manner rather than by an experimental or trial and error search. The mobility of spatial group 3 and 4 linkages can be identified progressively by treating two loops at a time. The ultimate objective is to establish a mobility theory treating the issues of discontinuity and singularity avoidance, full rotatability, and order or path of motion, which are intrinsic to all group 2, 3, and 4 spatial linkages.

VITA

Changyu Xue was born in Jiangsu, China, in 1972. He attended Tsinghua University in September 1990 and in July 1995 received a B.S. in Engineering. In January 2003, he attended Tennessee Technological University. He received an M.S. in Engineering in May 2005 and a Ph.D. in Engineering in August 2009 from Tennessee Technological University.